Title
Lewis Acid Mediated Reactions: Electronic Modification of Platinum Complexes and Metal-Free Catalysis

Author
Liberman-Martin, Allegra Lauren

Publication Date
2015

Peer reviewed|Thesis/dissertation

Lewis Acid Mediated Reactions: Electronic Modification of Platinum Complexes and Metal-Free Catalysis

by

Allegra Lauren Liberman-Martin

A dissertation submitted in partial satisfaction of the
Requirements for the degree of
Doctor of Philosophy
in
Chemistry
in the
Graduate Division
of the
University of California, Berkeley

Committee in charge:
Professor T. Don Tilley, Co-Chair
Professor Robert G. Bergman, Co-Chair
Professor Alexis T. Bell

Fall 2015

Abstract
Lewis Acid Mediated Reactions: Electronic Modification of
Platinum Complexes and Metal-Free Catalysis

Allegra Lauren Liberman-Martin
Doctor of Philosophy in Chemistry
University of California, Berkeley
Professor T. Don Tilley, Co-Chair
Professor Robert G. Bergman, Co-Chair

Chapter 1. A strategy for the control of electron density at a metal center is reported, using a remote chemical switch involving second-sphere Lewis acid binding that modulates electron density in the first coordination sphere. Binding of the Lewis acid $B(C_6F_5)_3$ at remote nitrogen positions of a bipyrazine-diarylplatinum(II) complex accelerates biaryl reductive elimination by a factor of 64,000.

Chapter 2. The silicon and zinc Lewis acids $Si(cat)_2$ (cat = catecholato), $Si(cat^F)_2$ (cat^F = tetrafluorocatecholato), and $Zn(C_6F_5)_2$ bind to the remote ligand site of a 2,2′-bipyrimidyl–platinum diaryl complex. This platinum complex provides a platform to systematically evaluate electronic and reactivity differences triggered by Lewis acid binding. The electron density of the bipyrimidine ligand is substantially depleted upon Lewis acid binding, as evidenced by UV-vis spectroscopy and cyclic voltammetry. Biaryl reductive elimination studies allowed quantification of the effect of Lewis acid binding on reactivity, and Lewis acid binding accelerated reductive elimination rates by up to eight orders of magnitude. Kinetics experiments in combination with DFT studies support an unusual mechanism featuring complete dissociation of the bidentate bipyrimidine ligand prior to reductive elimination.

Chapter 3. Z-type interactions between bis(perfluorophenyl)zinc and platinum(II) diaryl complexes supported by phenanthroline (phen), bipyridine (bpy), and bis(dimethylphosphino)ethane (dmpe) ligands are reported. In the solid state, there is an unsupported Pt–Zn bond for the phen complex, while the dmpe derivative features additional bridging aryl interactions. The Pt–Zn complexes featuring phen and bpy ligands undergo facile reductive elimination, whereas aryl exchange between Pt and Zn is observed for the dmpe complex.

Chapter 4. Bis(perfluorocatecholato)silane $Si(cat^F)_2$ was prepared, and stoichiometric binding to Lewis bases was demonstrated with fluoride, triethylphosphine oxide, and N,N'-diisopropylbenzamide. The potent Lewis acidity of $Si(cat^F)_2$ was suggested from catalytic hydrosilation and silylcyanation reactions with aldehydes. Mechanistic studies of hydrosilation using an optically active silane substrate, R-(+)-methyl(1-napthyl)phenylsilane, proceeded with predominant stereochemical retention at silicon, consistent with a carbonyl activation pathway. The enantiospecificity was dependent on solvent and salt effects, with increasing solvent polarity or addition of $NBu_4BAr^F{}_4$ leading to a diminished enantiomeric ratio. The medium effects are consistent with an ionic mechanism, wherein hydride transfer occurs prior to silicon–oxygen bond formation.

Lewis Acid Mediated Reactions: Electronic Modification of Platinum Complexes and Metal-Free Catalysis

Table of Contents

Introduction

The rate and selectivity of organometallic reactions can be dramatically influenced by the electronic environment of the metal center. Traditionally, to gain mechanistic insight on electronic preferences for a metal-mediated reaction, a series of independently-synthesized ligands and their corresponding metal complexes must be prepared. In this dissertation, an alternative strategy is explored, which uses the binding of an additive to electronically modify a complex. This modular approach allows a series of complexes to be rapidly assembled from a common precursor, and the differences in rates with and without the additive offer insight into the electronic preferences for a reaction.

Enzymes provided our inspiration for motifs by which post-synthetic modification could occur (Figure 1). In allosteric regulation, switching between catalyst states is controlled by effector binding to a remote protein site. Alternatively, coenzymes can interact directly with an active site to alter steric and electronic properties. For both pathways, the regulatory mechanism enables the active site to be protected in a stable resting state that is converted to a more reactive form during catalysis.

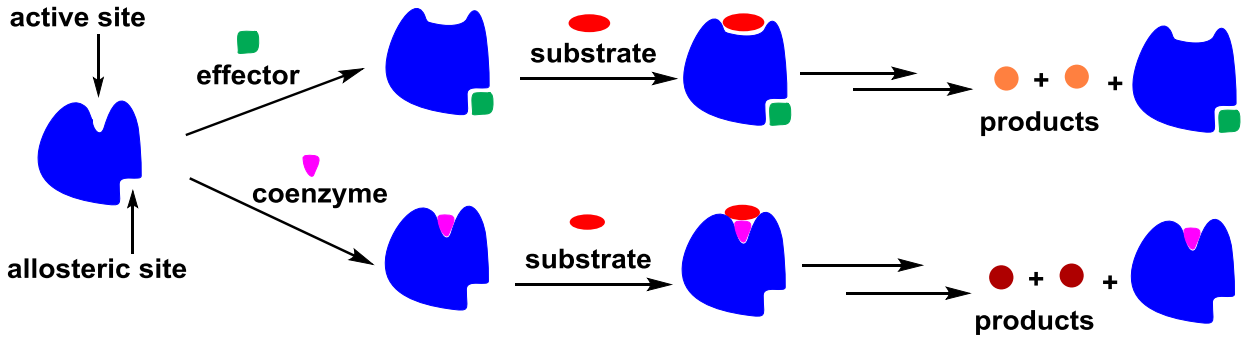

Figure 1. Regulatory mechanisms in enzyme catalysis.

This dissertation presents two strategies to modify the electronic properties of platinum complexes by addition of Lewis acids. Analogous to the allosteric mechanism described above, the first approach features Lewis acid binding to remote ligand sites (Figure 2). A second strategy, with parallels to the active site modification by a coenzyme, involves Lewis acid binding to the platinum center itself. While the remote binding strategy induces only electronic changes, direct binding alters both the electronic and steric environment of the platinum center.

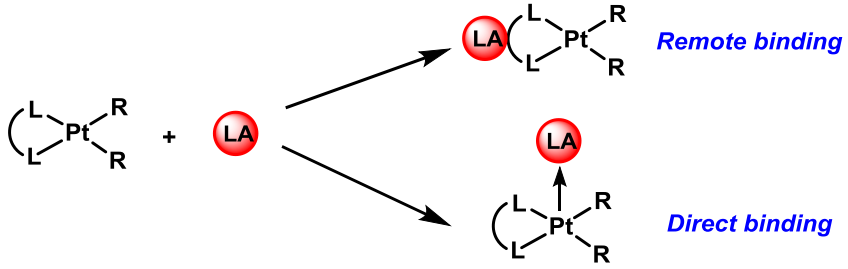

Figure 2. Lewis acid binding to modify platinum complexes.

Chelating bis-diazine ligands, which feature aromatic heterocycles with two nitrogen atoms per ring, were investigated as platforms for remote Lewis acid binding (Figure 3). The *para* and *meta* nitrogen placement in the diazine rings was selected to allow for electronic tuning without steric modification. In Chapter 1, binding of two equivalents of the strong Lewis acid bis(pentafluorophenyl)borane to the *para* nitrogen sites of a bipyrazine–platinum(II) diaryl complex is demonstrated. Boron binding depletes electron density from both the bipyrazine ligand and the platinum center, accelerating biaryl reductive elimination from platinum.

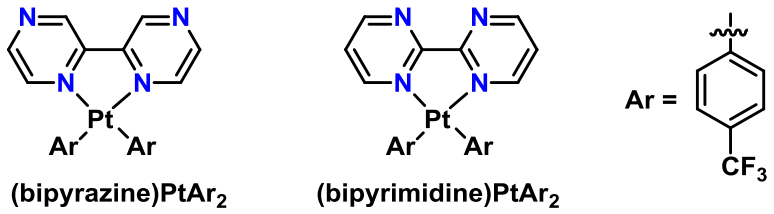

Figure 3. Ligand motifs for the remote binding of Lewis acids.

An analogous bipyrimidine–platinum complex with a bidentate remote binding site is presented in Chapter 2. Unconventional silicon and zinc Lewis acids were identified that interact strongly with the bipyrimidine ligand. The bipyrimidyl electron density is substantially depleted upon Lewis acid binding, while there is a smaller electronic effect on the platinum center. This electron withdrawal from the ligand causes biaryl reductive elimination from these complexes to proceed by an unusual mechanism, with bidentate ligand dissociation preceding carbon–carbon bond formation. This work demonstrates the ability of remote Lewis acid binding to profoundly alter ligand donor properties.

In Chapter 3, the direct binding of the bis(pentafluorophenyl)zinc Lewis acid to platinum(II) diaryl complexes is demonstrated. The Pt–Zn bond, which is formed by donation from platinum to zinc, is retained in solution and the solid state. Along with providing an unusual example of a Lewis acid-base interaction between two metal centers, this work demonstrates that the Pt–Zn interaction accelerates biaryl reductive elimination from the platinum center.

Lastly, a discussion of the metal-free reactivity of a bis(perfluorocatecholato)silane Lewis acid is presented in Chapter 4. This Lewis acid was initially prepared because it can readily adopt a six-coordinate structure, making it ideal for binding to the bidentate binding site of a bipyrimidine–platinum complex (discussed in Chapter 2). To gain additional insight into the strength and variety of Lewis acid-base interactions with bis(perfluorocatecholato)silane, binding studies of both neutral and anionic Lewis bases were performed, revealing the potent Lewis acidity of this reagent. Hydrosilation of aldehydes is catalyzed by bis(perfluorocatecholato)silane under mild conditions, providing a promising example of catalysis by a silicon Lewis acid.

Acknowledgements

I thank all of the people that have made it possible to complete my doctoral studies and have fun while doing it. Reaching this goal would not have been possible without the friends and mentors I've found at Berkeley.

I would first like to thank my two advisors, Profs. T. Don Tilley and Robert G. Bergman for the opportunity to work with them on a project that I have loved. They have given me tremendous support and freedom throughout my time at Berkeley. Their passion for chemistry and scientific rigor are inspirational, and I cannot imagine a better combination of mentors.

I thank my undergraduate research advisors, Profs. Kathleen L. Purvis-Roberts, Nancy B. S. Williams, and Alan S. Goldman who helped me discover my enthusiasm for research and for their continued mentorship during graduate school.

The departmental staff at Berkeley played a crucial role in supporting me throughout my time at Berkeley. I thank Rosemary Tilley and Anneke Runtupalit for personal support and their heroic efforts to keep chemicals on the shelves and money in my wallet. Drs. Chris Canlas, Antonio DiPasquale, and Kathleen Durkin also provided technical assistance on many occasions.

I am grateful for the opportunity I've had to work with my labmates in the Tilley and Bergman groups. It has been a wonderful experience to spend my days with such a smart, motivated, and fun group of people. I thank Daniel Levine, Micah Ziegler, and Dr. Wenjun Liu for their collaborations on DFT calculations, X-ray crystallography, and cyclic voltammetry that are presented in Chapters 2 and 3 of this dissertation. Drs. Miriam Bowring, Miles Johnson, Mark Lipke, and Mike Lipschutz and Beatriz Brando have been true friends and have also provided invaluable advice and insight about my chemistry.

Finally, I am incredibly grateful to my family for their love and support. I thank my parents, Sandy and Dean, for being a constant source of encouragement; I would not have made it through graduate school without them. Thank you to Zoe for being the best sister and friend I could ask for. Lastly, my husband, Henry Hallam, has brought love, friendship, and balance to my life. I am so lucky to have such a wonderful partner.

Chapter 1. A Remote Lewis Acid Trigger Dramatically Accelerates Biaryl Reductive Elimination from a Platinum Complex

INTRODUCTION

Biological catalysts utilize steric and electronic modifications to attain a remarkable degree of substrate specificity. One mechanism by which enzymes finely tune reactivity is through allosteric regulation, in which the enzyme responds to the presence of a distant activator that induces conformational changes to alter enzyme activity.[1] The operation of a chemical switching mechanism enables the active site to be protected in a stable resting state, which is converted to a more reactive form during catalysis. This allows many biological systems to be active only when a triggering signal is present, thus protecting them from decomposition.

Although tuning reactivity via chemical triggers is common in biological systems, there are currently few analogs for synthetic catalysts.[2] In particular, examples involving electronic triggers are rare. One reported strategy involves coordination of tris(pentafluorophenyl)borane, $B(C_6F_5)_3$, to carbonyl- and imine-containing nickel(II) complexes to activate these species toward ethylene polymerization catalysis.[3–5] Placement of the Lewis acid binding site remote from the reactive metal center allowed for electronic modifications without direct alteration of the coordination environment. Addition of the Lewis acid led to a three orders of magnitude increase in polymerization activity for these systems.

Herein, we report the synthesis and borane binding studies of platinum–bipyrazine (bpyz) complexes, as well as mechanistic studies of their biaryl reductive elimination. The *para*-arrangement of the nitrogen donors featured in bpyz was envisioned to allow borane binding with formation of a zwitterionic complex, which may have a significant resonance contributor that could be described as an electrophilic platinum(IV) species (Scheme 1). Because Lewis acid binding occurs at a remote ligand site, differences in the activity observed between borane-free and –bound complexes enable the role of electrophilicity on reactivity to be evaluated.

Scheme 1. Resonance contributors upon remote borane binding.

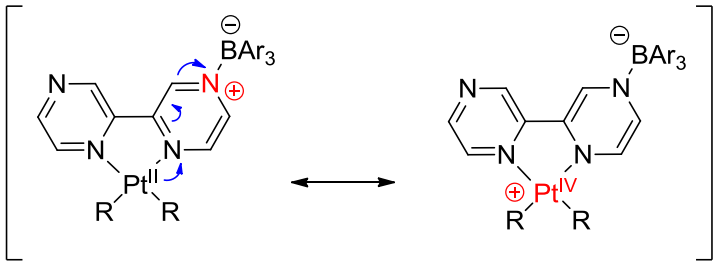

RESULTS AND DISCUSSION

A bipyrazine-diarylplatinum complex (bpyz)Pt(4-CF_3-Ph)$_2$ (**1**) was prepared by treatment of Pt(4-CF_3-Ph)$_2$(SEt_2)$_2$ with bpyz. Complex **1** was treated with variable amounts of $B(C_6F_5)_3$ in benzene to generate mono- or bis-borane adducts **2** and **3** (Scheme 2). Borane adduct formation resulted in dramatic color changes from red (**1**), to green (**2**), to brown (**3**). In the presence of one equiv of $B(C_6F_5)_3$, roughly equal amounts of **1**, **2**, and **3** were observed (34 %, 32 %, and 34 %, respectively), whereas with two equivs of $B(C_6F_5)_3$, the product distribution changed to 3 % **1**, 4 % **2**, and 93 % **3**. To test for the reversibility of borane coordination, isolated

3 was treated with an excess of 4-dimethylaminopyridine (DMAP), resulting in regeneration of **1** and formation of the DMAP–$B(C_6F_5)_3$ adduct (by ^1H and ^{19}F NMR spectroscopy).

Scheme 2. Reversible formation of mono-and bis-borane adducts.

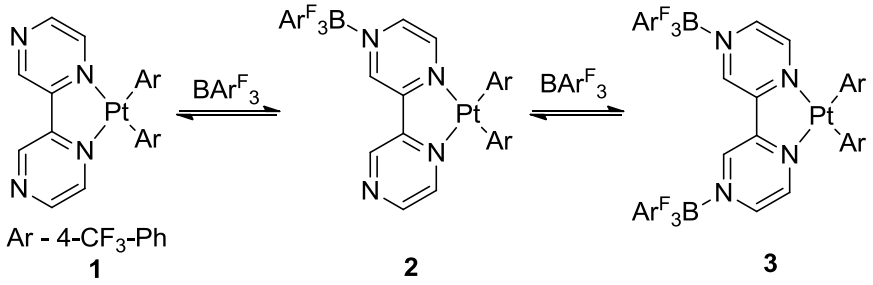

Comparisons of ^1H and ^{195}Pt NMR data for **1** and **3** suggest a substantial impact of Lewis acid binding on electron density at the platinum center. The ^1H NMR resonance for H-3 of the pyrazine ring shifts from 8.01 ppm for **1** to 8.68 ppm for **3** (Figure 1). This downfield shift is consistent with coordinated $B(C_6F_5)_3$ groups withdrawing electron density from the pyrazine rings. A gradual change in ^{195}Pt chemical shift was also observed between **1** (δ = -3197 ppm), **2** (-2654 ppm), and **3** (-2070 ppm), suggesting enhanced electron deficiency upon $B(C_6F_5)_3$ coordination.[6] The ^{19}F NMR separation of *para* and *meta* resonances of the $B(C_6F_5)_3$ fragments in **3** is 8.5 ppm, consistent with a four-coordinate geometry at boron.[7]

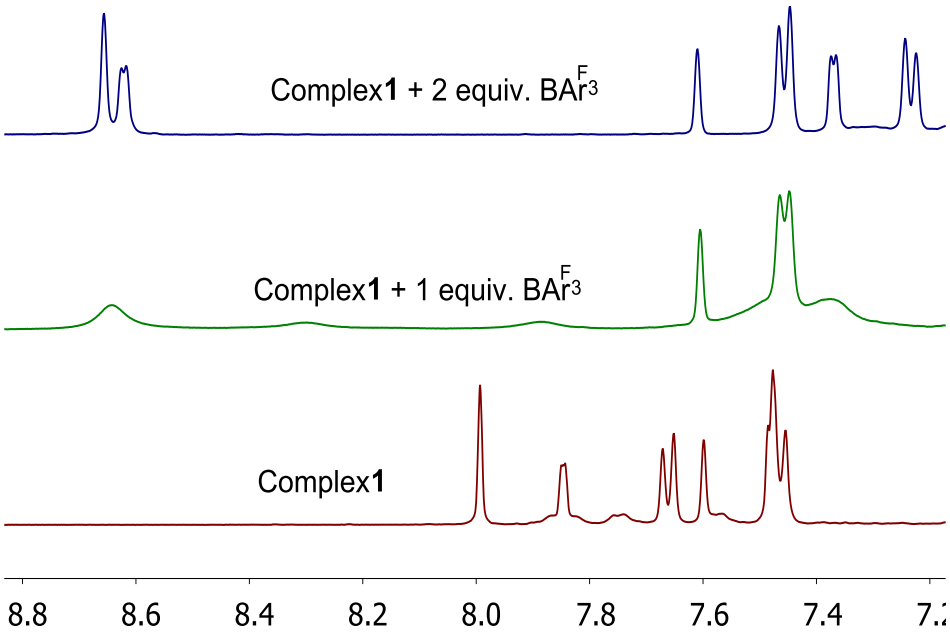

Figure 1. ^1H NMR spectra of **1** with added $B(C_6F_5)_3$, recorded in toluene-d_8 at 23 °C with a 1,3,5-tris(trifluoromethyl)benzene internal standard (δ = 7.61 ppm).

To probe the influence of borane binding on reactivity, reductive elimination studies were targeted, since group 10 metals have been shown to be highly useful catalysts for carbon–carbon coupling reactions.[8–10] Reductive elimination rates are dependent both on the nature of the transition metal, as well as the steric and electronic properties of the ancillary and reacting ligands.[11] Although the activity of many complexes toward reductive elimination has been attributed to electron deficiency of the metal center, few detailed studies have directly probed the role of this property on reactivity. For example, it has been shown that fluorinated phosphine ligands promote reductive elimination at platinum.[12,13] However, in such investigations, the steric environment of the platinum center is inevitably altered upon ligand modification, and the rate differences cannot be attributed to only electronic effects.

In the presence of two or more equivs of bis(trimethylsilyl)acetylene (BTMSA), the bis-borane adduct **3** was found to quantitatively undergo biaryl reductive elimination at 45 °C (eq 1). This is a remarkably low temperature for platinum biaryl reductive elimination, which requires temperatures above 90 °C for bis-phosphine systems.[12–14] In contrast, previous studies of diaryl(2,2'-bipyridine)platinum complexes demonstrated two consecutive roll-over metallations of the bipyridine ligand at 150 °C, along with generation of two equivs of Ar–H, rather than biphenyl formation.[15] In the current work, after reductive elimination from **3**, the bpyz ligand dissociated from platinum as a bis-borane adduct, yielding a platinum alkyne complex, [Pt_2(μ-$Me_3SiCCSiMe_3$)($Me_3SiCCSiMe_3$)$_2$] (**4**).[16,17] Analogous reactivity was observed with other internal alkynes, such as diphenylacetylene. Attempts to induce reductive elimination with other neutral donors, such as internal alkenes or phosphines, were unsuccessful.[18]

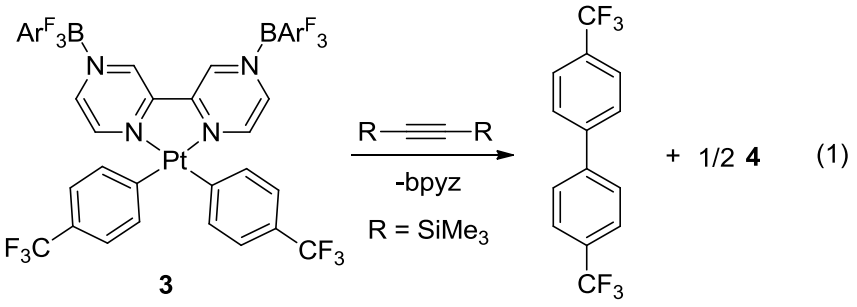

To investigate the mechanism of reductive elimination, the reaction order in each reagent was determined by monitoring ^{19}F NMR spectra. At 45 °C in *p*-xylene, reaction of **1** with two equivs of $B(C_6F_5)_3$ formed **3** as the exclusive platinum species. The disappearance of **3** and concomitant formation of 4,4'-bis(trifluoromethyl)-1,1'-biphenyl proceeded with clean first-order kinetics, and no intermediates were detected by ^{19}F NMR spectroscopy (see the Experimental Section).

The slope of the plot of ln(k_{obs}) versus ln[BTMSA] measured between 0.14 and 0.59 M BTMSA demonstrates that the reaction has a first-order dependence on the concentration of BTMSA (Figure 2).[19] Previously, diphosphine-nickel complexes have been observed to undergo sp^2–sp^3 reductive elimination via an associative mechanism in the presence of free phosphine.[20] In contrast, biphenyl reductive elimination from diphosphine-platinum complexes in the presence of diphenylacetylene was shown to proceed without prior alkyne association.[13]

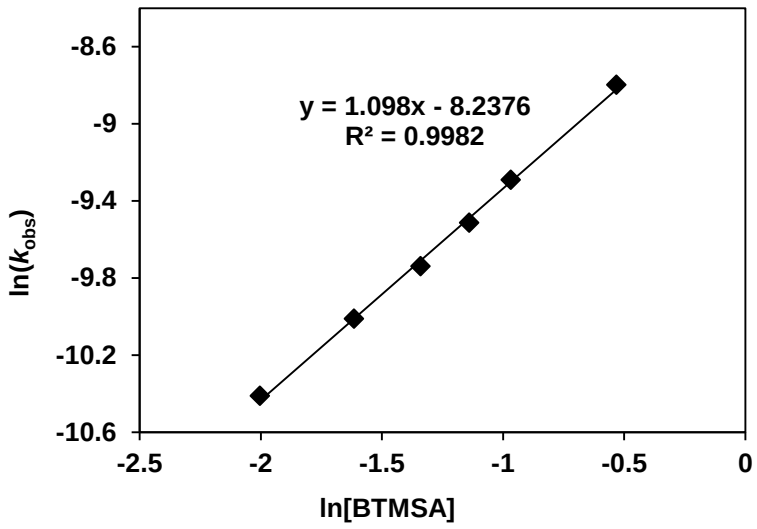

Figure 2. Plot of ln(k_{obs}) vs ln[BTMSA], indicating first-order behavior.

To probe the influence of the Lewis acid on reductive elimination**,** the concentration of $B(C_6F_5)_3$ was varied. In the presence of two equivs of $B(C_6F_5)_3$, a rate constant of k_{obs} = 1.74 ± 0.04 × 10^{-4} M·s^{-1} was determined. Doubling the concentration of $B(C_6F_5)_3$ had, within error, no effect on the observed rate constant (k_{obs} = 1.78 × 10^{-4} M·s^{-1}), suggesting that reductive elimination occurs with both equivs of $B(C_6F_5)_3$ still bound to the bpyz ligand. A decrease in rate with added $B(C_6F_5)_3$ present would be expected if borane dissociation occurred prior to C–C bond formation.

To verify that borane binding does not induce bpyz ligand dissociation prior to reductive elimination, experiments were performed in the presence of excess free bpyz. Identical reaction rates were observed in the presence or absence of two equivs of free bpyz relative to platinum (k_{obs} = 1.78 × 10^{-4} M·s^{-1}), suggesting that bpyz dissociation does not occur before the rate-determining step.

The mechanism presented in Scheme 3 is consistent with the observed kinetic data. Coordination of alkyne to **3** generates a five-coordinate platinum complex. Next, biaryl coupling expels a bpyzPt–(η^2-alkyne) adduct, from which displacement of bpyz by another equivalent of alkyne leads ultimately to **4**.

Scheme 3. Proposed mechanism of reductive elimination.

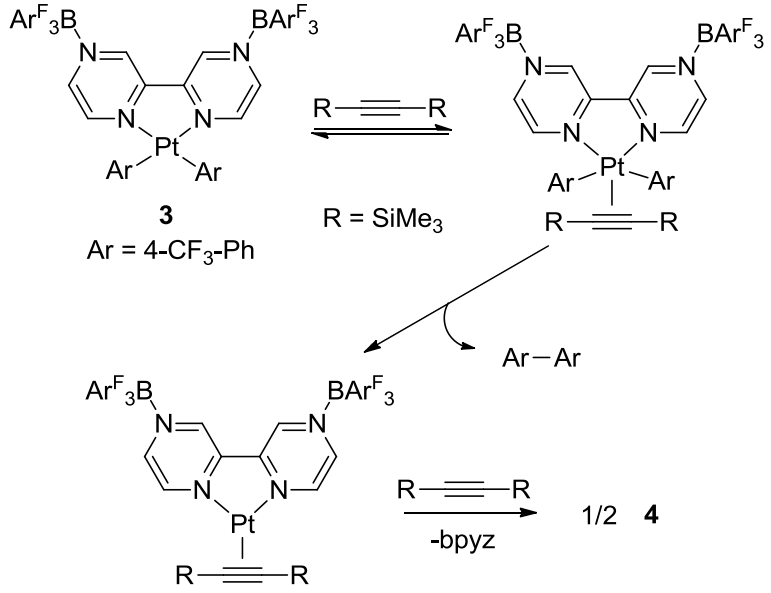

To determine the rate acceleration due to borane coordination, control experiments were performed in the absence of borane (eq 2). Biaryl reductive elimination was substantially slower under these conditions, requiring heating above 100 ^{o}C to observe any biaryl formation. In the absence of borane, the reaction of **1** exhibited first order dependence on [BTMSA] (see the Experimental Section), suggesting that the reductive elimination still proceeds *via* an associative mechanism.

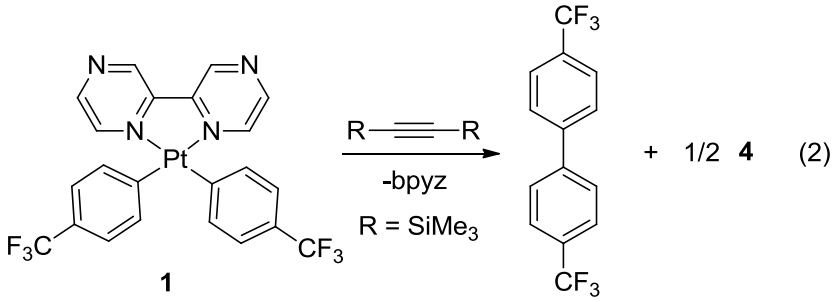

An Eyring plot was constructed for the background reaction of **1** with excess BTMSA from 110–150 ^{o}C without borane present (Figure 3). From the temperature dependence of the observed rate constant in the absence of borane, activation parameters of $\Delta H^{\ddagger}$ = 29.0 ± 1.3 kcal/mol and $\Delta S^{\ddagger}$ = -6.60 ± 3.2 e.u. were calculated. The small, negative value for $\Delta S^{\ddagger}$ is consistent with contributions from both the alkyne coordination and reductive elimination steps.

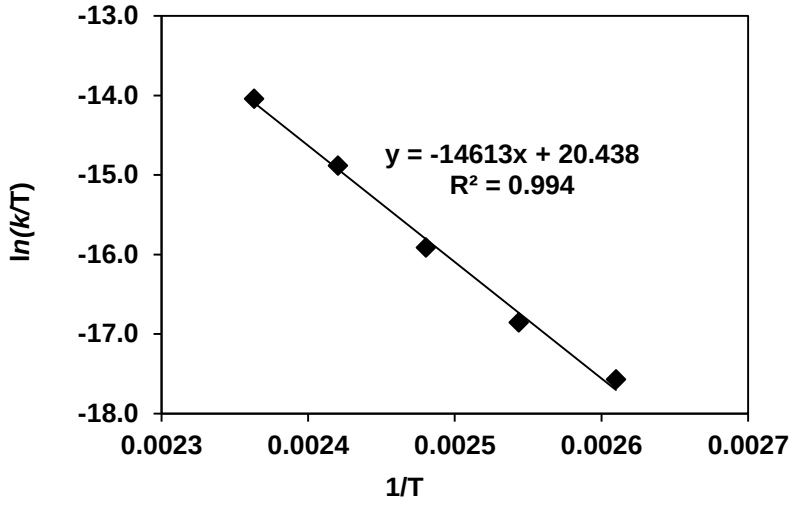

Figure 3. Eyring plot for the reaction of **1** with BTMSA.

Extrapolating to 45 °C, the temperature at which the kinetic experiments with **3** were performed, a rate constant of k_{obs} = 2.70 × 10^{-9} M·s^{-1} for the background reaction of **1** with BTMSA was estimated. Comparing the rates for the reaction of **3** or **1** with BTMSA gives a rate acceleration of ~64,000 for reductive elimination due to borane binding.

CONCLUSION

In conclusion, binding of Lewis acidic $B(C_6F_5)_3$ at remote nitrogen sites of a bipyrazine-diarylplatinum complex was observed. Reactions in the presence of BTMSA demonstrated facile biaryl reductive elimination, occurring in 95 % yield at 45 °C. To our knowledge, this is the fastest reported biaryl reductive elimination from a platinum center, and it represents the first example using a diimine ancillary ligand system. Kinetic analysis supports a mechanism involving association of an alkyne to a bis-borane adduct, and allowed calculation of a 64,000-fold rate acceleration due to borane binding. Future efforts will explore the generality of this Lewis acid binding strategy as a means for studying the role of electrophilicity in other metal-mediated reactions.[21]

EXPERIMENTAL SECTION

General. Unless otherwise noted, all experiments were conducted with dry, oxygen-free solvents using standard Schlenk techniques or in a N_2 atmosphere glovebox. Deuterated solvents were purchased from Cambridge Isotope Laboratory. Benzene-d_6, *p*-xylene-d_{10}, and mesitylene-d_{12} were dried by vacuum distillation from sodium metal. Tris(pentafluorophenyl)borane was purchased from Strem Chemicals and was recrystallized from pentane at -35 °C prior to use. Bipyrazine (bpyz) and *cis*/*trans*-$PtCl_2(SEt_2)_2$ were synthesized according to literature procedures.[22,23] Synthesis of $Pt(SEt_2)_2(4\text{-}CF_3\text{-}Ph)_2$ was performed analogous to the method of Puddephatt and coworkers.[24]

Analytical methods. Solution NMR spectroscopy was performed using Bruker AV-300, AVB-400, AVQ-400, AV-500, or AV-600 MHz spectrometers. ^{1}H NMR spectra were calibrated internally to either the resonance for the solvent or residual protio solvent relative to tetramethylsilane. ^{19}F chemical shifts were referenced to 1,3,5-tris(trifluoromethyl)benzene. ^{195}Pt chemical shifts were referenced to K_2PtCl_4 in D_2O. Elemental analyses were carried out by the College of Chemistry Microanalytical Laboratory at the University of California, Berkeley.

Synthesis of (bpyz)Pt(4-CF$_3$-Ph)$_2$. A suspension of $Pt(SEt_2)_2(4\text{-}CF_3\text{-}Ph)_2$ (0.625 g, 0.543 mmol) and 2,2'-bipyrazine (0.158 g, 0.998 mmol) was prepared in 15 mL of diethyl ether under air. The solution appeared red within minutes at 25 ^{o}C. After 15 hours, solvent was removed under vacuum. Product, (bpyz)Pt(4-CF$_3$-Ph)$_2$ (**1**), was obtained in 83 % yield after recrystallization by vapor diffusion of hexane into dichloroethane at 25 ^{o}C. NMR in $CDCl_3$: δ(^{1}H): 9.57 ppm (d, J = 1.8 Hz, 2H), 8.89 (d, J = 4.2 Hz, 2H), 8.52 (dd with Pt satellites, J_{HH} = 3.0, 1.2 Hz, J_{PtH} = 30 Hz, 2H), 7.52 (dd with Pt satellites, J_{HH} = 8.2 Hz, J_{PtH} = 108 Hz, 4H), 7.31 (d, J = 8.2 Hz, 4H). δ(^{13}C): 149.61, 148.51, 147.78, 143.30, 141.46, 137.75, 126.41, 124.61, 123.51 (q, J_{CF} = 3.8 Hz). δ(^{19}F): -61.07. δ(^{195}Pt): -3197. Anal. Calc'd (%) C 41.07, H 2.19, N 8.71; Found C 40.73, H 2.21, N 8.60.

Solution characterization of (bpyz-B(C$_6$F$_5$)$_3$)Pt(4-CF$_3$-Ph)$_2$. Solutions of (bpyz)Pt(4-CF$_3$-Ph)$_2$ (4.2 mg, 0.0065 mmol) in 0.250 mL of benzene-d_6 and tris(pentafluorophenyl)borane (3.3 mg, 0.0065 mmol) in 0.250 mL of benzene-d_6 were combined in a J. Young NMR tube. An immediate color change from red to green was observed. NMR spectra indicated a mixture of (bpyz)Pt(4-CF$_3$-Ph)$_2$, (bpyz-B(C$_6$F$_5$)$_3$)Pt(4-CF$_3$-Ph)$_2$ (**2**), and (bpyz-2B(C$_6$F$_5$)$_3$)Pt(4-CF$_3$-Ph)$_2$ (**3**). δ(^{1}H of (bpyz-B(C$_6$F$_5$)$_3$)Pt(4-CF$_3$-Ph)$_2$): 8.65 (br), 8.30 (br), 7.89 (br), 7.46 (br), 7.37 (br). δ(^{19}F): -60.88 (br), -60.97 (br), -130.04, -151.29, -159.74. δ(^{195}Pt): -2654.

Synthesis of (bpyz-2B(C$_6$F$_5$)$_3$)Pt(4-CF$_3$-Ph)$_2$. Solutions of (bpyz)Pt(4-CF$_3$-Ph)$_2$ (4.2 mg, 0.0065 mmol) in 0.250 mL of benzene-d_6 and tris(pentafluorophenyl)borane (6.6 mg, 0.013 mmol) in 0.250 mL of benzene-d_6 were combined in a J. Young NMR tube. An immediate color change from red to black was observed. The bis(borane) adduct (bpyz-2B(C$_6$F$_5$)$_3$)Pt(4-CF$_3$-Ph)$_2$ (**3**) was isolated by removal of solvent under vacuum, followed by washes with pentane (2 x 3 mL). NMR in C_6D_6: δ(^{1}H): 8.68 (s, 2H), 8.64 (d, J_{HH} = 6 Hz, 2H), 7.64 (s, 2H), 7.48 (d, J_{HH} = 12 Hz, 4H), 7.39 (d, J_{HH} = 6 Hz, 2H), 7.26 (d with Pt satellites, J_{HH} = 12 Hz, J_{PtH} = 84Hz, 4H). δ(^{13}C): 149.93, 147.49, 147.48 (d, J_{CF} = 243 Hz), 146.87, 143.72, 141.35 (d, J_{CF} = 258 Hz), 138.41, 137. 65 (d, J_{CF} = 246 Hz) 136.90, 125.58, 124.26, 123.78, 114.24. δ(^{19}F): -61.12, -130.25, -151.84, -160.23. δ(^{195}Pt): -2070. Anal. Calc'd for **3**·C_6H_6 (%) C 44.04, H 1.15, N 3.21; Found C 44.11, H 1.11, N 3.28.

Reaction of 3 with DMAP. A solution of **3** was prepared by combining **1** (7.2 mg, 0.011 mmol) and B(C$_6$F$_5$)$_3$ (11.3 mg, 0.022 mmol) in 0.500 mL of *p*-xylene-d_{10} in a J. Young NMR tube, resulting in a black solution. Complete conversion to **3** was assessed by ^{1}H and ^{19}F NMR spectroscopy. DMAP (2.7 mg, 0.022 mmol) was added, resulting in an immediate color change to red. NMR spectra (^{1}H and ^{19}F) indicated complete conversion to **1** and two equivalents of B(C$_6$F$_5$)$_3$–DMAP. δ(^{1}H of (B(C$_6$F$_5$)$_3$–DMAP): 7.63 (br d, J_{HH} = 6.4 Hz, 2H), 5.39 (d, J_{HH} = 7.6 Hz, 2H), 1.89 (s, 6H). δ(^{19}F): -130.78, -156.78, -162.89.

Reaction of 3 with bis(trimethylsilyl)acetylene. Complex **1** (4.2 mg, 0.0065 mmol) and B(C$_6$F$_5$)$_3$ (6.6 mg, 0.013 mmol) were dissolved in 0.500 mL of *p*-xylene-d_{10} in a J. Young NMR tube. Bis(trimethylsilyl)acetylene (15.0 μL, 0.0695 mmol) was added via syringe. The NMR tube was heated to 45 ^{o}C for 16 hours. NMR spectra indicated complete disappearance of **3**, along

with formation of bipyrazine, bis(4-CF_3-phenyl)acetylene, and [Pt_2(μ-$Me_3SiCCSiMe_3$)(Me_3-$SiCCSiMe_3$)$_2$].[17]

Reaction of 3 with diphenylacetylene. Complex **1** (4.2 mg, 0.0065 mmol), diphenylacetylene (12.4 mg, 0.0695 mmol), and $B(C_6F_5)_3$ (6.6 mg, 0.013 mmol) were dissolved in 0.500 mL of *p*-xylene-d_{10} in a J. Young NMR tube. The NMR tube was heated to 45 ^oC for 16 hours. NMR spectra indicated complete disappearance of **3**, along with formation of bipyrazine, bis(4-CF_3-phenyl)acetylene, and $Pt(PhCCPh)_2$.[16]

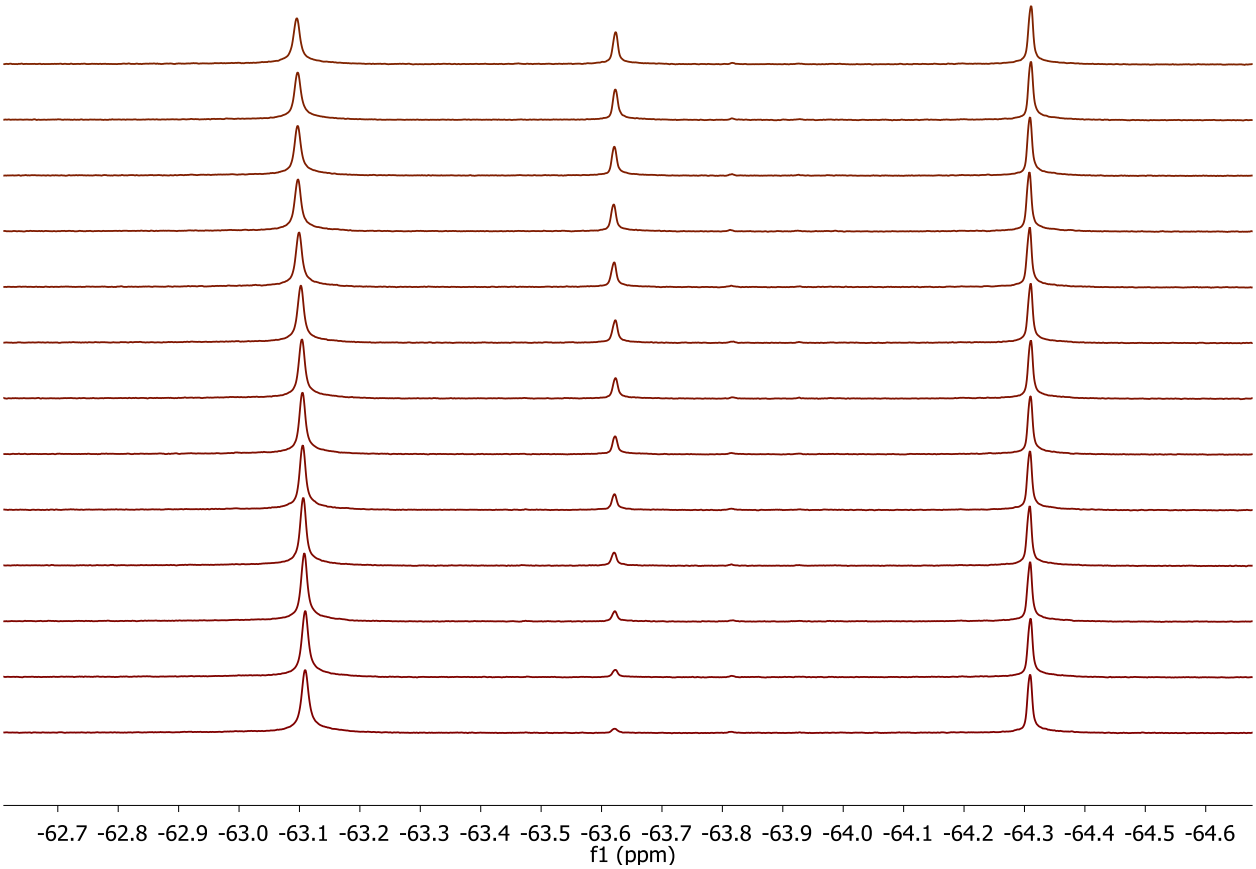

Figure 4. Stacked ^{19}F NMR spectra of reductive elimination from **3** (0.011 M) in the presence of BTMSA (0.61 M) at 45 ^oC in *p*-xylene-d_{10}. Peak assignments: **3** (-63.1 ppm), bis(4-CF_3-phenyl)acetylene (-63.6 ppm), 1,3,5-tris(trifluoromethyl)benzene internal standard (-64.3 ppm).

Reaction order in platinum with 3 and BTMSA. Complex **1** (4.2 mg to 12.6 mg, 0.0065 to 0.020 mmol) and $B(C_6F_5)_3$ (6.6 mg to 19.8 mg, 0.013 to 0.040 mmol) were dissolved in 0.500 mL of *p*-xylene-d_{10} in a J. Young NMR tube. An internal standard, 1,3,5-tris(trifluoromethyl)benzene (0.25 μL), and bis(trimethylsilyl)acetylene (75.0 μL, 0.348 mmol) were added via syringe. The NMR tube was stored at 0 ^oC prior to use. The tube was placed in an NMR spectrometer with the temperature pre-equilibrated to 45 ^oC, and the temperature was allowed to equilibrate for two minutes. The rate of reductive elimination was monitored by ^{19}F NMR spectroscopy to between 2-3 half lives.

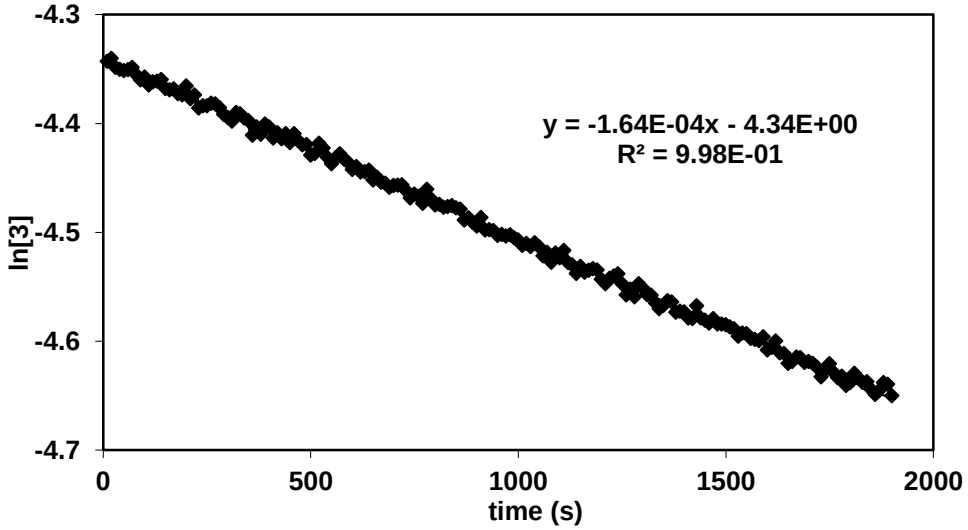

Figure 5. Representative rate data for reductive elimination from **3** (0.011 M) in the presence of BTMSA (0.61 M) at 45 ^{o}C in *p*-xylene-d_{10}.

Table 1. Rate as a function of [**3**] at 45 ^{o}C.

[**3**] (M)	k_{obs} (M/s)
0.011	1.64×10^{-4}
0.023	1.63×10^{-4}
0.028	1.66×10^{-4}
0.035	1.65×10^{-4}

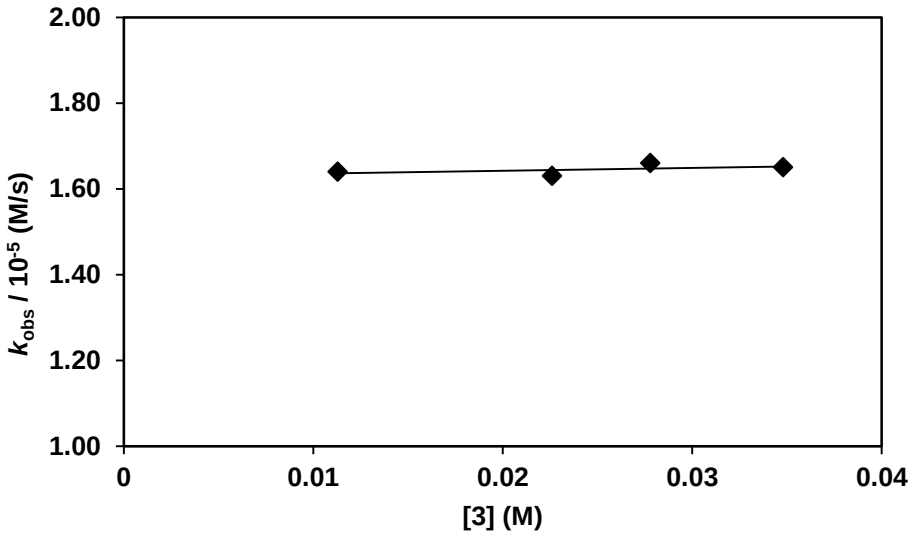

Figure 6. Plot of rate as a function of [**3**] at 45 °C.

Reaction order in BTMSA with 3 at 45 °C. Complex **1** (4.2 mg, 0.0065 mmol) and $B(C_6F_5)_3$ (6.6 mg, 0.013 mmol) were dissolved in 0.500 mL of *p*-xylene-d_{10} in a J. Young NMR tube. An internal standard, 1,3,5-tris(trifluoromethyl)benzene (0.25 μL), and bis(trimethylsilyl)acetylene (15.0 to 75.0 μL, 0.0695 to 0.348 mmol) were added via syringe. Additional *p*-xylene-d_{10} was added as necessary to achieve a total volume of 0.575 mL. The NMR tube was stored at 0 °C prior to use. The tube was placed in an NMR spectrometer with the temperature pre-equilibrated to 45 °C, and the temperature was allowed to equilibrate for two minutes. The rate of reductive elimination was monitored to between 2-3 half lives by ^{19}F NMR spectroscopy.

Table 2. Rate as a function of [BTMSA] at 45 °C.

[BTMSA] (M)	k_{obs} (M/s)
0.135	3.01×10^{-5}
0.199	4.49×10^{-5}
0.262	5.89×10^{-5}
0.320	7.38×10^{-5}
0.380	9.23×10^{-5}
0.588	1.51×10^{-4}

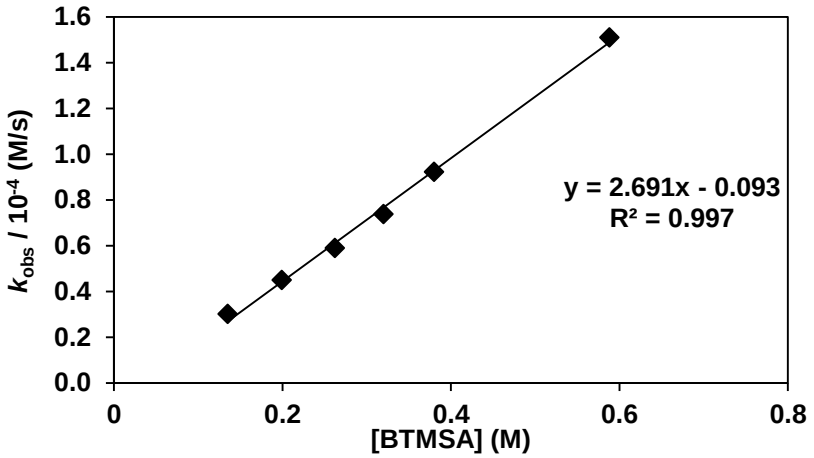

Figure 7. Plot of k_{obs} for elimination from **3** as a function of [BTMSA] at 45 °C.

Reaction order in $B(C_6F_5)_3$ with 3 and BTMSA at 45 °C. Complex **1** (4.2 mg, 0.0065 mmol) and $B(C_6F_5)_3$ (8.3 mg, 0.016 mmol) were dissolved in 0.500 mL of *p*-xylene-d_{10} in a J. Young NMR tube. An internal standard, 1,3,5-tris(trifluoromethyl)benzene (0.25 μL), and bis(trimethylsilyl)acetylene (75.0 μL, 0.348 mmol) were added via syringe. The NMR tube was stored at 0 °C prior to use. The tube was placed in an NMR spectrometer with the temperature pre-equilibrated to 45 °C, and the sample temperature was allowed to equilibrate for two minutes. The rate of reductive elimination was monitored to three half-lives by ^{19}F NMR spectroscopy. Reactions performed in triplicate provided a rate constant of $k_{obs} = 1.74 \pm 0.04 \times 10^{-4}$ M/s for reductive elimination.

For comparison, complex **1** (4.2 mg, 0.0065 mmol) and $B(C_6F_5)_3$ (16.5 mg, 0.0325 mmol) were combined in 0.500 mL of *p*-xylene-d_{10} in a J. Young NMR tube. An internal standard, 1,3,5-tris(trifluoromethyl)benzene (0.25 μL), and bis(trimethylsilyl)acetylene (75.0 μL, 0.348 mmol) were added via syringe. From monitoring the rate of reductive elimination at 45 °C by ^{19}F NMR spectroscopy, a rate constant of $k_{obs} = 1.78 \times 10^{-4}$ M/s was determined.

Reaction of 3 and BTMSA in the presence of excess bpyz at 45 °C. Complex **1** (4.2 mg, 0.0065 mmol), $B(C_6F_5)_3$ (23.1 mg, 0.0451 mmol), and bipyrazine (2.0 mg, 0.013 mmol) were combined in 0.500 mL of *p*-xylene-d_{10} in a J. Young NMR tube. An internal standard, 1,3,5-tris(trifluoromethyl)benzene (0.25 μL), and bis(trimethylsilyl)acetylene (75.0 μL, 0.348 mmol) were added via syringe. The NMR tube was placed in an NMR spectrometer with the temperature pre-equilibrated to 45 °C, and the sample temperature was allowed to equilibrate for two minutes. The rate of reductive elimination was monitored by ^{19}F NMR spectroscopy to determine a rate constant of $k_{obs} = 1.78 \times 10^{-4}$ M/s.

Reaction order in BTMSA with 1 at 130 °C. Complex **1** (4.2 mg, 0.0065 mmol) was dissolved in 0.250 mL of mesitylene-d_{12} in a J. Young NMR tube. An internal standard, 1,3,5-tris(trifluoromethyl)benzene (0.25 μL), and bis(trimethylsilyl)acetylene (50.0 to 120.0 μL, 0.232 to 0.557 mmol) were added via syringe. Additional mesitylene-d_{12} was added to achieve a total sample volume of 0.575 mL. The NMR tube was heated to 130 °C in an oil bath, and the rate of reductive elimination was monitored by ^{19}F NMR spectroscopy.

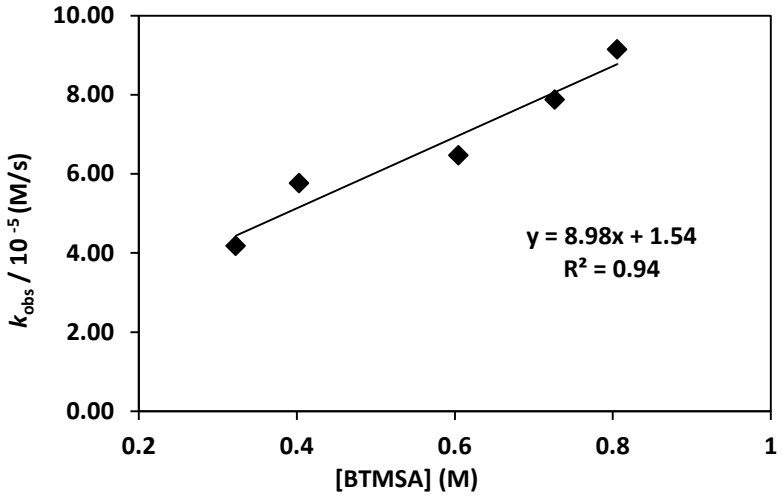

Figure 8. Plot of k_{obs} for elimination from **1** as a function of [BTMSA] at 130 ^{o}C.

Eyring analysis of 1 and BTMSA in the absence of $B(C_6F_5)_3$ between 110–150 ^{o}C. Five J. Young NMR tube samples were prepared, each containing complex **1** (4.2 mg, 0.0065 mmol) dissolved in 0.500 mL of mesitylene-d_{12}. An internal standard, 1,3,5-tris(trifluoromethyl)benzene (0.25 μL), and bis(trimethylsilyl)acetylene (75.0 μL, 0.348 mmol) were added via syringe to each sample. The NMR tubes were placed in an oil bath with the temperature pre-equilibrated to between 110–150 ^{o}C. The rate of biaryl formation was monitored by ^{19}F NMR spectroscopy.

Table 3. Temperature dependence of k_{obs} for biaryl reductive elimination from **1**.

Temp. (^{o}C)	1/T (K^{-1})	k_{obs} (M/s)	ln(k/T)
110	0.00261	8.97×10^{-6}	-17.57
120	0.00254	1.88×10^{-5}	-16.86
130	0.00248	4.95×10^{-5}	-15.91
140	0.00242	1.42×10^{-4}	-14.88
150	0.00236	3.37×10^{-4}	-14.04

The plot of ln(k/T) as a function of T^{-1} (Figure 3) was fit by a line according to the expression:

$$\ln\frac{k}{T} = -\frac{\Delta H^{\neq}}{R}\cdot\frac{1}{T} + \ln\frac{k_B}{h} + \frac{\Delta S^{\neq}}{R}$$

The enthalpy and entropy of activation were extracted from the slope and intercept, respectively. Standard deviations for $\Delta H^{‡}$ and $\Delta S^{‡}$ were evaluated using the LINEST routine in Excel.

REFERENCES

(1) Lehninger, A. L.; Nelson, D. L.; Cox, M. M. *Principles of Biochemistry*, 5th ed.; W. H. Freeman: New York, 2008.
(2) Gianneschi, N. C.; Masar III, M. S.; Mirkin, C. A. *Acc. Chem. Res.* **2005**, *38*, 825.
(3) Lee, B. Y.; Bazan, G. C.; Vela, J.; Komon, Z. J. A.; Bu, X. *J. Am. Chem. Soc.* **2001**, *123*, 5352.
(4) Kim, Y. H.; Kim, T. H.; Lee, B. Y.; Woodmansee, D.; Bu, X.; Bazan, G. C. *Organometallics*, **2002**, *21*, 3082.
(5) Azoulay, J. D.; Koretz, Z. A.; Wu, G.; Bazan, G. C. *Angew. Chem. Int. Ed.* **2010**, *49*, 7890.
(6) Gabano, E.; Marengo, E.; Bobba, M.; Robotti, E.; Cassino, C.; Botta, M.; Osella, D. *Coord. Chem. Rev.* **2006**, *250*, 2158.
(7) Beringhelli, T.; Donghi, D.; Maggioni, D.; D'Alfonso, G. *Coord. Chem. Rev.* **2008**, *252*, 2292.
(8) Martin, R.; Buchwald, S. L. *Acc. Chem. Res.* **2008**, *41*, 1461.
(9) Phapale, V. B.; Cardenas, D. J. *Chem. Soc. Rev.* **2009**, *38*, 1598.
(10) Brown, J. M.; Cooley, N. A. *Chem. Rev.* **1988**, *88*, 1031.
(11) Hartwig, J. F. *Inorg. Chem.* **2007**, *46*, 1936.
(12) Merwin, R. K.; Schnabel, R. C.; Koola, J. D.; Roddick, D. M. *Organometallics* **1992**, *11*, 2972.
(13) Korenaga, T.; Abe, K.; Ko, A.; Maenishi, R.; Sakai, T. *Organometallics* **2010**, *29*, 4025.
(14) Shekhar, S.; Hartwig, J. F. *J. Am. Chem. Soc.* **2004**, *126*, 13016.
(15) Skapski, A. C.; Sutcliffe, V. F.; Young, G. B. *J. Chem. Soc., Chem. Commun.* **1985**, 609.
(16) Boag, N. M.; Green, M.; Grove, D. M.; Howard, J. A. K.; Spencer, J. L.; Stone, F. G. A. *J. C. S., Dalton* **1980**, 2170.
(17) Boag, N. M.; Green, M.; Howard, J. A. K.; Stone, F. G. A.; Wadepohl, H. *J. C. S., Dalton* **1981**, 862.
(18) No reaction was observed between **3** and cyclohexene or norbornene up to 100 ^{o}C. The reaction of **3** with triphenylphosphine showed displacement of the bpyz ligand by two equivs of phosphine.
(19) In the absence of alkyne, reductive elimination from **1** is sluggish, requiring heating to 170 ^{o}C for 40 hours to produce 4,4'-bis(trifluoromethyl)-1,1'-biphenyl in 80 % yield. Attempts to study reductive elimination from **3** were complicated due to the necessity of high reaction temperatures (> 80^{o}C) to observe reductive elimination, and under these conditions, borane dissociation was observed. Heating **3** in the presence of excess $B(C_6F_5)_3$ (5 or 10 equiv) lead to decomposition, with minimal biaryl formation (18 %).
(20) Komiya, S.; Abe, Y.; Yamamoto, A.; Yamamoto, T. *Organometallics* **1983**, *2*, 1466.
(21) The work in this chapter was adapted with permission from Liberman-Martin, A. L.; Bergman, R. G.; Tilley, T. D. *J. Am. Chem. Soc.* **2013**, *135*, 9612.
(22) Boully, L.; Darabantu, M.; Turck, A.; Ple, N. *J. Heterocyclic Chem.* **2005**, *42*, 1423.
(23) De Crisci, A. G.; Lough, A. J.; Multani, K.; Fekl, U. *Organometallics* **2008**, *27*, 1765.
(24) Rashidi, M.; Fakhroeian, Z.; Puddephatt, R. J. *J. Organomet. Chem.* **1991**, *406*, 261.

Chapter 2. Biaryl Reductive Elimination is Dramatically Accelerated by a Remote Lewis Acid Chemical Switch: Evidence for an Unusual Bidentate Ligand Dissociation Mechanism

INTRODUCTION

Lewis acid activators can be used in combination with transition metal complexes to generate highly reactive intermediates. For example, boron and aluminum compounds are used to irreversibly abstract hydride and alkyl ligands from a wide range of transition metals.[1] In particular, $B(C_6F_5)_3$ is well known as an activator for metallocene alkene polymerization catalysts.[2] Recent research has extended the utility of Lewis acids as activators for chemical switches that operate by reversible abstraction of ligands. For example, alkali metal salts have been used to alter metal–oxygen interactions in iridium and rhodium complexes with ligands bearing aza-crown ether substituents.[3] In these cases, the Lewis acid activator operates by modifying the coordination environment of the metal center.

In contrast to the traditional Lewis acid-promoted ligand abstractions, the binding of additives can also occur on the periphery of appropriately designed ligands, allowing for electronic tuning without steric modification. The ligands in these systems feature pendant nitrogen- or oxygen-based functional groups that are in electronic communication with the primary metal center. There are relatively few systems that utilize these remote chemical switches, which operate by coordination of protons or neutral Lewis acids.[4,5] Despite continued interest in creating electronic switches that are reversible, modular, and tunable, the effect of Lewis acid binding on a ligand's donor properties or a metal center's electronic environment remains poorly understood.

Herein, we report a 2,2′-bipyrimidyl–platinum (bpym–Pt) complex and employ it as a platform to investigate chemical switching by remote Lewis acid coordination. Silicon- and zinc-based Lewis acids have a strong affinity for coordination to the bidentate binding site of the bpym–Pt complex. A combination of methods, including ^{1}H, ^{13}C, ^{195}Pt NMR and UV-vis spectroscopies, and cyclic voltammetry, were used to probe ligand-based electronic perturbations that occur upon Lewis acid binding. Biaryl reductive elimination reactions provide a benchmark for evaluation of reactivity, and tunable rate enhancements ranging from 10^3 to 10^8 were observed in the presence of Lewis acids. Mechanistic studies revealed an unexpected mechanism involving complete dissociation of the bidentate bipyrimidine ligand prior to C–C bond formation, demonstrating the ability of remote Lewis acid switches to profoundly alter ligand donor properties and reaction mechanisms.

RESULTS AND DISCUSSION

Synthesis of bpymPtAr$_2$ and Lewis acid adducts

Bis(4-trifluoromethylphenyl)platinum-2,2′-bipyrimidine (bpymPtAr$_2$, **1**) was prepared by treatment of (4-CF_3-Ph)Pt(SEt_2)$_2$ with 2 equiv of bpym in dichloromethane. Following purification by column chromatography on silica, yellow crystals of **1** were obtained by layering a toluene solution with pentane at –30 ^{o}C.

An initial attempt to bind tris(pentafluorophenyl)borane to the remote nitrogen site of **1** was unsuccessful, as no interaction was observed by ^{1}H or ^{19}F NMR spectroscopy. This is likely due to steric constraints enforced by the 2,2′-bipyrimidyl nitrogen placement. Instead, silicon and zinc compounds were sought as alternative Lewis acids that could simultaneously coordinate to both distal nitrogen sites of **1**.

Treatment of **1** with bis(catecholato)silane, $Si(cat)_2$,[6] in toluene caused rapid formation of a red silicon–bpym–platinum complex (**2**, eq 1). We have previously reported that the bis(tetrafluorocatecholato)silane $Si(cat^F)_2$ is more Lewis acidic than the parent $Si(cat)_2$ complex.[7] For comparison with **2**, the dark brown $Si(cat^F)_2$ adduct **3** was prepared by treatment of **1** with $Si(cat^F)_2(MeCN)_2$. Lastly, treatment of **1** with bis(pentafluorophenyl)zinc(η^2-toluene)[8] allowed isolation of a platinum–zinc heterobimetallic complex **4** containing a bridging bpym ligand. Red single crystals of **2** and **4** were obtained by vapor diffusion of pentane into toluene solutions at -30 °C.

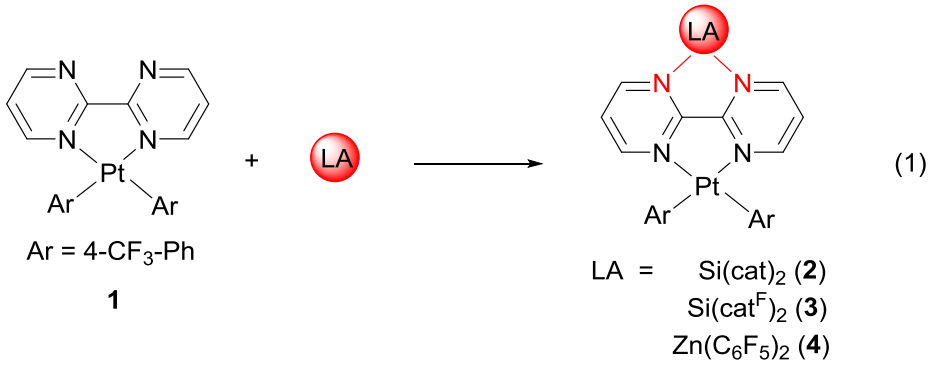

(1)

X-ray diffraction studies of **1**, **2**, and **4** provided solid state structural comparisons (Figure 1). All complexes feature the expected square planar geometry at platinum. Complex **2** contains a hexacoordinate silicon center with approximately octahedral geometry. The zinc center of **4** is tetrahedral, as has been previously observed for pyridine adducts of diaryl zinc species.[9] There are negligible differences in the bond lengths of the bpym rings, platinum–bpym bonds, and platinum–aryl bonds of **1**, **2**, and **4**.

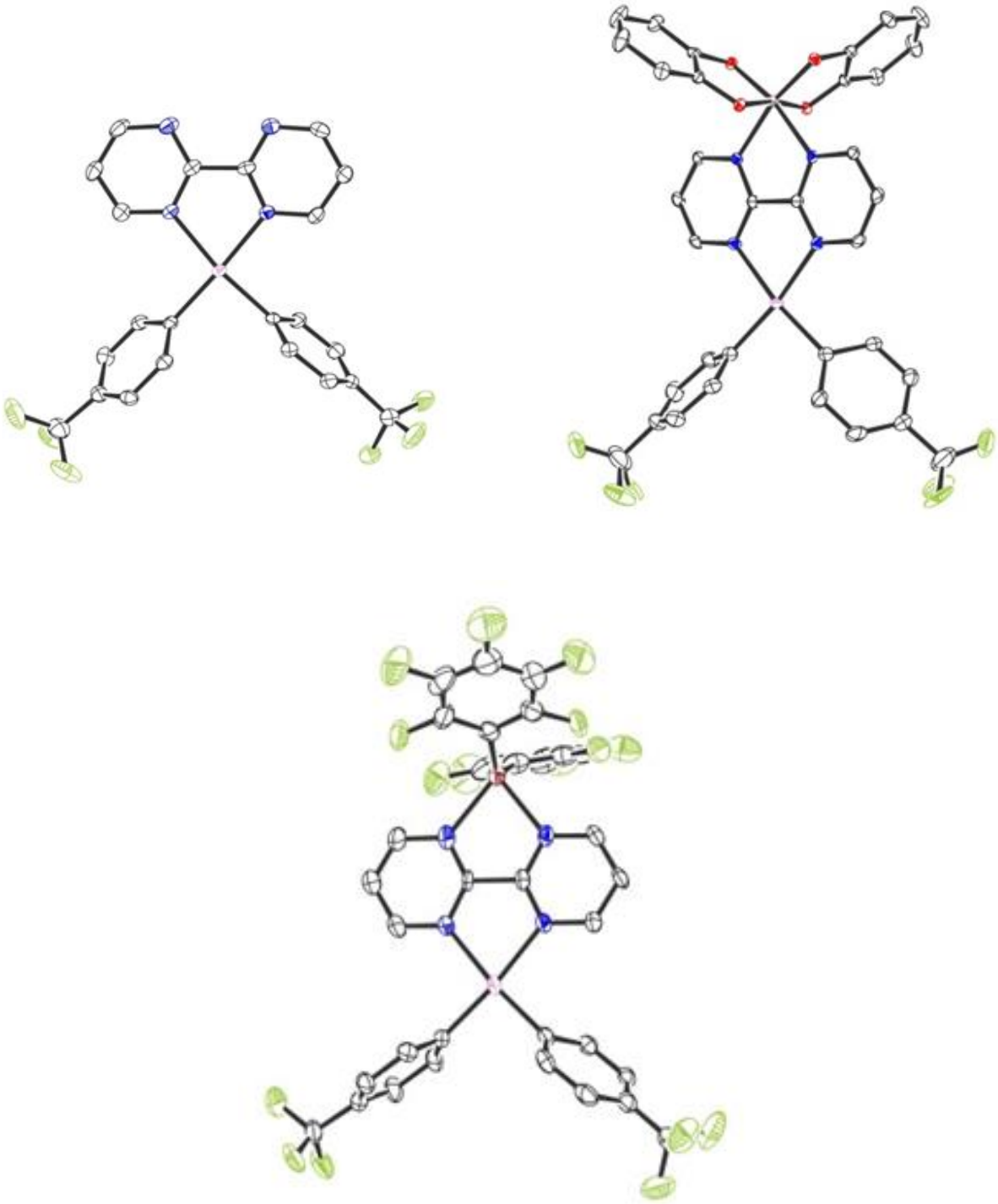

Figure 1. ORTEP diagrams of complexes **1** (top left), **2** (top right) and **4** (bottom), with thermal ellipsoids shown at 50% probability.

NMR spectroscopy

The bpym ^{1}H NMR chemical shifts of **1**–**4** were compared to assess trends that result from Lewis acid binding. Signals due to the bpym protons *ortho* to platinum for adducts **2**–**4** are upfield-shifted by 0.10 – 0.37 ppm relative to those for **1** (see SI). Resonances due to the protons *ortho* to the remote nitrogen site of **2**–**4** appear downfield by 0.24 – 0.28 ppm compared to the corresponding signals in the parent complex. There is no trend in the ^{1}H NMR chemical shift of the bpym *meta* position. The ^{195}Pt NMR signals for **1**–**4** occur in a small region of the ~6,000 ppm range typically observed for organo-platinum(II) complexes (see SI).[10] There is similarly no trend in the ^{13}C NMR chemical shifts of the bpym ligand. Taken together, these observations suggest that NMR chemical shifts are poorly correlated with the electronic properties of the complexes in this series. To provide additional information about electronic changes upon Lewis acid binding, UV-vis spectroscopy and cyclic voltammetry were employed as complementary diagnostic techniques.

UV-vis Spectroscopy

UV-vis spectra of **1**–**4** are presented in Figure 2. An intense bipyrimidyl ligand π–π* transition is observed in the near UV region for all complexes (not shown, λ_{max} ~ 300 nm). There are two diagnostic absorptions that have been assigned as MLCT transitions for similar platinum–bpym complexes.[11] The higher of the two in energy is not observed for the parent complex **1** (likely due to overlap with the intense π–π* transition), but occurs between 400–425 nm for adducts **2**–**4**. A lower energy absorption is observed at 450 nm for **1**, and is shifted to 525–600 nm for the Lewis acid adducts. For both MLCT transitions, the shift in the absorption maxima to longer wavelengths is consistent with a significant lowering of the bpym π* orbital levels upon Lewis acid binding.

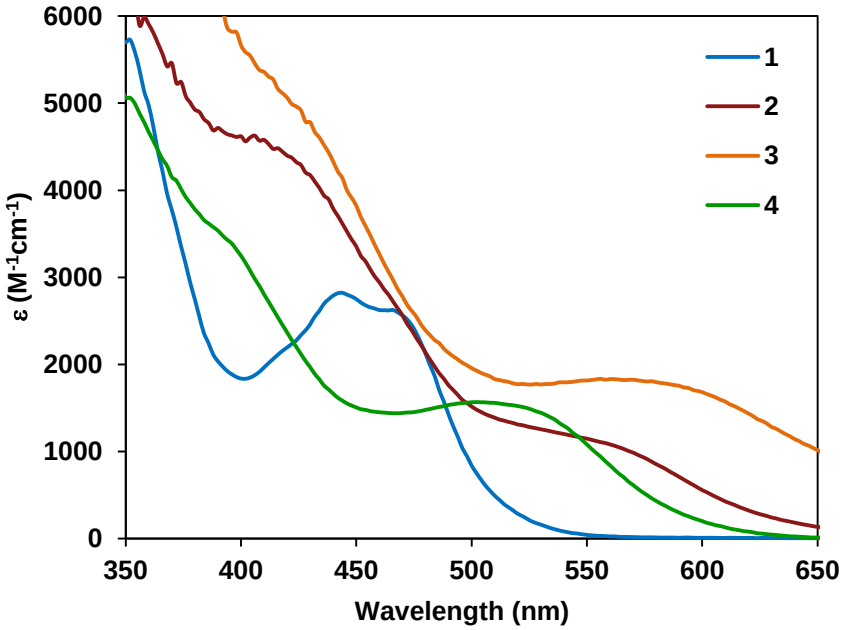

Figure 2. Absorption spectra of compounds **1** – **4**.

Electrochemical Experiments

Cyclic voltammetry was performed on complexes **1**–**4**. Silicon adducts **2** and **3** showed complicated, irreversible behavior upon reduction, likely due to the redox activity of the silicon-bound catecholate ligands.[12] In contrast, for the parent complex and $ZnAr^{F}_{2}$ adduct, **1** and **4**, two reversible bpym-based redox processes and one irreversible platinum-based oxidation event were observed (Figure 3). The first bpym reduction event ($bpym^{0}/bpym^{1-}$) for **4** is 600 mV less negative than that observed for complex **1**. Similarly, a shift of 400 mV was observed for the second bpym reduction event ($bpym^{1-}/bpym^{2-}$). In addition, the platinum-based oxidation requires a +100 mV greater potential upon remote zinc binding. These electrochemical data indicate that the electron density of the bpym ligand is substantially depleted upon zinc coordination, but the electronic perturbation at the platinum center is modest.

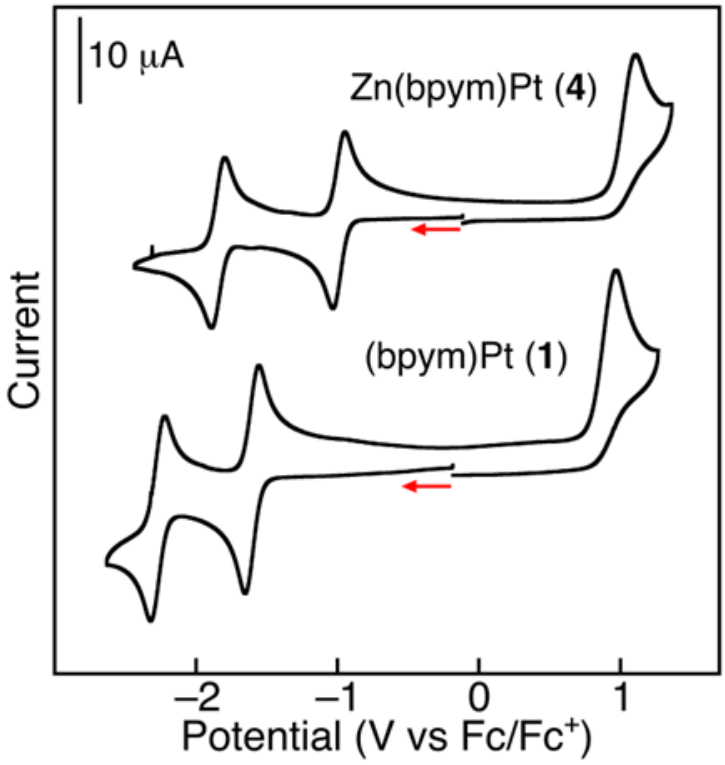

Figure 3. Cyclic voltammograms of **1** and **4** in *o*-difluorobenzene (1.0 mM with 0.1 M $[^{n}Bu_4N][B(C_6F_5)_4]$).

Lewis Acid Binding Constants

Variable temperature ^{1}H NMR experiments were performed to determine the relative strength of Lewis acid interactions in complexes **2**–**4** (eq 2). For complex **2**, partial, reversible dissociation of $Si(cat)_2$ occurs upon mild heating (40 ^{o}C), leading to a shift in the observed bipyrimidyl resonances due to averaging on the NMR timescale. Equilibrium constants were calculated based on the observed ^{1}H NMR chemical shift of the bpym resonances as a function of temperature. From Van't Hoff analysis of the equilibrium constants between 30 and 80 ^{o}C, the enthalpy and entropy for binding of $Si(cat)_2$ to **1** were measured as $\Delta H = -18.2 \pm 1.5$ kcal/mol and $\Delta S = -47 \pm 4.7$ cal/mol ($\Delta G = -4.2$ kcal/mol, $K_{eq} = \sim 1200\ M^{-1}$ at 25 ^{o}C).

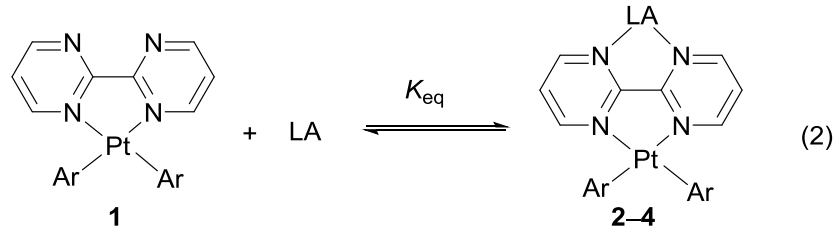

(2)

For $Si(cat)_2$, $\Delta G_{298} = -4.2$ kcal/mol
For $Si(cat^F)_2$, $\Delta G_{298} = -5.9$ kcal/mol
For $Zn(C_6F_5)_2$, $\Delta G_{298} \leq -8.6$ kcal/mol

In contrast to the behavior of $Si(cat)_2$, dissociation of $Si(cat^F)_2$ and $Zn(C_6F_5)_2$ from **3** and **4**, respectively, could not be observed at temperatures as high as 120 °C. Instead, competition experiments were performed to determine relative binding strengths. Mixing **3** with a 10-fold excess of $Si(cat)_2$ yielded a 1:1 mixture of **2** and **3**, allowing the free energy of $Si(cat^F)_2$ binding to **1** to be calculated as $\Delta G = -5.9$ kcal/mol at 25 °C. Treatment of **3** with $Zn(C_6F_5)_2$ led to the quantitative formation of **4** and free $Si(cat^F)_2$, suggesting that $\Delta G \leq -8.6$ kcal/mol for $Zn(C_5F_5)_2$ binding to **1** at 25 °C. Therefore, the relative strength of Lewis acid interactions with **1** increases in the order $Si(cat)_2 < Si(cat^F)_2 < Zn(C_6F_5)_2$.

Competition experiments were performed to establish the relative strength of Lewis acid interactions with bpym versus **1** (eq 3). For all Lewis acids, there is a preference for binding to free bpym rather than the platinum-bound bpym. Treatment of $Si(cat)_2$ with bpym and excess **1** led to a mixture of **1**, **2**, bpym, and bpym–$Si(cat)_2$ at 25 °C ($\Delta G = -3.4$ kcal/mol, see the Experimental Section for details). In contrast, only **1** and bpym–$Si(cat^F)_2$ or bpym–$Zn(C_6F_5)_2$ could be observed in the analogous experiments with these Lewis acids. Based on the concentrations employed, and assuming 99% conversion to products based on the ^{1}H NMR detection limits, for both $Si(cat^F)_2$ and $Zn(C_6F_5)_2$, $\Delta G \leq -5.4$ kcal/mol at 25 °C.

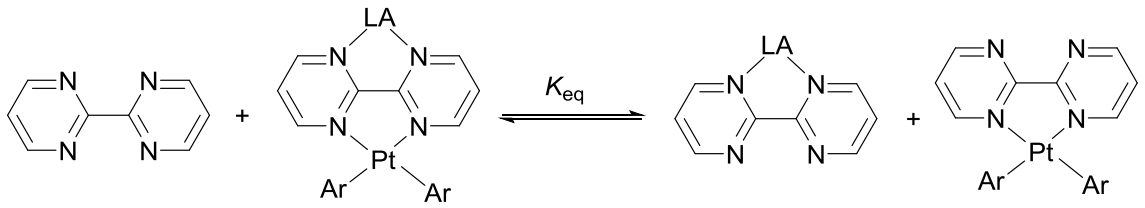

(3)

For $Si(cat)_2$, $\Delta G_{298} = -3.4$ kcal/mol
For $Si(cat^F)_2$, $\Delta G_{298} \leq -5.4$ kcal/mol
For $Zn(C_6F_5)_2$, $\Delta G_{298} \leq -5.4$ kcal/mol

Biaryl Reductive Elimination

Biaryl formation from complexes **1**–**4** was investigated, as this reaction represents a crucial step in carbon–carbon coupling reactions that often utilize Group 10 catalysts.[13] We and others have shown that electron-deficient platinum complexes undergo facile reductive

elimination compared to more electron rich analogues.[5e,14] Therefore, this elementary step provides a benchmark for the impact of remote Lewis acid binding on platinum-based reactivity.

Biaryl reductive elimination was exceptionally slow from **1**, requiring heating to 225 °C in nitrobenzene-d_5 to produce 4,4′-bis(trifluoromethyl)-1,1′-biphenyl, free bpym, and insoluble platinum(0) material. Coordination of $Zn(C_6F_5)_2$ promoted reductive elimination, with biaryl formation occurring at 140 °C ($k_{obs} = 1.5 \pm 0.1 \times 10^{-5}$ s^{-1}).[15]

The addition of bis(trimethylsilyl)acetylene (BTMSA) provided a lower energy pathway to reductive elimination (eq 4). Kinetics experiments in the initial rate regime indicated that biaryl formation from **1** proceeded slowly in the presence of excess BTMSA at 150 °C ($k_{obs} = 1.2 \pm 0.1 \times 10^{-6}$ s^{-1}), exhibiting first-order decay of **1** and concomitant appearance of the biaryl product. The reaction was determined to exhibit a first-order dependence on the concentration of BTMSA (Figure 4), consistent with an associative mechanism.[5e]

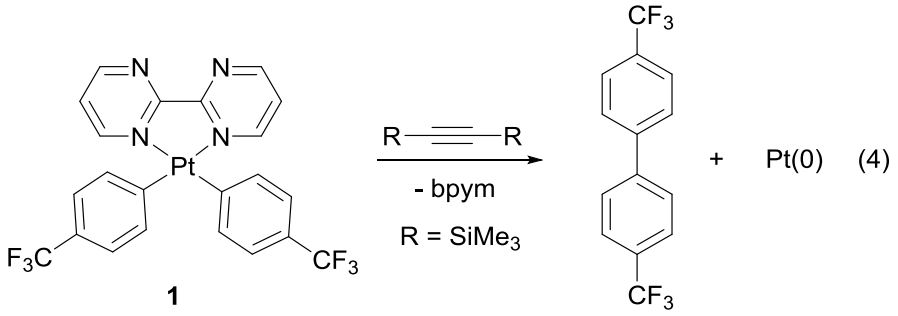

Next, experiments were performed to probe whether bpym dissociation occurs prior to reductive elimination. We have previously found that reductive elimination from a borane-activated bipyrazine (bpyz) platinum complex was not inhibited by addition of excess bpyz ligand.[5e] Surprisingly, the rate of reductive elimination from **1** slowed dramatically upon the addition of bpym. Quantitative kinetics experiments were performed, and a linear dependence was observed in a plot of k_{obs} vs 1/[bpym] (Figure 4), indicating that the reductive elimination is inverse first-order in bpym. Therefore, different reaction profiles are observed in the alkyne-promoted biaryl reductive elimination reactions from the similar bipyrazine- and 2,2′-bipyrimidine-platinum complexes.

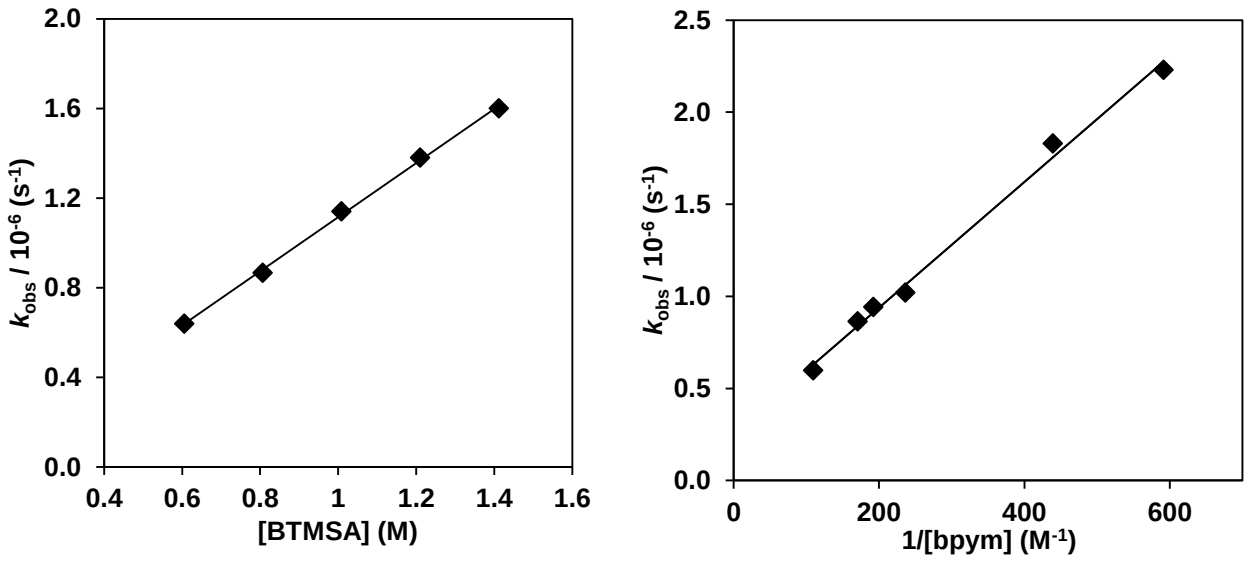

Figure 4. Effect of bis(trimethylsilyl)acetylene (left) and bpym (right) on the biaryl reductive elimination from **1** at 150 °C. A standard error of < 5 % is estimated from experiments performed in triplicate.

Complexes **2**–**4** also underwent reductive elimination in the presence of BTMSA, with widely varying temperatures required to induce C–C bond formation at rates convenient for monitoring by NMR spectroscopy. Biaryl elimination occurred at 120 °C for the $Si(cat)_2$ adduct **2**, 70 °C for the $Si(cat^F)_2$ adduct **3**, and 45 °C for the $Zn(C_6F_5)_2$ adduct **4** (see below for quantitative rate constant comparisons). For reactions at temperatures below 100 °C, the platinum(0) product was trapped as the soluble alkyne adduct, [Pt_2(μ-$Me_3SiCCSiMe_3$)($Me_3SiCCSiMe_3$)$_2$] (**5**).[16] At higher temperatures, this alkyne complex was unstable, and the platinum slowly precipitated as a black solid.

In all reactions, disappearance of **2**–**4** was first order in the initial rate regime, and no intermediates were observed. The reductive elimination exhibited a first-order dependence on the concentration of BTMSA, and was inverse first order in bpym-$Si(cat)_2$ and bpym-$Si(cat^F)_2$ for complexes **2** and **3**, respectively. It is fortuitous that under the reaction conditions, complexes **2** and **3** remain intact in the presence of added bpym-$Si(cat)_2$ and bpym-$Si(cat^F)_2$ (i.e., binding of a second equivalent of Lewis acid to bpym does not compete with binding to the bpym-platinum complex). In contrast, experiments with **4** in the presence of added bpym-$Zn(C_6F_5)_2$ were complicated by preferential dissociation of $Zn(C_6F_5)_2$ from **4** to generate **1** and the bis(zinc) adduct $(C_6F_5)_2$Zn-bpym-$Zn(C_6F_5)_2$. For **2**–**4**, addition of excess Lewis acid had no effect on reaction rate, suggesting that the Lewis acid does not dissociate from bpym during the reaction.

A proposed mechanism is shown in Scheme 1. First, there is ligand exchange of bpym for BTMSA to generate a three-coordinate platinum–alkyne complex (**A**). This must be reversible to account for the inhibition observed in experiments with added bpym. Biaryl reductive elimination occurs from the (BTMSA)$PtAr_2$ complex (**A**) in the rate determining step to generate 4,4′-bis(trifluoromethyl)-1,1′-biphenyl, which is followed by trapping of platinum with additional alkyne to form **5**. Applying the steady-state approximation to the concentration of

intermediate (BTMSA)$PtAr_2$, the rate expression for the mechanism shown in Scheme 1 is given in eq 5. If k_{-1}[bpym] >> k_2, this equation can be simplified to the form shown in eq 6. These expressions account for the observed first-order dependences for platinum and BTMSA as well as the inverse first-order behavior for bpym.

Scheme 1. Reductive elimination mechanism.

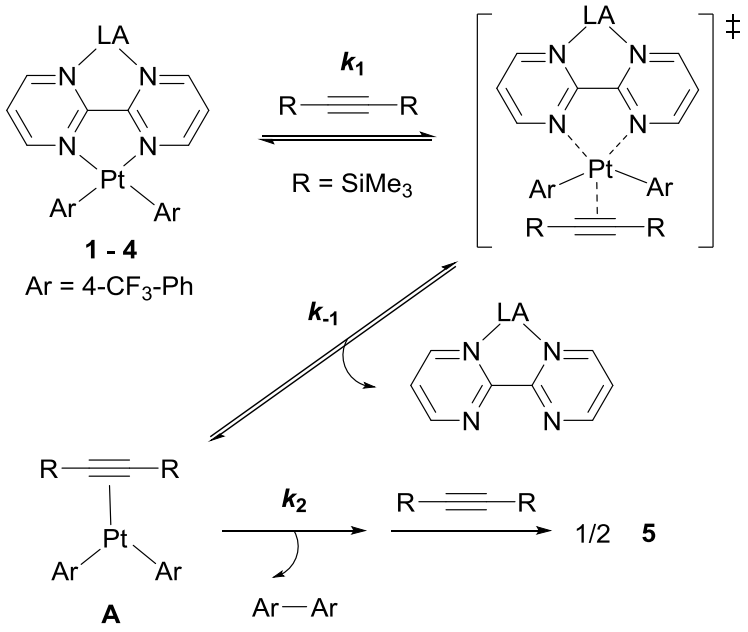

$$\text{rate} = \frac{k_1 k_2[\text{Pt}][\text{BTMSA}]}{k_{-1}[\text{bpym}] + k_2} \qquad (5)$$

$$\text{rate} = \frac{k_1 k_2[\text{Pt}][\text{BTMSA}]}{k_{-1}[\text{bpym}]} = \frac{K_{eq} k_2[\text{Pt}][\text{BTMSA}]}{[\text{bpym}]} \qquad (6)$$

The complete dissociation of the bidentate bpym ligand in this reductive elimination reaction is unusual, although exchange of monodentate ligands is a well precedented mechanism. For example, carbon–silicon reductive elimination from *cis*-$PtMe(SiPh_3)(PMePh_2)_2$ in the presence of diphenylacetylene proceeds by displacement of one phosphine ligand by alkyne.[17] Additionally, aryl–allyl reductive elimination from palladium(II) complexes was found to involve exchange of a triphenylarsine ligand for an alkene.[18] In contrast, with bidentate ancillary ligands, dissociation of one donor group is a more common pathway, as has been observed in studies of reductive elimination from octahedral platinum(IV) complexes.[19] Dissociation of bidentate ligands is often overlooked as a potential mechanism.

Biaryl formation from **1** was investigated by DFT calculations to determine the mechanism of ligand substitution (associative vs. dissociative) and to calculate the expected barrier for biaryl reductive elimination (Figure 5). The barrier for direct bpym dissociation from (bpym)$PtAr_2$ was determined to be 52.0 kcal/mol, while associative interchange, involving the

concerted exchange of bpym for an incoming alkyne, was found to have a much lower barrier of 33.6 kcal/mol (favored mechanism shown in Scheme 1). This supports an associative ligand exchange process as would be expected for a square planar d^8 platinum complex.[20]

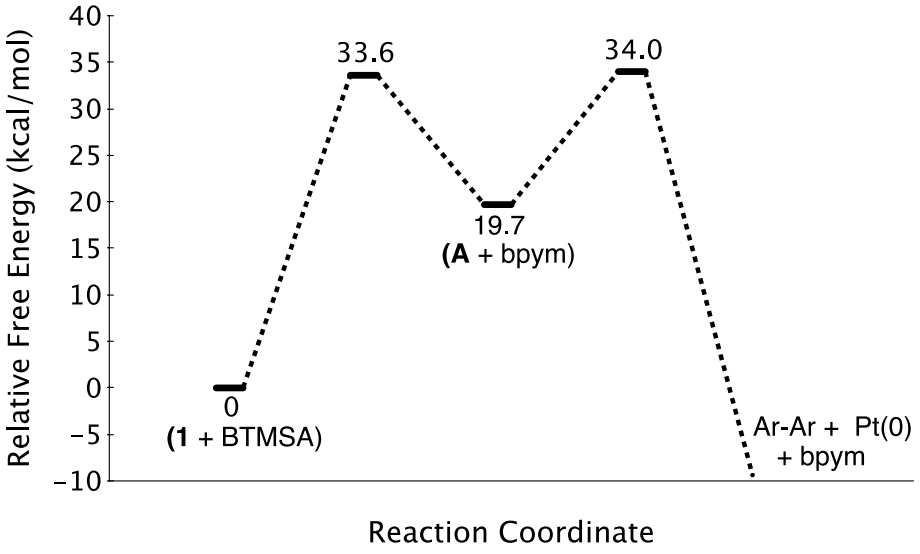

Figure 5. Reaction energy profile diagram (298K, 1 atm).

It is fortuitous that complexes **1**–**4** display the same kinetics profiles, as the conserved mechanism allows for quantification of relative rates. Eyring analysis was performed for the reaction of **1** and excess BTMSA from 140 – 180 ^{o}C (Figure 6). The temperature dependence of the observed rate constant afforded activation parameters of $\Delta H^{\ddagger}$ = + 31.6 ± 0.96 kcal/mol and $\Delta S^{\ddagger}$ = – 11.4 ± 2.2 eu. The experimentally determined free energy of activation ($\Delta G^{\ddagger}_{298K}$ = + 35.0 ± 1.6 kcal/mol) matches the calculated value of 33.6 kcal/mol within error.

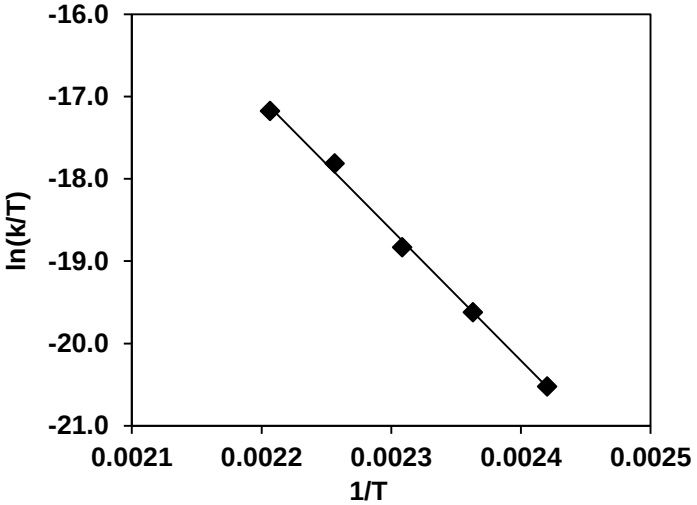

Figure 6. Eyring analysis of reductive elimination from **1** in the presence of BTMSA from 140 – 180 ^{o}C . A standard error of <5% is estimated based on triplicate experiments at one temperature.

Initial rates of reductive elimination for complexes **2**–**4** were measured in triplicate in the presence of 0.35 M BTMSA (Table 1). To determine relative rates vs. **1**, estimated rate constants for reductive elimination from **1** at 120 °C ($k = 5.8 \times 10^{-8}$ s^{-1}), 70 °C ($k = 1.6 \times 10^{-10}$ s^{-1}), and 45 °C ($k = 4.2 \times 10^{-12}$ s^{-1}) were calculated by extrapolation using the measured Eyring parameters. By comparing measured rate constants for **2**–**4** with extrapolated values for **1**, relative rates due to Lewis acid binding were calculated for **2** (1.5×10^3 at 120 °C), **3** (1.2×10^6 at 70 °C), and **4** (1.2×10^8 at 45 °C).

Table 1. Comparison of reductive elimination rates from **1**–**4**.

Complex	Lewis acid	Temp. (°C)	k_{obs} (s^{-1})	Relative Rate
1	None	150	$1.2 \pm 0.1 \times 10^{-6}$	1
2	$Si(cat)_2$	120	$8.7 \pm 0.1 \times 10^{-5}$	1.5×10^3 (at 120 °C)
3	$Si(cat^F)_2$	70	$1.9 \pm 0.1 \times 10^{-4}$	1.2×10^6 (at 70 °C)
4	$Zn(C_6F_5)_2$	45	$4.8 \pm 0.1 \times 10^{-4}$	1.2×10^8 (at 45 °C)

We sought to determine whether the Lewis acid binding leads to rate acceleration by shifting the bpym and alkyne exchange equilibrium, changing the rate at which the equilibrium is established, or both. The value of K_{eq} can be calculated based on a Boltzmann distribution with the energy difference between **1** and **A** from the DFT calculations and taking into account the effects of Lewis acid coordination from the binding constant measurements. For $Si(cat)_2$, the change in equilibrium constant accounts for an 80-fold rate acceleration for reductive elimination, while the remaining 20-fold rate acceleration is due to kinetic effects (see the Experimental Section for details). Therefore, changes to both the location of the equilibrium position and the kinetics of the ligand exchange step due to Lewis acid binding give rise to the observed rate acceleration.

CONCLUSIONS

A platinum–bipyrimidine complex was synthesized and employed as a platform to investigate the ability of silicon and zinc Lewis acids to act as chemical switches for electronic properties. Spectroscopic and electrochemical studies evidence substantial depletion of electron density in the bpym ligand upon binding of the Lewis acids. The electronic effects of remote

Lewis acid binding dramatically accelerated reductive elimination from the platinum center, providing a rare example of *tunable* reactivity using a remote chemical switch.

Mechanistic experiments and DFT calculations unexpectedly revealed complete dissociation of the bpym ligand prior to reductive elimination. The combined experimental and theoretical results indicate that bidentate ligand dissociation is kinetically favored by Lewis acid coordination (i.e. bpym is more labile with Lewis acids bound). However, a *thermodynamic* driving force also favors ligand dissociation, due to stronger binding of the Lewis acids to free bpym than the platinum-bound bpym ligand. Combined, these effects drastically modify the rate of biaryl elimination by factors of 10^3 to 10^8.

EXPERIMENTAL SECTION

General Considerations. Unless otherwise noted, all experiments were conducted using standard Schlenk techniques or in a nitrogen atmosphere glovebox. Solvents were stored in PTFE-valved flasks after drying using Vacuum Atmospheres solvent purification systems or by distillation from appropriate drying agents. Deuterated solvents were purchased from Cambridge Isotope Laboratory, dried using appropriate drying agents, and vacuum transferred prior to use. $Pt(SEt_2)_2(4\text{-}CF_3\text{-}Ph)_2$,[5a] $Si(cat)_2$,[6] $Si(cat^F)_2$,[7] and $Zn(C_6F_5)_2(\eta^2\text{-toluene})$[8] were prepared according to literature procedures. The 2,2′-bipyrimidine ligand was purchased from Aldrich and purified by vacuum sublimation. Bis(trimethylsilyl)acetylene and 1,3,5-tris(trifluoromethyl)benzene were purchased from Aldrich and were degassed and stored over activated 3Å molecular sieves prior to use.

Solution NMR spectroscopy was performed using Bruker NMR spectrometers at 20 ^oC unless otherwise noted. ^1H NMR spectra were calibrated internally to either the resonance for the solvent or residual proteo solvent relative to tetramethylsilane. ^{19}F NMR chemical shifts were referenced to 1,3,5-tris(trifluoromethyl)benzene. ^{195}Pt NMR chemical shifts were referenced to K_2PtCl_4 in D_2O. Solution UV-vis spectra were collected using a Varian Cary 300 series spectrophotometer. Elemental analyses were performed by the University of California, Berkeley College of Chemistry Microanalytical Facility.

Cyclic voltammetry experiments were conducted with a BioLogic SP-200 potentiostat. The measurements were done in an electrochemical cell located inside a N_2-filled glovebox, with a standard three-electrode configuration. A 3 mm diameter glassy carbon electrode was used as the working electrode, and was polished with 1 μm alumina prior to each use. A platinum wire was used as the counter electrode, and a Ag/Ag^+ electrode (0.01 M of $AgNO_3$ in MeCN with 0.1 M of $^nBu_4NPF_6$) was used as the reference electrode. Cyclic voltammograms of all the compounds were obtained in the *o*-diflurobenzene solution at a concentration of 1.0 mM containing 0.1 M of $^nBu_4NB(C_6F_5)_4$ as the electrolyte, at a scan rate of 100 mV/s. Ferrocene was added at the end of each experiment to obtain a cyclic voltammogram containing Fc/Fc^+ redox wave as the internal standard, so the potential value can be reported versus Fc/Fc^+ redox couple.

Single crystal X-ray diffraction was performed at the UC Berkeley CHEXRAY crystallographic facility. Measurements were performed on a Bruker APEX-II CCD area detector with Mo Kα radiation (λ = 0.71073 Å) monochromated using QUAZAR multilayer mirrors. Crystals were maintained at 100(2) K during collection. Data collection, refinement, and reduction were performed with Bruker APEX2 software (v. 2013.4 or 2014.1). Structures were

refined with SHELXL-2013 direct methods[21] or SHELXT-2014 with refinement of F^2 against all reflections by full-matrix least squares. Non-hydrogen atoms were refined anisotropically, and hydrogen atoms were included at geometrically-calculated positions and refined using a riding model. The structure of **4** contained voids partially occupied by highly disordered solvent molecules, likely pentane. SQUEEZE was employed to treat electron density in these voids as a diffuse solvent contribution to the calculated structure factors.[22]

Calculations were carried out in the UC Berkeley Molecular Graphics and Computation Facility with the Gaussian09 rev D01 suite of programs,[23] employing the B3LYP functional with the D3 version of Grimme's dispersion with Becke-Johnson damping[24] and 6-31+G** basis set for non-metal atoms. Platinum was treated with the relativistic ECP[25] and basis set of Los Alamos National Lab (LANL2DZ). All free energies were calculated at 298 K and 1 atm of pressure in the gas phase.

Synthesis of (2,2′-bpym)Pt(4-CF_3-Ph)$_2$ (1). A solution of Pt(SEt_2)$_2$(4-CF_3-Ph)$_2$ (0.450 g, 0.676 mmol) in 5 mL of dichloromethane was added dropwise to a solution of 2,2′-bipyrimidine (0.213 g, 1.35 mmol) in 5 mL of dichloromethane under air. The solution appeared red within minutes at 25 °C. After 48 hours, solvent was removed under vacuum. Microcrystalline orange (2,2′-bpym)Pt(4-CF_3-Ph)$_2$ was obtained in 89 % yield (0.390 g) after purification by silica column chromatography (eluent: CH_2Cl_2/1% MeOH), and was recrystallized by layering pentane on a benzene solution of **1**. ^{1}H NMR (C_6D_6) δ 7.97 (m, 4H), 7.80 (d with Pt satellites, J_{HH} = 7.6 Hz, J_{PtH} = 72 Hz, 4H), 7.52 (d, J_{HH} = 7.7 Hz, 4H), 5.70 (dd, J_{HH} = 5.4, 4.7 Hz, 2H); ^{19}F NMR (C_6D_6) -60.34; ^{13}C{^{1}H} NMR (C_6D_6) δ 161.58, 156.68, 154.53, 150.14, 138.21, 124.92, 124.73, 123.56 (q, J_{CF} = 3.0 Hz), 122.74; ^{195}Pt NMR (*o*-$C_6H_4F_2$) –3393. Anal. Calc'd for $C_{22}H_{14}F_6N_4Pt\cdot 0.5C_6H_6$ (%) C 44.00, H 2.53, N 8.21; Found C 43.75, H 2.45, N 7.92.

Synthesis of (2,2′-bpym-Si(cat)$_2$)Pt(4-CF_3-Ph)$_2$ (2). A solution of bis(catecholato)silane (7.7 mg, 0.031 mmol) in 4 mL of toluene was added to a solution of **1** (20. mg, 0.031 mmol) in 4 mL of toluene. An immediate color change to red was observed. The solution was layered with 2 mL of pentane and cooled to -35 °C overnight to obtain red crystals of **2** (23 mg, 84 % yield). ^{1}H NMR (toluene-d_8) 8.45 (br, 2H), 7.84 (br, 2H), 7.62 (d with Pt satellites, J_{HH} = 6.0 Hz, J_{PtH} = 60 Hz, 4H), 7.43 (d, J_{HH} = 6.0 Hz, 4H), 6.50–6.96 (m, 8H), 5.77 (t, J_{HH} = 5.4 Hz, 2H); ^{19}F NMR (toluene-d_8) -60.44; ^{13}C{^{1}H} NMR (CD_2Cl_2) δ 156.78, 156.61, 147.75, 137.67, 137.44, 131.84, 128.72, 127.83, 126.04, 125.43, 125.05, 124.24, 123.45, 120.04, 112.23; ^{195}Pt NMR (*o*-$C_6H_4F_2$) –3005. Anal. Cal'd for $C_{34}H_{22}F_6N_4O_4PtSi\cdot C_7H_8$ (%) C 50.26, H 3.09, N 5.72; Found C 50.43, H 3.13, N 5.53.

Synthesis of (2,2′-bpym-Si(cat^F)$_2$)Pt(4-CF_3-Ph)$_2$ (3). A solution of **1** (16.8 mg, 0.0261 mmol) and bis(perfluorocatecholato)silane(NCMe)$_2$ (36.8 mg, 0.0782 mmol) was prepared in 3 mL of benzene. After 15 minutes, solvent was removed under reduced pressure. The product was redissolved in 1 mL of bromobenzene, filtered to remove excess Si(cat^F)$_2$, and dried *in vacuo* to afford **3** as a brown powder (12.4 mg, 40 % yield). Solid samples of **3** must be stored below 0 °C to prevent decomposition. ^{1}H NMR (C_6D_6) δ 8.25 (dd, J = 5.5, 1.8 Hz, 2H), 7.60 (dd, J = 5.5, 1.9 Hz, 2H), 7.51 (m, 8H), 5.57 (t, J = 5.5 Hz, 2H); ^{19}F NMR (C_6D_6) δ -60.60 (6F), -163.34 (ddd, J = 21.7, 9.7, 5.5 Hz, 2F), -164.83 (ddd, J = 21.7, 9.5, 5.4 Hz, 2F), -169.14 (td, J = 21.8, 5.6 Hz, 2F), -169.57 (td, J = 21.6, 5.5 Hz, 2F); ^{13}C{^{1}H} NMR (*o*-$C_6H_4F_2$) δ 159.22, 155.76, 152.49, 151.52, 151.11, 144.74, 138.34, 136.59 (br d, J_{CF} = 231 Hz), 133.98 (br d, J_{CF} = 222 Hz), 130.53 (d, J_{CF} = 7.6 Hz), 128.67, 124.42 (q, J_{CF} = 3.9 Hz); ^{195}Pt NMR (*o*-$C_6H_4F_2$) –3324. Anal. Cal'd for $C_{34}H_{14}F_{14}N_4O_4PtSi\cdot C_6H_5Br$ (%) C 40.42, H 1.61, N 4.71; Found C 40.40, H 1.72, N 5.09.

Synthesis of (2,2′-bpym-Zn(C_6F_5)$_2$)Pt(4-CF_3-Ph)$_2$ (4). A solution of **1** (20.0 mg, 0.0311 mmol) and bis(pentafluorophenyl)zinc(μ^2-toluene) (15.5 mg, 0.0311 mmol) was prepared in 8 mL of toluene. An immediate color change from yellow to red was observed. Layering the solution with pentane and storing at –30 °C overnight yielded red crystals of **4** (25.0 mg, 77 % yield). ^{1}H NMR (toluene-d_8) δ 8.54–8.41 (m, 2H), 7.95 (dd, J = 5.6, 2.0 Hz, 2H), 7.51 (d with Pt satellites, J_{PtH} = 73.6 Hz, J_{HH} = 7.8 Hz, 4H), 7.39 (d, J = 7.8 Hz, 4H), 5.91 (t, J = 5.4 Hz, 2H); ^{19}F NMR (toluene-d_8) δ -60.56 (6H), -114.95 (m, 4 H), -153.24 (t, J = 19.5 Hz, 2H), -158.35 (m, 4H); ^{13}C{^{1}H} NMR (C_6D_6) δ 159.85, 157.96, 156.14, 151.19, 150.78, 147.23, 138.16, 126.42, 124.10 (q, J_{CF} = 3.6 Hz), resonances for Zn-C_6F_5 groups were not observable; ^{195}Pt NMR (*o*-$C_6H_4F_2$) –3350. Anal. Calc'd for $C_{34}H_{14}F_{16}N_4PtZn\cdot 0.5C_7H_8$ (%) C 41.36, H 1.67, N 5.14; Found C 41.25, H 1.67, N 5.14.

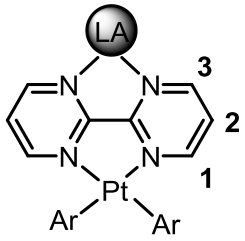

Table 2. Comparison of ^{1}H,[a] ^{195}Pt,[b] and ^{13}C[c] NMR signals (in ppm) for **1**–**4**.

	1	**2**	**3**	**4**
H1	7.97	7.75	7.60	7.87
H2	5.70	5.58	5.57	5.73
H3	7.98	8.23	8.25	8.21
Pt	– 3393	– 3005	– 3324	– 3350
C1	154.53	152.43	151.29	156.14
C2	122.74	124.54	126.67	124.10
C3	154.53	155.81	157.83	157.96

[a] ^{1}H NMR chemical shifts are reported in benzene-d_6 with assignments based on NOESY crosspeaks between H1 and the platinum-bound aryl groups. [b] ^{195}Pt{^{1}H} NMR data is reported in *o*-difluorobenzene. [c] ^{13}C NMR data is reported in benzene-d_6 with assignments based on ^{1}H–^{13}C HSQC crosspeaks.

Van't Hoff analysis for the binding of Si(cat)$_2$ to 1. A solution of **1** (4.0 mg, 0.0062 mmol) and Si(cat)$_2$ (1.5 mg, 0.0062 mmol) was prepared in 0.500 mL of toluene-d_8 in a J. Young NMR tube. An internal standard, tetrakis(trimethylsilyl)silane, was added. The NMR tube was placed in the NMR spectrometer with the temperature pre-equilibrated to 30 ^{o}C. The temperature was increased, allowing 10 minutes for equilibration at each temperature. Concentrations of **1** and **2** were determined by chemical shift analysis of the H1 position of bpym (*ortho* to Pt, chemical shift varies between 7.84 and 8.10 ppm over this temperature range). Spectra of **1** and **2** with a 7-fold excess of Si(cat)$_2$ were also collected at all temperatures for comparison.

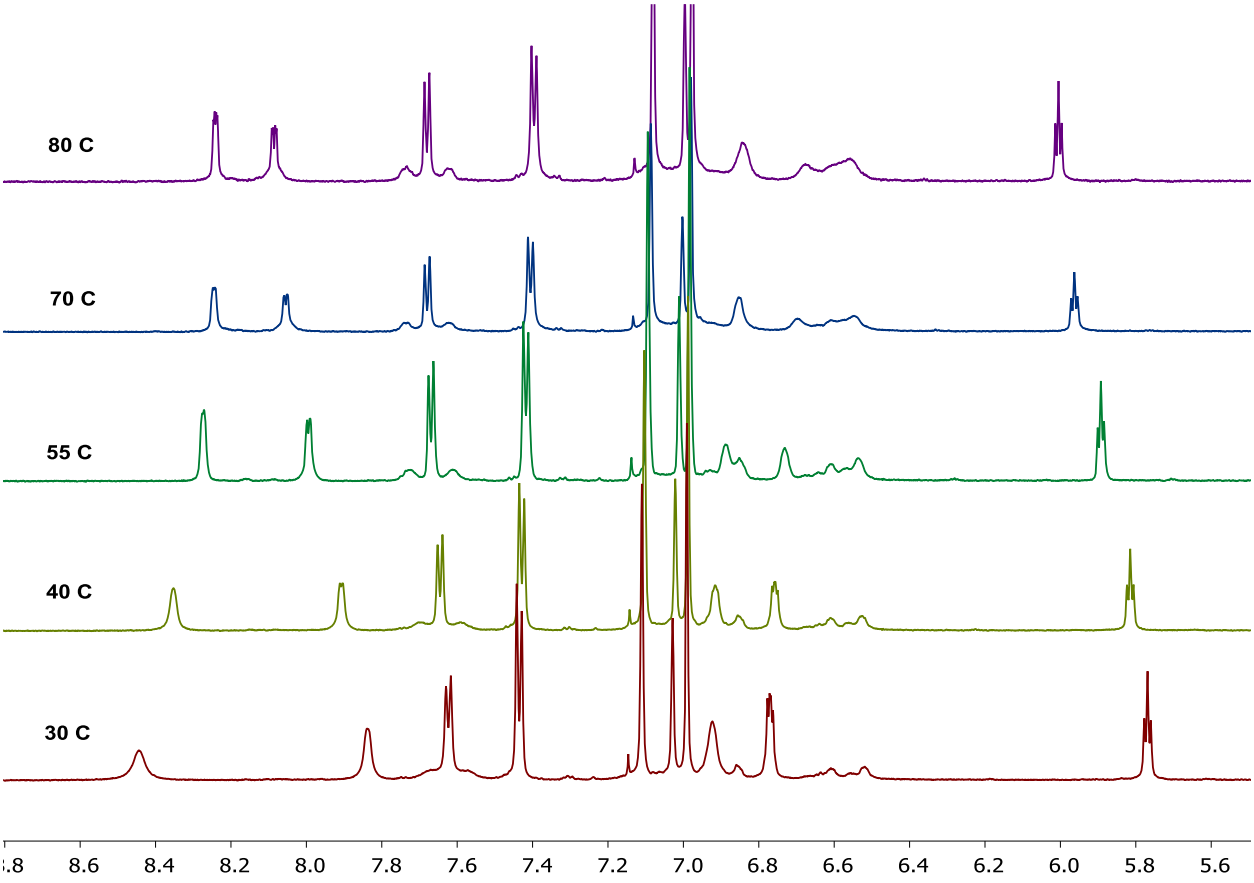

Figure 7. ^{1}H NMR spectra (in ppm) for binding of Si(cat)$_2$ to **1** between 30 and 80 ^{o}C.

Table 3. Temperature dependence of K_{eq} for $Si(cat)_2$ binding to **1**.

Temp. (^oC)	1/T (K^{-1})	K_{eq} (M^{-1})	ln(K_{eq})
30.0	0.00333	1210	7.10
40.0	0.00323	229	5.43
55.0	0.00308	92.8	4.53
70.0	0.00294	22.4	3.11
80.0	0.00286	13.3	2.59

The plot of ln(K_{eq}) as a function of T^{-1} (Figure 8) was fit by a line according to the expression

$$\ln K_{eq} = \frac{-\Delta H}{RT} + \frac{\Delta S}{R}$$

The enthalpy and entropy of $Si(cat)_2$ binding to 1 were extracted from the slope and intercept, respectively. Standard deviations for ΔH and ΔS were evaluated using the LINEST routine in Excel.

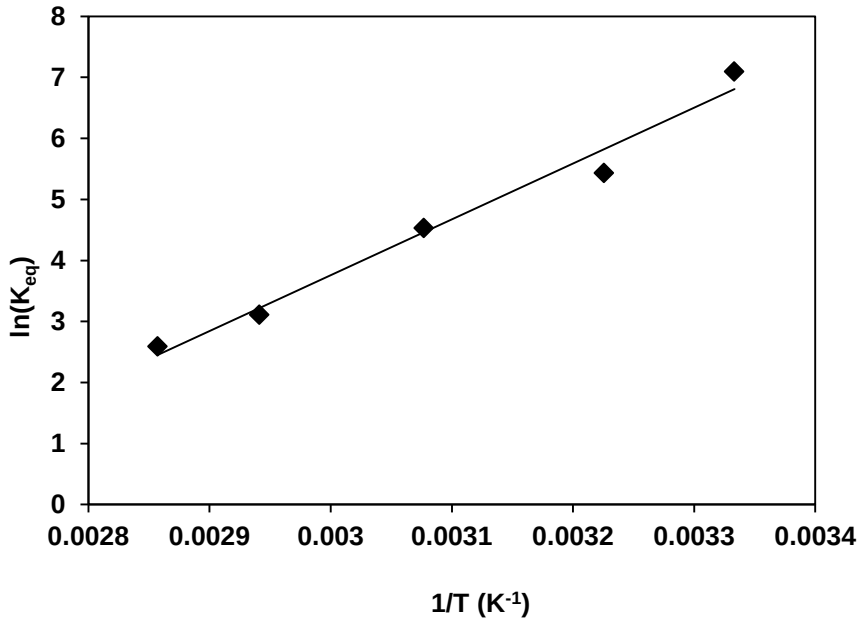

Figure 8. Van't Hoff plot for $Si(cat)_2$ binding to **1** between 30 and 80 ^oC.

Variable temperature NMR studies of 3. A solution of **3** (0.0065 mmol) was prepared in 1.00 mL of toluene-d_8 in a J. Young NMR tube. A known amount of internal standard, tetrakis(trimethylsilyl)silane, was added. The NMR tube was placed in an NMR spectrometer with the temperature pre-equilibrated to 30 ^{o}C. The temperature was increased, allowing 10 minutes for equilibration at each temperature. Between 30 and 100 ^{o}C, there was no evidence of Si(cat^{F})$_2$ dissociation from **3**. Spectra of **3** in the presence of a 3-fold excess of Si(cat^{F})$_2$ were also collected at all temperatures for comparison.

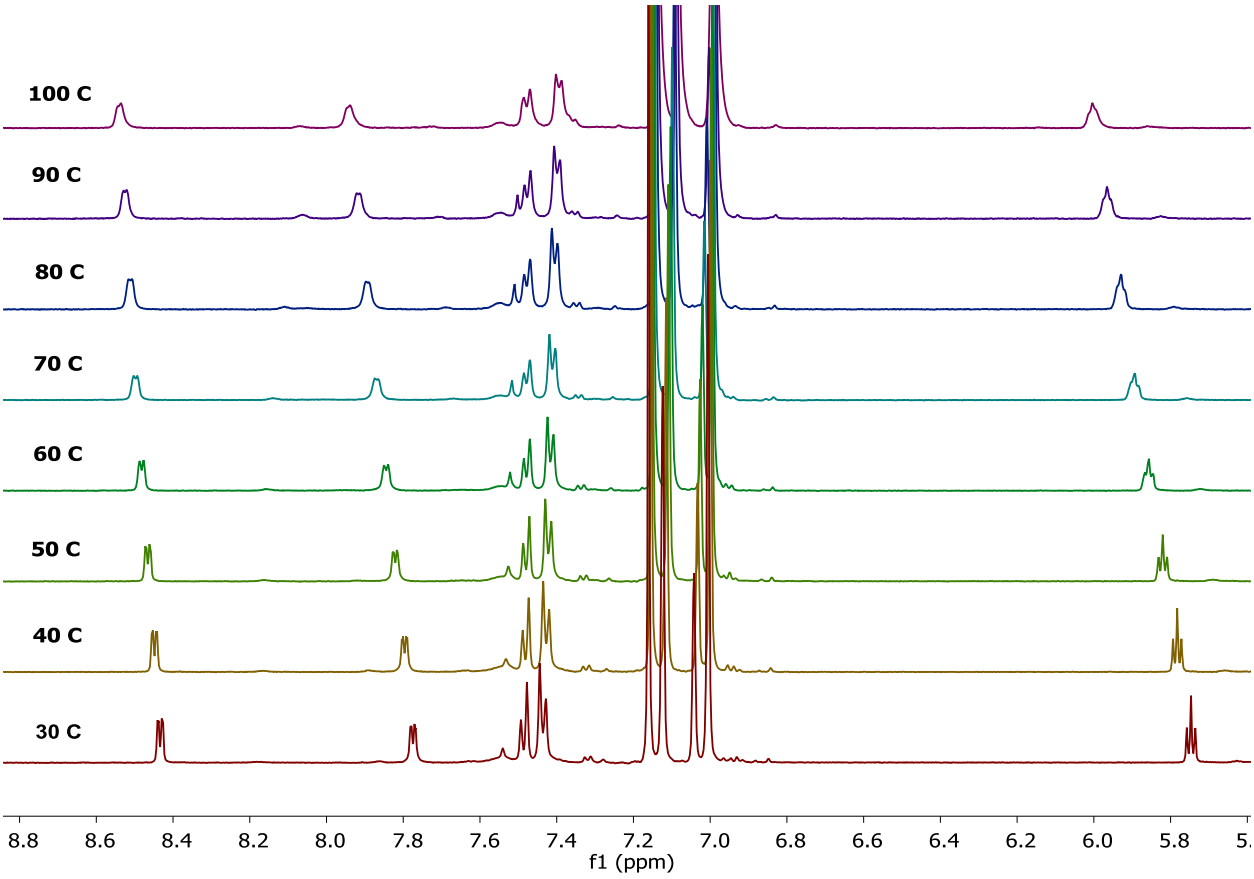

Figure 9. ^{1}H NMR spectra (in ppm) of **3** in toluene-d_8 from 30 to 100 ^{o}C.

Competition experiment for Si(cat)$_2$ and Si(cat^{F})$_2$ binding to 1. A solution of **3** (0.0065 mmol), Si(cat)$_2$ (0.065 mmol), and tetrakis(trimethylsilyl)silane as an internal standard was prepared in 0.500 mL of toluene-d_8 in a J. Young NMR tube. The ^{1}H and ^{19}F NMR spectra indicated formation of **2** and **3** in a 1:1 ratio at 25 ^{o}C.

Variable temperature NMR studies of 4. A solution of **4** (0.0065 mmol) and 1,3,5-tris(trifluoromethyl)benzene as an internal standard was prepared in 0.500 mL of *o*-dichlorobenzene and 0.050 mL benzene-d_6 in a J. Young NMR tube. The NMR tube was placed in an NMR spectrometer with the temperature pre-equilibrated to 20 °C. The temperature was increased, allowing 10 minutes for equilibration at each temperature. Between 20 and 120 °C, there was no evidence of $Zn(C_6F_5)_2$ dissociation from **4**. Spectra of **4** in the presence of a 5-fold excess of $Zn(C_6F_5)_2$ were also collected at all temperatures for comparison.

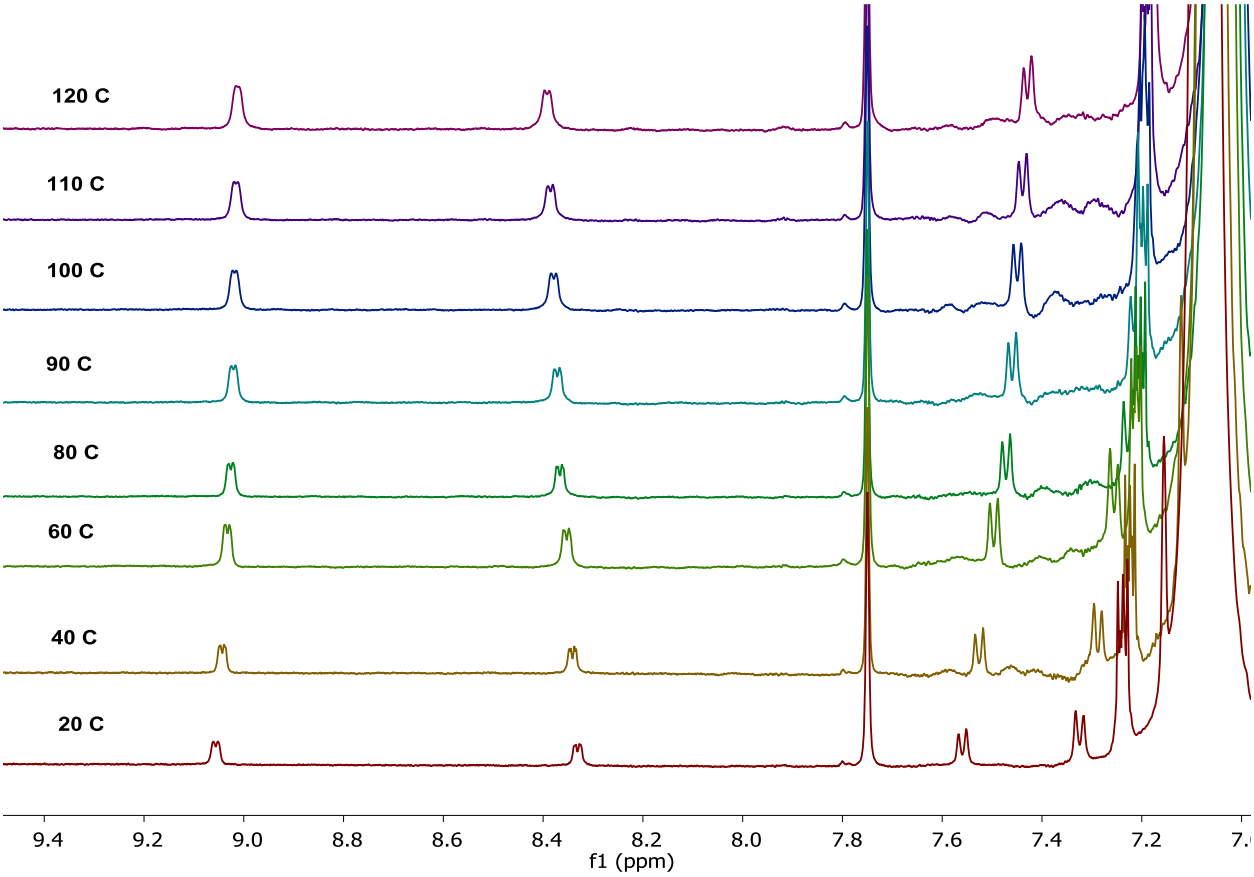

Figure 10. ^{1}H NMR spectra (in ppm) of **4** in *o*-dichlorobenzene from 20 to 120 °C. Peaks below 7.2 ppm are *o*-dichlorobenzene solvent; the singlet at 7.75 ppm is the 1,3,5-tris(trifluoromethyl)benzene internal standard.

Competition experiment for $Si(cat^F)_2$ and $Zn(C_6F_5)_2$ binding to 1. A solution of **3** (0.0065 mmol) and $Zn(C_6F_5)_2$•(η^2-toluene) (0.0065 mmol) was prepared in 0.500 mL of toluene-d_8 in a J. Young NMR tube, and a known amount of internal standard, tetrakis(trimethylsilyl)silane, was added. Complete formation of **4** and $Si(cat^F)_2$ was confirmed by ^{1}H and ^{19}F NMR spectroscopy.

Competition experiment for Si(cat)$_2$ binding to 1 versus bpym. A solution of **1** (6.5×10^{-3} mmol), 2,2′-bipyrimidine (6.5×10^{-4} mmol), Si(cat)$_2$ (6.5×10^{-4} mmol), and ferrocene as an internal standard was prepared in 0.500 mL of *o*-dichlorobenzene and 0.050 mL of benzene-d_6 in a J. Young NMR tube. Integration of the relative amounts of **1** (6.4×10^{-3} mmol), **2** (1.1×10^{-4} mmol), bpym (1.1×10^{-4} mmol), and bpym–Si(cat)$_2$ (5.4×10^{-4} mmol) by ^{1}H NMR spectroscopy at 25 ^{o}C allowed calculation of $K_{eq} = 315$ and $\Delta G_{298} = -3.4$ kcal/mol.

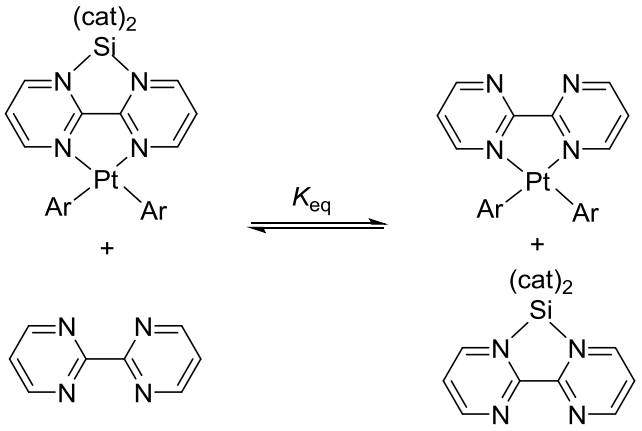

Competition experiment for Si(cat^F)$_2$ or Zn(C$_6$F$_5$)$_2$ binding to 1 versus bpym. A solution of **1** (3.6×10^{-3} mmol), 2,2′-bipyrimidine (6.5×10^{-4} mmol), Si(cat^F)$_2$ or Zn(C$_6$F$_5$)$_2$(toluene) (6.5×10^{-4} mmol), and ferrocene as an internal standard was prepared in 0.500 mL of *o*-dichlorobenzene and 0.050 mL of benzene-d_6 in a J. Young NMR tube. By ^{1}H NMR spectroscopy at 25 ^{o}C, there was complete formation of **1** and bpym–Si(cat^F)$_2$ or bpym–Zn(C$_6$F$_5$)$_2$. Assuming 99 % conversion based on ^{1}H NMR detection limits, $K_{eq} > 9.6 \times 10^3$ and $\Delta G_{298} \leq -5.4$ kcal/mol.

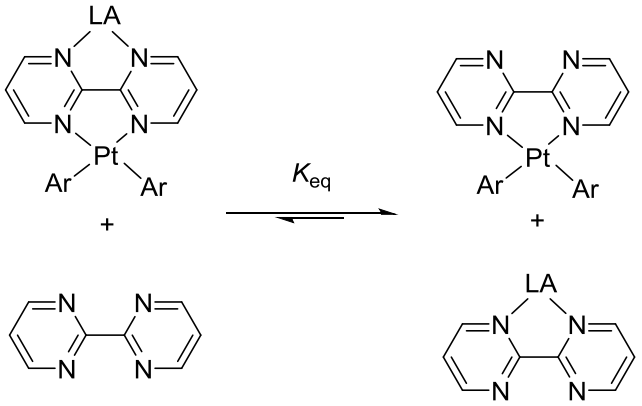

LA = Si(cat^F)$_2$, Zn(C$_6$F$_5$)$_2$

Reaction order in BTMSA with 1 at 150 °C. Complex **1** (4.2 mg, 0.0065 mmol) was dissolved in 0.400 mL of mesitylene-d_{12} in a J. Young NMR tube. An internal standard, 1,3,5-tris(trifluoromethyl)benzene (0.25 μL), and bis(trimethylsilyl)acetylene (75.0 to 175 μL, 0.348 to 0.812 mmol) were added via syringe. Additional mesitylene-d_{12} was added as necessary to achieve a total volume of 0.575 mL. The NMR tube was heated to 150 °C in a temperature-controlled oil bath. The rate of reductive elimination was monitored by ^{19}F NMR spectroscopy.

Table 4. Observed rate constant as a function of [BTMSA] for reductive elimination from **1** at 150 °C.

[BTMSA] (M)	k_{obs} (s^{-1})
0.605	6.40×10^{-6}
0.807	8.66×10^{-6}
1.01	1.14×10^{-5}
1.21	1.38×10^{-5}
1.41	1.60×10^{-5}

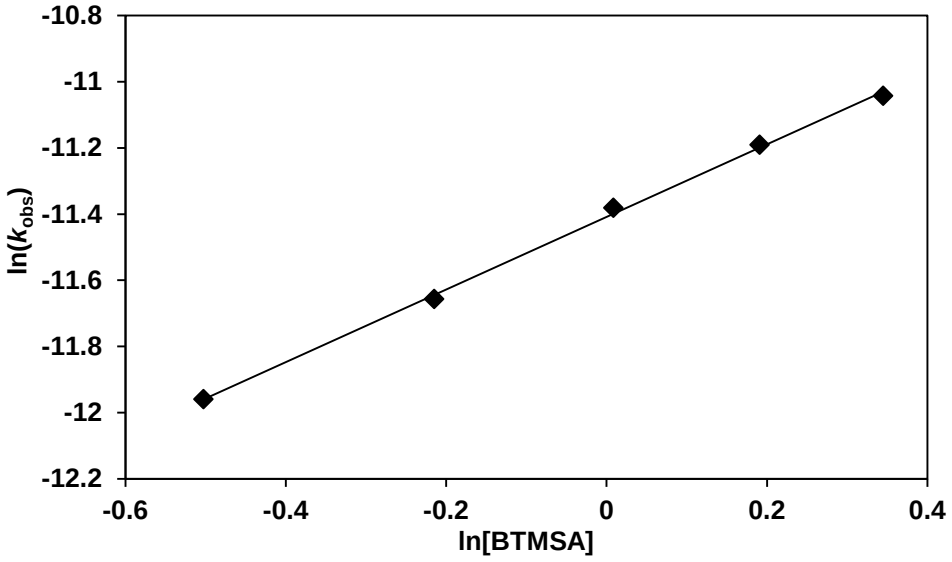

Figure 11. Plot of ln(k_{obs}) vs ln[BTMSA] for **1** at 150 °C, indicating first-order behavior.

Reaction order in BTMSA with 2 at 120 °C. Complex **1** (4.2 mg, 0.0065 mmol) and $Si(cat)_2$ (7.9 mg, 0.033 mmol) were dissolved in 0.400 mL of fluorobenzene and 0.050 mL of benzene-d_6 in a J. Young NMR tube. An internal standard, 1,3,5-tris(trifluoromethyl)benzene (0.25 μL), and bis(trimethylsilyl)acetylene (50.0 to 90.0 μL, 0.232 to 0.418 mmol) were added via syringe. Additional fluorobenzene was added to achieve a total volume of 0.575 mL. The NMR tube was heated to 120 °C in a temperature-controlled oil bath. The rate of reductive elimination was monitored by ^{19}F NMR spectroscopy.

Table 5. Observed rate constant as a function of [BTMSA] for reductive elimination from **2** at 120 °C.

[BTMSA] (M)	k_{obs} (s^{-1})
0.403	5.14×10^{-5}
0.483	6.67×10^{-5}
0.605	7.67×10^{-5}
0.645	8.52×10^{-5}
0.727	9.57×10^{-5}

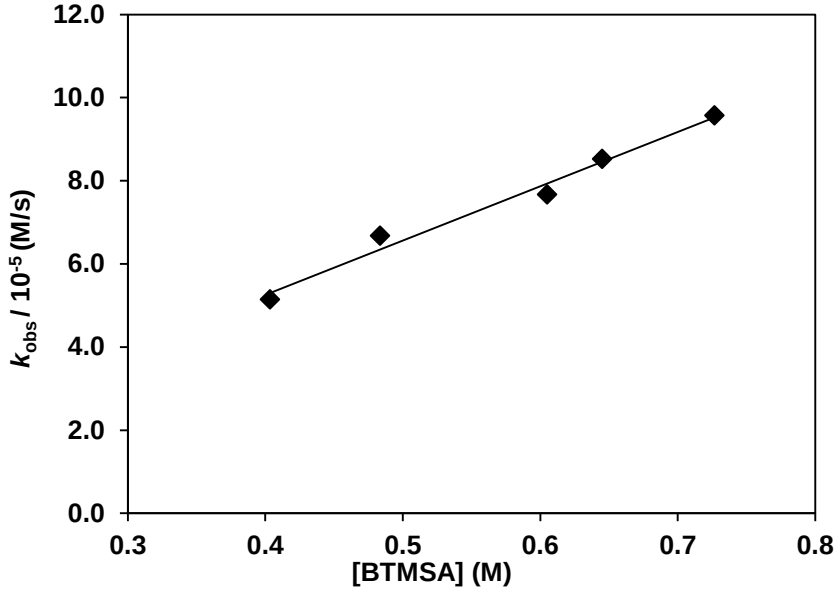

Figure 12. Plot of k_{obs} for reductive elimination from **2** as a function of [BTMSA] at 120 °C.

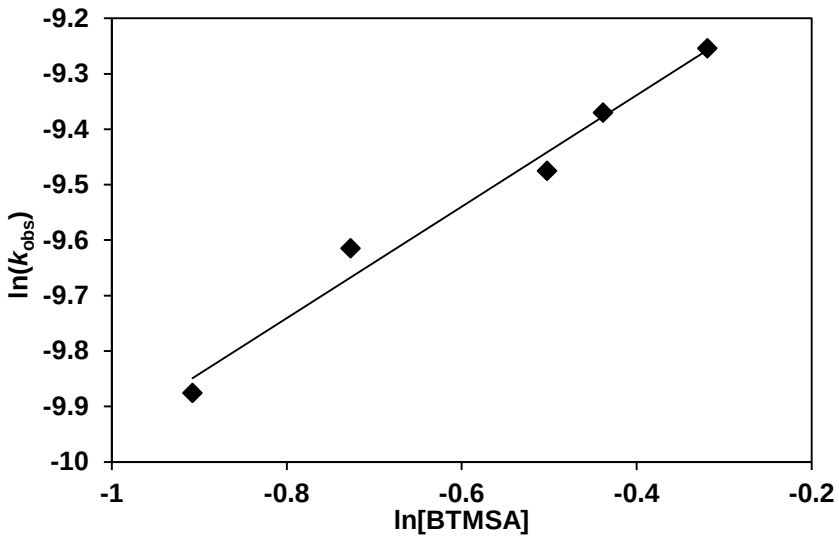

Figure 13. Plot of ln(k_{obs}) vs ln[BTMSA] for **2** at 120 ^{o}C, indicating first-order behavior.

Reaction order in BTMSA with 3 at 70 ^{o}C. Complex **1** (4.2 mg, 0.0065 mmol) and $Si(cat^{F})_2(NCMe)_2$ (9.2 mg, 0.020 mmol) were dissolved in 0.400 mL of fluorobenzene and 0.050 mL of benzene-d_6 in a J. Young NMR tube. An internal standard, 1,3,5-tris(trifluoromethyl)benzene (0.25 μL), and bis(trimethylsilyl)acetylene (50.0 to 90.0 μL, 0.232 to 0.418 mmol) were added via syringe. Additional fluorobenzene was added to achieve a total volume of 0.575 mL. The NMR tube was stored at 0 ^{o}C prior to use. The tube was placed in an NMR spectrometer with the temperature pre-equilibrated to 70 ^{o}C. After allowing the temperature to equilibrate for two minutes, the rate of reductive elimination was monitored by ^{19}F NMR spectroscopy.

Table 6. Observed rate constant as a function of [BTMSA] for reductive elimination from **3** at 70 ^{o}C.

[BTMSA] (M)	k_{obs} (s^{-1})
0.403	1.46×10^{-4}
0.483	1.68×10^{-4}
0.605	2.16×10^{-4}
0.645	2.30×10^{-4}
0.727	2.50×10^{-4}

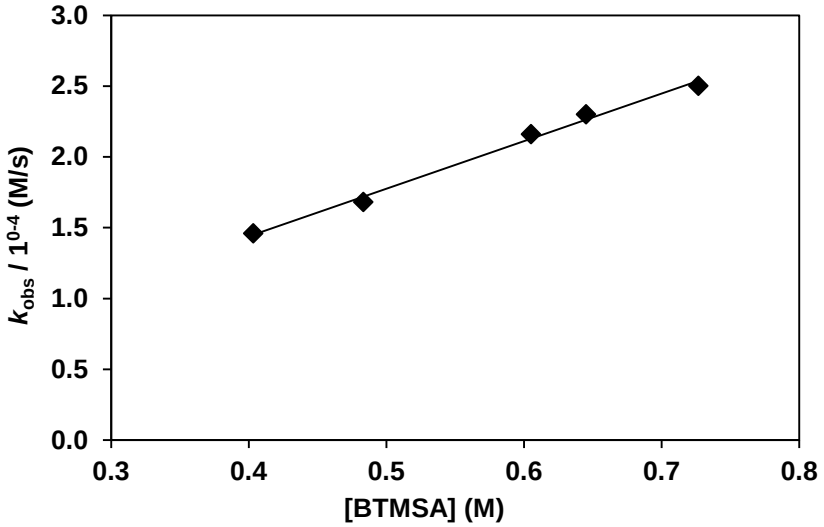

Figure 14. Plot of k_{obs} for reductive elimination from **3** as a function of [BTMSA] at 70 °C.

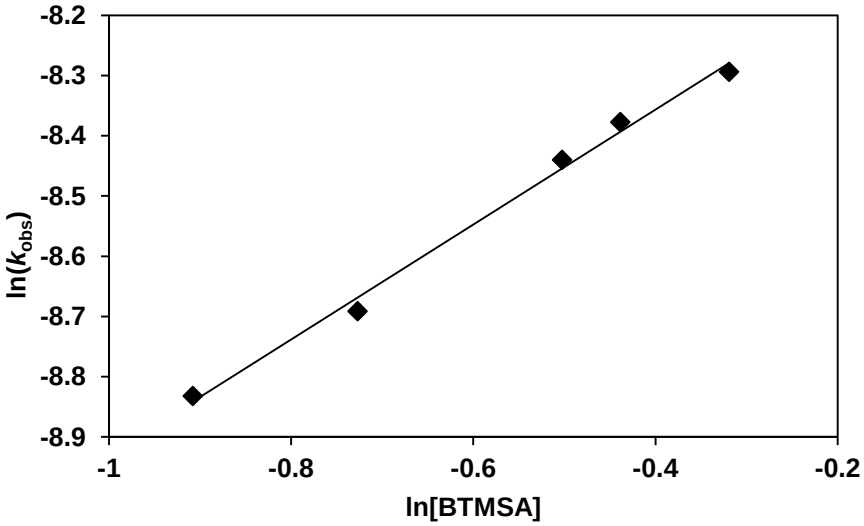

Figure 15. Plot of ln(k_{obs}) vs ln[BTMSA] for **3** at 70 °C, indicating first-order behavior.

Reaction order in BTMSA with 4 at 45 °C. Complex **1** (4.2 mg, 0.0065 mmol) and $Zn(C_6F_5)_2$•(η^2-toluene) (6.4 mg, 0.013 mmol) were dissolved in 0.400 mL of *o*-difluorobenzene and 0.050 mL of benzene-d_6 in a J. Young NMR tube. An internal standard, 1,3,5-tris(trifluoromethyl)benzene (0.25 μL), and bis(trimethylsilyl)acetylene (50.0 to 90.0 μL, 0.232 to 0.418 mmol) were added via syringe. Additional *o*-difluorobenzene was added to achieve a total volume of 0.575 mL. The NMR tube was stored at 0 °C prior to use. The tube was placed in an NMR spectrometer with the temperature pre-equilibrated to 45 °C. After allowing the temperature to equilibrate for two minutes, the rate of reductive elimination was monitored by ^{19}F NMR spectroscopy.

Table 7. Observed rate constant as a function of [BTMSA] for reductive elimination from **4** at 45 °C.

[BTMSA] (M)	k_{obs} (s^{-1})
0.403	4.87×10^{-4}
0.483	5.94×10^{-4}
0.605	7.47×10^{-4}
0.645	8.16×10^{-4}
0.727	8.74×10^{-4}

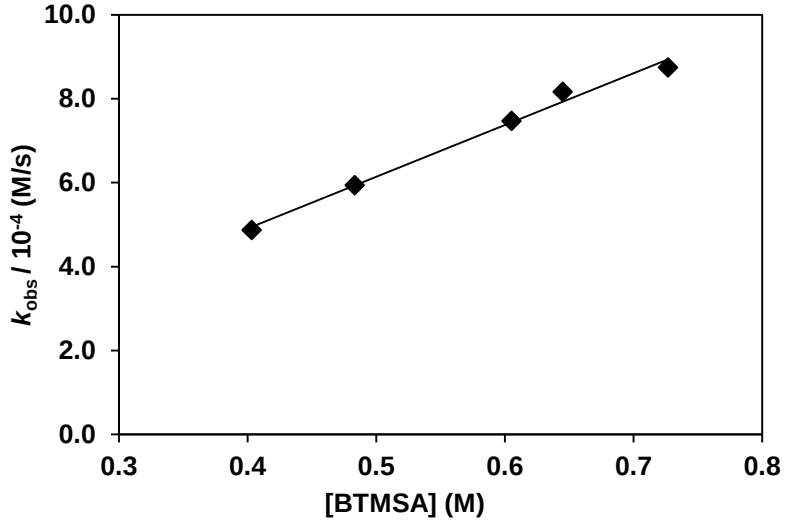

Figure 16. Plot of k_{obs} for reductive elimination from **4** as a function of [BTMSA] at 45 °C.

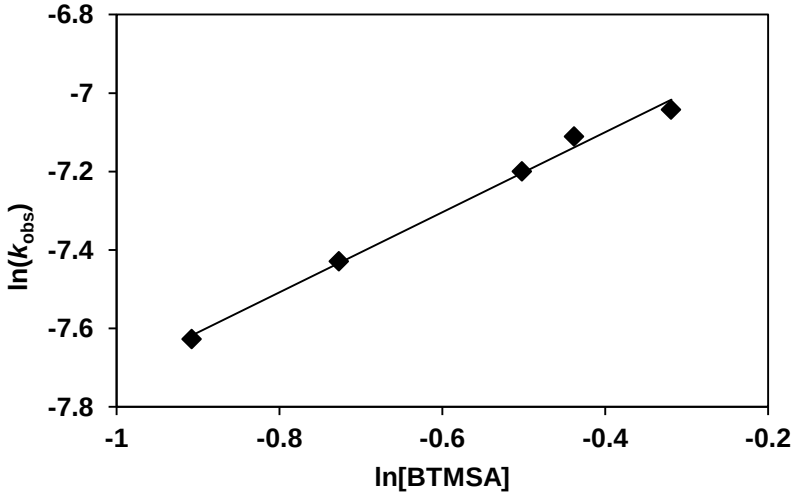

Figure 17. Plot of ln(k_{obs}) vs ln[BTMSA] for **4** at 45 °C, indicating first-order behavior.

Reaction order in bpym with 1 at 150 °C. Complex **1** (0.0065 mmol) and 2,2′-bipyrimidine (0.0020 to 0.0091 mmol) were dissolved in 0.450 mL of mesitylene and 0.050 mL of benzene-d_6 in a J. Young NMR tube. An internal standard, 1,3,5-tris(trifluoromethyl)benzene (0.25 μL), and bis(trimethylsilyl)acetylene (75.0, 0.348 mmol) were added via syringe. The NMR tube was heated to 150 °C in a temperature-controlled oil bath. The rate of reductive elimination was monitored by ^{19}F NMR spectroscopy.

Table 8. Reductive elimination rate as a function of [bpym] for **1** at 150 °C.

equiv bpym	[bpym] (M)	[1/bpym] (M^{-1})	k_{obs} (s^{-1})
0.26	0.0029	340	2.2×10^{-6}
0.35	0.0040	250	1.8×10^{-6}
0.65	0.0074	140	1.0×10^{-6}
0.80	0.0090	110	9.4×10^{-7}
0.90	0.010	98	8.6×10^{-7}
1.4	0.016	63	6.0×10^{-7}

Reaction order in bpym with 2 at 120 °C. Complex **1** (0.0065 mmol), $Si(cat)_2$ (0.033 mmol), and 2,2′-bipyrimidine (0.0017 to 0.0091 mmol) were dissolved in 0.450 mL of fluorobenzene and 0.050 mL of benzene-d_6 in a J. Young NMR tube. An internal standard, 1,3,5-tris(trifluoromethyl)benzene (0.25 μL), and bis(trimethylsilyl)acetylene (75.0 μL, 0.348 mmol) were added via syringe. The NMR tube was heated to 120 °C in a temperature-controlled oil bath. The rate of reductive elimination was monitored by ^{19}F NMR spectroscopy.

Table 9. Reductive elimination rate as a function of [bpym] for **2** at 120 °C.

equiv bpym	[bpym] (M)	[1/bpym] (M^{-1})	k_{obs} (s^{-1})
0.30	0.0034	290	5.8×10^{-5}
0.50	0.0057	180	4.2×10^{-5}
0.60	0.0068	150	4.3×10^{-5}
0.90	0.010	98	3.7×10^{-5}
1.1	0.012	80.	3.4×10^{-5}
1.3	0.015	68	3.2×10^{-5}

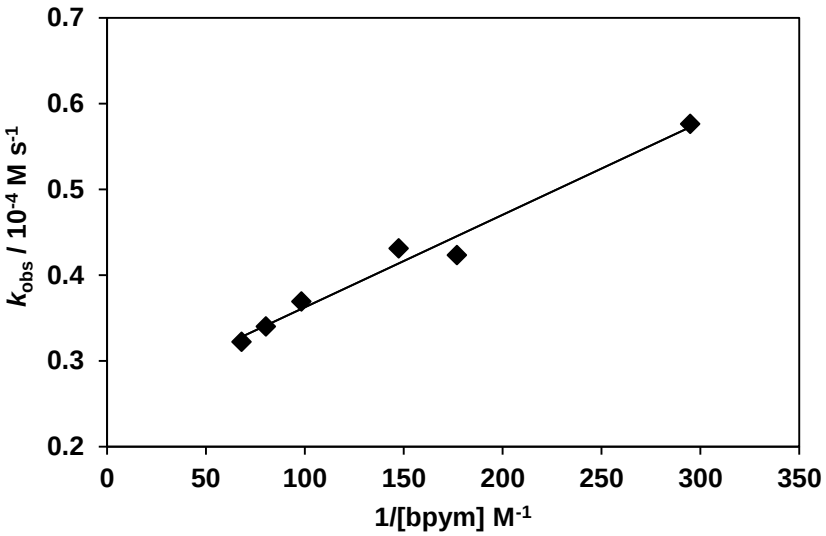

Figure 18. Effect of added bpym on the reductive elimination from **2** at 120 °C.

Reaction order in bpym with 3 at 70 °C. Complex **1** (0.0065 mmol), $Si(cat^F)_2(NCMe)_2$ (0.020 mmol), and 2,2′-bipyrimidine (0.0016 to 0.0072 mmol) were dissolved in 0.450 mL of fluorobenzene and 0.050 mL of benzene-d_6 in a J. Young NMR tube. An internal standard, 1,3,5-tris(trifluoromethyl)benzene (0.25 μL), and bis(trimethylsilyl)acetylene (75.0 μL, 0.348 mmol) were added via syringe. The NMR tube was stored at 0 °C prior to use. The tube was placed in an NMR spectrometer with the temperature pre-equilibrated to 70 °C. After allowing the temperature to equilibrate for two minutes, the rate of reductive elimination was monitored by ^{19}F NMR spectroscopy.

Table 10. Reductive elimination rate as a function of [bpym] for **3** at 70 °C.

equiv bpym	[bpym] (M)	[1/bpym] (M^{-1})	k_{obs} (s^{-1})
0.25	0.0028	350	9.8×10^{-4}
0.50	0.0057	180	6.3×10^{-4}
0.70	0.0079	130	4.4×10^{-4}
0.90	0.010	98	3.8×10^{-4}
1.1	0.012	80	3.2×10^{-4}

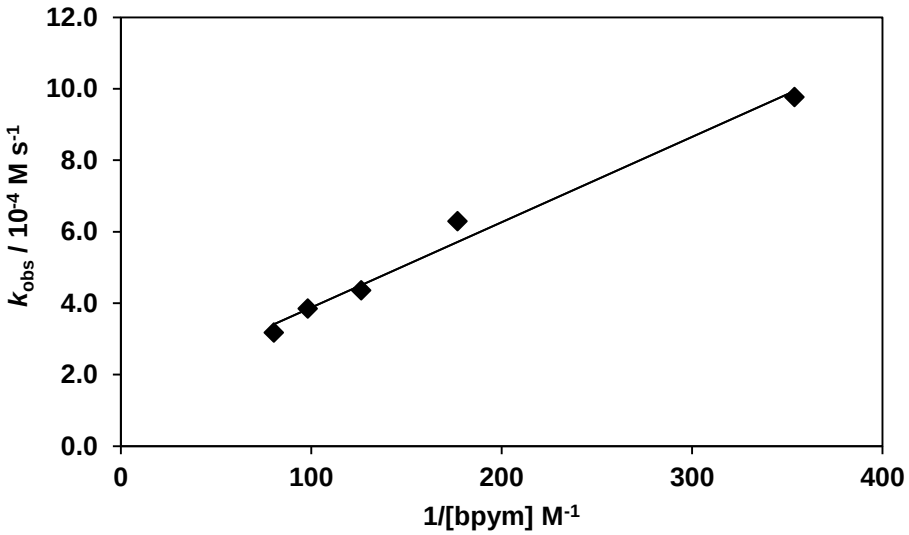

Figure 19. Effect of added bpym on the reductive elimination from **3** at 70 °C.

Eyring analysis for reductive elimination from 1 between 140 – 180 °C. Five J. Young NMR tube samples were prepared, each containing **1** (4.2 mg, 0.0065 mmol) in 0.500 mL of mesitylene-d_{12}. Bis(trimethylsilyl)acetylene (75.0 μL, 0.348 mmol) and 1,3,5-tris(trifluoromethyl)benzene (0.25 μL) as an internal standard were added via syringe to each sample. The NMR tubes were placed in oil baths with temperatures pre-equilibrated between 140 – 180 °C. The rate of disappearance of **1** and biaryl formation was monitored by ^{19}F NMR spectroscopy.

Table 11. Temperature dependence of k_{obs} for biaryl reductive elimination from **1**.

Temp. (°C)	1/T (K^{-1})	k_{obs} (s^{-1})	ln(k/T)
140.	0.00242	5.04×10^{-7}	-20.5
150.	0.00236	1.27×10^{-6}	-19.6
160.	0.00231	2.87×10^{-6}	-18.8
170.	0.00226	8.11×10^{-6}	-17.8
180.	0.00221	1.57×10^{-5}	-17.2

The plot of ln(k/T) as a function of T^{-1} (Figure 5) was fit by a line according to the expression

$$\ln\frac{k}{T} = -\frac{\Delta H^{\neq}}{R}\cdot\frac{1}{T} + \ln\frac{k_B}{h} + \frac{\Delta S^{\neq}}{R}$$

The enthalpy and entropy of activation were extracted from the slope and intercept, respectively. Standard deviations for $\Delta H^{\ddagger}$ and $\Delta S^{\ddagger}$ were evaluated using the LINEST routine in Excel.

Rate acceleration analysis. If the initial pre-equilibrium is fast relative to k_2, changes to k_1 and k_{-1} have no direct role in rate acceleration; their effect is accounted by the changes to the value of $K_{eq.}$ This is the equilibrium effects-only regime.

In this case, if **A** refers to the parent complex **1**, and **B** is the $Si(cat)_2$ adduct **2**:

$$\boldsymbol{k_{obsA} = K_{eqA} k_2}$$
$$\boldsymbol{k_{obsB} = K_{eqB} k_2}$$

The observed rate acceleration is:

$$\frac{\boldsymbol{k_{obsB}}}{\boldsymbol{k_{obsA}}} = \frac{\boldsymbol{K_{eqB} k_2}}{\boldsymbol{K_{eqA} k_2}} = \frac{\boldsymbol{K_{eqB}}}{\boldsymbol{K_{eqA}}}$$

The value of K_{eq} can be evaluated by considering a Boltzmann distribution between products and reactants at the given temperature based on the free energy difference. That is,

$$\boldsymbol{K_{eq} = \frac{e^{-\Delta G/RT}}{1 + e^{-\Delta G/RT}}}$$

Where ΔG is the free energy difference between the products and reactants, R is the gas constant, and T is the temperature in Kelvin.

If the change to ΔG on adding $Si(cat)_2$ is δ, then the rate acceleration is:

$$\frac{\boldsymbol{K_{eqB}}}{\boldsymbol{K_{eqA}}} = \frac{\boldsymbol{e^{-\frac{\Delta G+\delta}{RT}}}}{\boldsymbol{1 + e^{-\frac{\Delta G+\delta}{RT}}}} \frac{\boldsymbol{1 + e^{-\frac{\Delta G}{RT}}}}{\boldsymbol{e^{-\frac{\Delta G}{RT}}}}$$
$$= \frac{\boldsymbol{e^{-\frac{\Delta G}{RT}} e^{-\frac{\delta}{RT}}}}{\boldsymbol{1 + e^{-\frac{\Delta G}{RT}} e^{-\frac{\delta}{RT}}}} \frac{\boldsymbol{1 + e^{-\frac{\Delta G}{RT}}}}{\boldsymbol{e^{-\frac{\Delta G}{RT}}}}$$
$$= \left(\frac{\boldsymbol{1 + e^{-\frac{\Delta G}{RT}}}}{\boldsymbol{1 + e^{-\frac{\Delta G}{RT}} e^{-\frac{\delta}{RT}}}} \right) \boldsymbol{e^{-\frac{\delta}{RT}}}$$

The term in parentheses is approximately 1 as long ΔG and ΔG + δ are at least 3-4 kcal/mol. Based on the DFT calculations, ΔG ~ 20 kcal/mol and δ was experimentally measured to be -3.4 kcal/mol. The rate enhancement due to equilibrium effects for $Si(cat)_2$ is $e^{-\delta/RT} = 77.8$. Thus, of the 1500 fold rate acceleration observed with $Si(cat)_2$, about 80-fold of it may be attributed to equilibrium effects. Therefore, kinetic changes to the equilibration must be responsible for the balance of the rate enhancement (about 20-fold acceleration). We therefore conclude that both changes to the location of the equilibrium position of the first step, as well as changes to the kinetics of the first step give rise to the observed rate acceleration.

REFERENCES

(1) (a) Piers, W. E.; Chivers, T. *Chem. Soc. Rev.* **1997**, *26*, 345. (b) Chivers, T. *J. Fluorine Chem.* **2002**, *115*, 1. (c) Erker, G. *Dalton Trans.* **2005**, 1883.

(2) Chen, E. Y.-X.; Marks, T. J. *Chem. Rev.* **2000**, *100*, 1391.

(3) (a) Kita, M. R.; Miller, A. J. M. *J. Am. Chem. Soc.* **2014**, *136*, 14519. (b) Ouyang, G.-H.; He, Y.-M.; Li, Y.; Xiang, J.-F.; Fan, Q.-H. *Angew. Chem. Int. Ed.* **2015**, *54*, 4334.

(4) (a) Periana, R. A.; Taube, D. J.; Gamble, S.; Taube, H.; Satoh, T.; Fujii, H. *Science*, **1998**, *280*, 560. (b) Hashiguchi, B. G.; Young, K. J. H.; Yousufuddin, M.; Goddard, W. A.; Periana, R. A. *J. Am. Chem. Soc.* **2010**, *132*, 12542. (c) Himeda, Y.; Onozawa-Komatsuzaki, N.; Sugihara, H.; Kasuga, K. *Organometallics* **2007**, *26*, 702. (d) Dixon, N. A.; McQuarters, A. B.; Kraus, J. S.; Soffer, J. B.; Lehnert, N.; Schweitzer-Stenner, R.; Papish, E. T. *Chem Commun.* **2013**, *49*, 5571. (e) Hesp, K. D.; McDonald, R.; Ferguson, M. J.; Schatte, G.; Stradiotto, M. *Chem. Commun.* **2008**, 5645. (f) Hesp, K. D.; McDonald, R.; Ferguson, M. J.; Stradiotto, M. *J. Am. Chem. Soc.* **2008**, *130*, 16394.

(5) (a) Lee, B. Y.; Bazan, G. C.; Vela, J.; Komon, Z. J. A.; Bu, X. *J. Am. Chem. Soc.* **2001**, *123*, 5352. (b) Kim, Y. H.; Kim, T. H.; Lee, B. Y.; Woodmansee, D.; Bu, X.; Bazan, G. C. *Organometallics* **2002**, *21*, 3082. (c) Azoulay, J. D.; Rojas, R. S.; Serrano, A. V.; Ohtaki, H.; Galland, G. B.; Qu, G.; Bazan, G. C. *Angew. Chem. Int. Ed.* **2009**, *48*, 1089. (d) Azoulay, J. D.; Koretz, Z. A.; Wu, G.; Bazan, G. C. *Angew. Chem. Int. Ed.* **2010**, *49*, 7890. (e) Liberman-Martin, A. L.; Bergman, R. G.; Tilley, T. D. *J. Am. Chem. Soc.* **2013**, *135*, 9612. (f) Trofymchuk, O. S.; Gutsulyak, D. V.; Quintero, C.; Parvez, M.; Daniliuc, C. G.; Piers, W. E.; Rojas, R. S. *Organometallics* **2013**, *32*, 7323. (g) Brennan, C.; Draksharapu, A.; Browne, W. R.; McGarvey, J. J.; Vos, J. G.; Pryce, M. T. *Dalton Trans.* **2013**, *42*, 2546. (h) Tseng, K.-N. T.; Kampf, J. W.; Szymczak, N. K. *ACS Catal.* **2015**, *5*, 411.

(6) Allcock, H. R.; Nugent, T. A.; Smeltz, L. A. *Synth. Inorg. Met.-Org. Chem.* **1972**, *2*, 97.

(7) Liberman-Martin, A. L.; Bergman, R. G.; Tilley, T. D. *J. Am. Chem. Soc.* **2015**, *137*, 5328.

(8) Walker, D. A.; Woodman, T. J.; Hughes, D. L.; Bochmann, M. *Organometallics* **2001**, *20*, 3772.

(9) Martin, E.; Spendley, C.; Mountford, A. J.; Coles, S. J.; Horton, P. N.; Hughes, D. L.; Hursthouse, M. B.; Lancaster, S. J. *Organometallics* **2008**, *27*, 1436.

(10) Priqueler, J. R. L.; Butler, I. S.; Rochon, F. D. *Appl. Spec. Rev.* **2006**, *41*, 185.

(11) (a) Sutcliffe, V. F.; Young, G. B. *Polyhedron*, **1984**, *3*, 87. (b) Thomson, S. K.; Young, G. B. *Polyhedron*, **1988**, *7*, 1953. (c) Scott, J. D.; Puddephatt, R. J. *Organometallics* **1986**, *5*, 1538. (d) Braterman, P. S.; Song, J.-I.; Vogler, C.; Kaim, W. *Inorg Chem.* **1992**, *31*, 222. (e) Klein, A.; Kaim, W.; Hornung, F. M.; Fiedler, J.; Zalis, S. *Inorg. Chim. Acta* **1997**,*264*, 269.

(12) (a) Zanello, P.; Corsini, M. *Coord. Chem. Rev.*, **2006**, ***250***, 2000; (b) Broere, D. L. J.; Plessius, R.; van der Vlugt, J. I. *Chem. Soc. Rev.*, **2015**, ***44***, 6886.

(13) (a) Martin, R.; Buchwald, S. L. *Acc. Chem. Res.* **2008**, *41*, 1461. (b) Phapale, V. B.; Cardenas, D. J. *Chem. Soc. Rev.* **2009**, *38*, 1598. (c) Brown, J. M.; Cooley, N. A. *Chem. Rev.* **1988**, *88*, 1031.

(14) (a) Merwin, R. K.; Schnabel, R. C.; Koola, J. D.; Roddick, D. M. *Organometallics* **1992**, *11*, 2972. (b) Korenaga, T.; Abe, K.; Ko, A.; Maenishi, R.; Sakai, T. *Organometallics* **2010**, *29*, 4025. (c) Shiba, Y.; Inagaki, A.; Akita, M. *Organometallics* 2015, **34**, 4844-4853.

(15) Decomposition of the silane adducts **2** and **3** occurs at 140 ^{o}C, with no biaryl reductive elimination observed by ^{1}H or ^{19}F NMR spectroscopy.

(16) (a) Boag, N. M.; Green, M.; Grove, D. M.; Howard, J. A. K.; Spencer, J. L.; Stone, F. G. A. *J. Chem. Soc., Dalton Trans.* **1980**, 2170. (b) Boag, N. M.; Green, M.; Howard, J. A. K.; Stone, F. G. A.; Wadepohl, H. *J. Chem. Soc., Dalton Trans.* **1981**, 862.
(17) Ozawa, F.; Hikida, T.; Hayashi, T. *J. Am. Chem. Soc.* **1994**, *116*, 2844.
(18) Kurosawa, H.; Emoto, M.; Urabe, A.; Miki, K.; Kasai, N. *J. Am. Chem. Soc.* **1985**,*107*, 8253.
(19) (a) Crumpton-Bregel, D. M.; Goldberg, K. I. *J. Am. Chem. Soc.* **2003**,*125*, 9442. (b) Arthur, K. L.; Wang, Q. L.; Bregel, D. M.; Smythe, N. A.; O'Neill, B. A.; Goldberg, K. I.; Moloy, K. G. *Organometallics* **2005**, *24*, 4624.
(20) Hartwig, J. F. Ligand Substitution Reactions. *Organotransition Metal Chemistry: From Bonding to Catalysis.* University Science Books: United States, 2010; pp 217-261.
(21) Sheldrick, G. M. *Acta. Cryst. A* **2008**, *64*, 112.
(22) Spek, A. L. *Acta Cryst.* **2015**,*C71*, 9.
(23) Frisch, M. J.; Trucks, G. W.; Schlegel, H. B.; Scuseria, G. E.; Robb, M. A.; Cheeseman, J. R.; Scalmani, G.; Barone, V.; Mennucci, B.; Petersson, G. A.; Nakatsuji, H.; Caricato, M.; Li, X.; Hratchian, H. P.; Izmaylov, A. F.; Bloino, J.; Zheng, G.; Sonnenberg, J. L.; Hada, M.; Ehara, M.; Toyota, K.; Fukuda, R.; Hasegawa, J.; Ishida, M.; Nakajima, T.; Honda, Y.; Kitao, O.; Nakai, H.; Vreven, T.; Montgomery, J. A., Jr.; Peralta, J. E.; Ogliaro, F.; Bearpark, M.; Heyd, J. J.; Brothers, E.; Kudin, K. N.; Staroverov, V. N.; Kobayashi, R.; Normand, J.; Raghavachari, K.; Rendell, A.; Burant, J. C.; Iyengar, S. S.; Tomasi, J.; Cossi, M.; Rega, N.; Millam, J. M.; Klene, M.; Knox, J. E.; Cross, J. B.; Bakken, V.; Adamo, C.; Jaramillo, J.; Gomperts, R.; Stratmann, R. E.; Yazyev, O.; Austin, A. J.; Cammi, R.; Pomelli, C.; Ochterski, J. W.; Martin, R. L.; Morokuma, K.; Zakrzewski, V. G.; Voth, G. A.; Salvador, P.; Dannenberg, J. J.; Dapprich, S.; Daniels, A. D.; Farkas, O.; Foresman, J. B.; Ortiz, J. V.; Cioslowski, J.; Fox, D. J.; Gaussian 09, revision C.01; Gaussian Inc.: Wallingford, CT, 2010.
(24) Grimme, S.; Ehrlich, S.; Goerigk, L. *J. Comp. Chem.* **2011**, *32*, 1456.
(25) Wadt, W. R.; Hay, P. J. *J. Chem. Phys.* **1985**, *82*, 270, 284. 299.

Chapter 2. Appendix

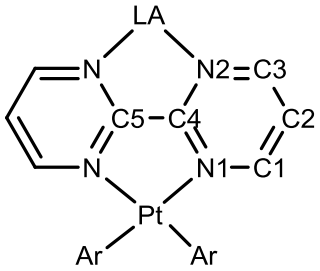

Table A1. Selected bond lengths (in Å) for **1**, **2**, and **4**.

	1	**2**	**4**
Pt–N1	2.103(3)	2.138(2)	2.103(8)
Pt–C6	1.993(3)	1.994(3)	2.005(10)
N2–LA	N/A	2.030(2)	2.145(9)
N1–C1	1.346(4)	1.353(3)	1.369(14)
C1–C2	1.377(4)	1.381(4)	1.362(19)
C2–C3	1.372(4)	1.379(4)	1.383(18)
C3–N2	1.335(4)	1.346(3)	1.348(14)
N2–C4	1.324(4)	1.329(3)	1.320(14)
C4–C5	1.494(4)	1.464(5)	1.489(12)

Table A2. Crystal data and structure refinement for **1**.

Identification code	ALM-III-101	
Empirical formula	'C26.50 H18.50 F6 N4 Pt'	
Formula weight	702.04	
Temperature	100(2) K	
Wavelength	0.71073 Å	
Crystal system	Monoclinic	
Space group	P 21/c	
Unit cell dimensions	a = 18.9500(18) Å	α= 90°.
	b = 9.5863(9) Å	β= 90.839(5)°.
	c = 27.069(3) Å	γ = 90°.
Volume	4916.8(8) $Å^3$	
Z	8	
Density (calculated)	1.897 Mg/m^3	
Absorption coefficient	5.777 mm^{-1}	
F(000)	2700	
Crystal size	0.100 x 0.080 x 0.040 mm^3	
Theta range for data collection	1.505 to 25.470°.	
Index ranges	-22<=h<=22, -11<=k<=11, -30<=l<=32	
Reflections collected	78209	
Independent reflections	9114 [R(int) = 0.0361]	
Completeness to theta = 25.000°	100.0 %	
Absorption correction	Semi-empirical from equivalents	
Max. and min. transmission	0.1560 and 0.1035	
Refinement method	Full-matrix least-squares on F^2	
Data / restraints / parameters	9114 / 0 / 704	
Goodness-of-fit on F^2	1.046	
Final R indices [I>2sigma(I)]	R1 = 0.0194, wR2 = 0.0381	
R indices (all data)	R1 = 0.0250, wR2 = 0.0397	
Extinction coefficient	n/a	
Largest diff. peak and hole	0.930 and -0.520 $e.Å^{-3}$	

Table A3. Crystal data and structure refinement for **2**.

Identification code	ALM-III-81	
Empirical formula	C46 H34 F6 N4 O4 Pt Si	
Formula weight	1043.95	
Temperature	100(2) K	
Wavelength	0.71073 Å	
Crystal system	Monoclinic	
Space group	C 2/c	
Unit cell dimensions	a = 14.1091(4) Å	α= 90°.
	b = 32.5954(8) Å	β= 121.3810(10)°.
	c = 10.4710(3) Å	γ = 90°.
Volume	4111.1(2) $Å^3$	
Z	4	
Density (calculated)	1.687 Mg/m^3	
Absorption coefficient	3.520 mm^{-1}	
F(000)	2064	
Crystal size	0.080 x 0.050 x 0.030 mm^3	
Theta range for data collection	1.249 to 25.343°.	
Index ranges	-15<=h<=16, -39<=k<=39, -11<=l<=12	
Reflections collected	14377	
Independent reflections	3747 [R(int) = 0.0212]	
Completeness to theta = 25.000°	99.3 %	
Absorption correction	Semi-empirical from equivalents	
Max. and min. transmission	0.7452 and 0.6588	
Refinement method	Full-matrix least-squares on F^2	
Data / restraints / parameters	3747 / 12 / 456	
Goodness-of-fit on F^2	1.112	
Final R indices [I>2sigma(I)]	R1 = 0.0191, wR2 = 0.0467	
R indices (all data)	R1 = 0.0203, wR2 = 0.0473	
Extinction coefficient	n/a	
Largest diff. peak and hole	0.952 and -0.334 $e.Å^{-3}$	

Table A4. Crystal data and structure refinement for **4**.

Identification code	ALM-VII-50	
Empirical formula	C34 H14 F16 N4 Pt Zn	
Formula weight	1042.95	
Temperature	100(2) K	
Wavelength	0.71073 Å	
Crystal system	Tetragonal	
Space group	I 41/a	
Unit cell dimensions	a = 30.154(2) Å	α= 90°.
	b = 30.154(2) Å	β= 90°.
	c = 16.1171(14) Å	γ = 90°.
Volume	14654(3) $Å^3$	
Z	16	
Density (calculated)	1.891 Mg/m^3	
Absorption coefficient	4.582 mm^{-1}	
F(000)	7968	
Crystal size	0.080 x 0.060 x 0.060 mm^3	
Theta range for data collection	1.351 to 25.644°.	
Index ranges	-36<=h<=36, -35<=k<=34, -19<=l<=19	
Reflections collected	147948	
Independent reflections	6878 [R(int) = 0.0777]	
Completeness to theta = 25.000°	100.0 %	
Absorption correction	Semi-empirical from equivalents	
Max. and min. transmission	0.2171 and 0.1707	
Refinement method	Full-matrix least-squares on F^2	
Data / restraints / parameters	6878 / 0 / 505	
Goodness-of-fit on F^2	1.087	
Final R indices [I>2sigma(I)]	R1 = 0.0676, wR2 = 0.1344	
R indices (all data)	R1 = 0.0882, wR2 = 0.1472	
Extinction coefficient	n/a	
Largest diff. peak and hole	2.438 and -2.132 $e.Å^{-3}$	

DFT results

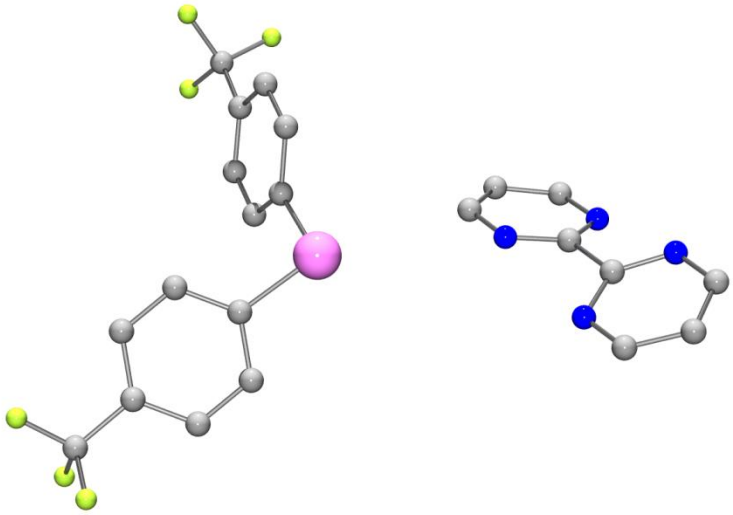

Figure A1. Transition state for bpym dissociation from **1**.

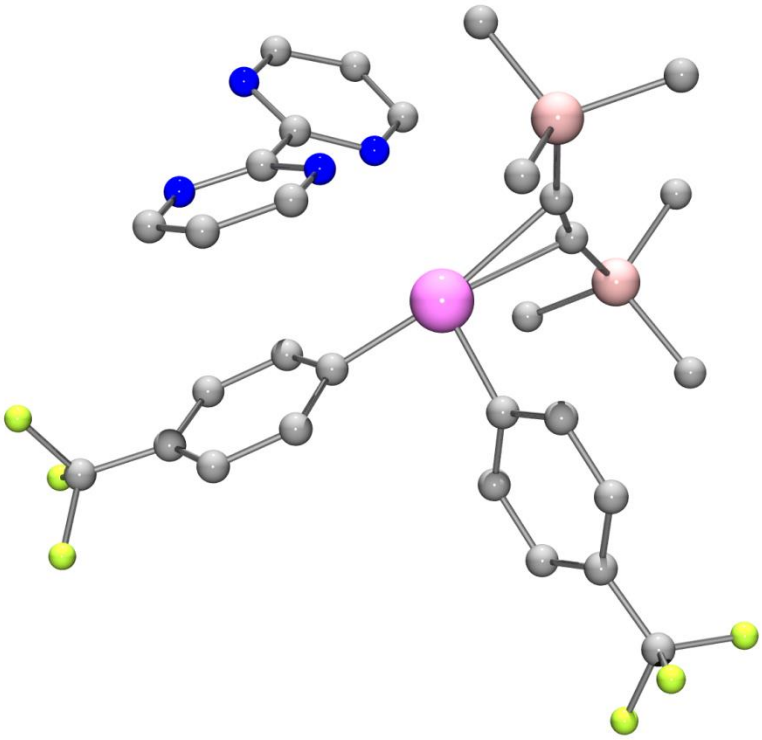

Figure A2. Transition state for associative interchange of BTMSA for bpym from **1**.

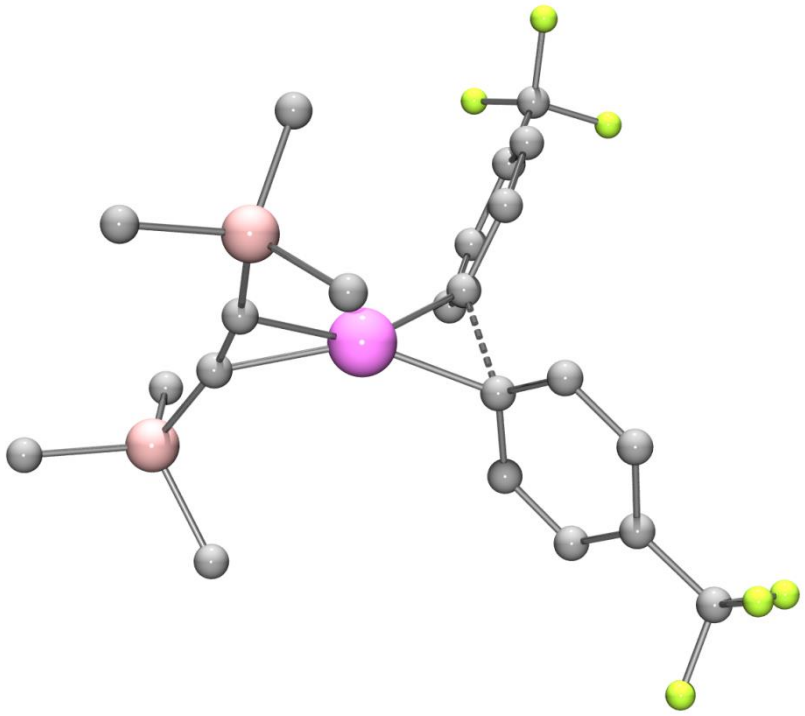

Figure A3. Transition state for biaryl reductive elimination from (η^2-$Me_3SiCCSiMe_3$)$PtAr_2$.

Bipyrimidine

Symbolic Z-matrix:
Charge = 0 Multiplicity = 1

C	-4.43834	-0.74121	-0.00768
C	-2.33238	0.46141	-0.00768
C	-3.01847	1.6757	-0.01044
C	-4.41312	1.6838	-0.01179
C	-5.17877	-2.00165	-0.00643
C	-5.45555	-4.27957	-0.79117
C	-6.59853	-4.41863	-0.00409
C	-7.03297	-3.35147	0.78175
H	-1.23253	0.45133	-0.00441
H	-2.4615	2.62375	-0.01154
H	-4.95741	2.63958	-0.01618
H	-5.11141	-5.11836	-1.4139
H	-7.15543	-5.36672	-0.00318
H	-7.93272	-3.45836	1.40532
N	-4.7474	-3.07967	-0.79292
N	-3.03593	-0.74121	-0.00768
N	-6.32974	-2.14864	0.78117
N	-5.12108	0.48374	-0.00898

Zero-point correction = 0.133812 (Hartree/Particle)
Thermal correction to Energy = 0.142386
Thermal correction to Enthalpy = 0.143330
Thermal correction to Gibbs Free Energy = 0.098709
Sum of electronic and zero-point Energies = -527.382930
Sum of electronic and thermal Energies = -527.374356
Sum of electronic and thermal Enthalpies = -527.373412
Sum of electronic and thermal Free Energies = -527.418033

Bis(trimethylsilyl)acetylene

Symbolic Z-matrix:
Charge = 0 Multiplicity = 1

C	-4.51642	-1.33212	0
C	-3.31522	-1.33212	0
Si	-6.45642	-1.33212	0
Si	-1.37522	-1.33212	0
C	-0.72856	-2.29836	1.553
H	0.34144	-2.30004	1.55195
H	-1.08361	-1.82188	2.44284
H	-1.08684	-3.30607	1.52076
C	-0.72856	-2.19393	-1.61329
H	-1.08529	-1.66106	-2.46984
H	0.34144	-2.19386	-1.61333
H	-1.08515	-3.20222	-1.6465
C	-0.72856	0.49594	0.06029
H	0.34144	0.49588	0.06224
H	-1.08363	1.02833	-0.79726
H	-1.08682	0.97187	0.94913
C	-7.10309	-0.47343	1.61496
H	-6.74639	0.53475	1.65018
H	-8.17309	-0.47339	1.61493
H	-6.74646	-1.00804	2.47047
C	-7.10309	-0.36287	-1.55112
H	-6.74639	-0.83645	-2.44184
H	-8.17309	-0.3629	-1.55114
H	-6.74645	0.64533	-1.5159
C	-7.10309	-3.16005	-0.06383
H	-6.74809	-3.63303	-0.95555
H	-6.74476	-3.69519	0.79064
H	-8.17309	-3.16012	-0.06179

Zero-point correction = 0.232712 (Hartree/Particle)
Thermal correction to Energy = 0.249456
Thermal correction to Enthalpy = 0.250401
Thermal correction to Gibbs Free Energy = 0.189327

Sum of electronic and zero-point Energies = -894.580070
Sum of electronic and thermal Energies = -894.563326
Sum of electronic and thermal Enthalpies = -894.562382
Sum of electronic and thermal Free Energies = -894.623455

(bpym)$PtAr_2$ (1)

Symbolic Z-matrix:
Charge = 0 Multiplicity = 1

C	1.45872	0.422	0.01712
C	2.41862	0.38508	-1.02035
H	2.29361	-0.31653	-1.84007
C	3.52238	1.24163	-1.02809
H	4.24687	1.19718	-1.83354
C	3.6988	2.1568	0.01628
C	2.7537	2.2258	1.04932
H	2.88877	2.93948	1.85423
C	1.64932	1.37371	1.04257
H	0.91838	1.45067	1.83914
C	-1.32577	0.69059	0.01774
C	-1.33026	1.66445	-1.00439
H	-0.59345	1.60585	-1.797
C	-2.25505	2.70914	-1.01093
H	-2.24336	3.44613	-1.80584
C	-3.19064	2.82285	0.0265
C	-3.19571	1.88477	1.06567
H	-3.90511	1.98614	1.87947
C	-2.27301	0.83606	1.05753
H	-2.27843	0.12604	1.87955
C	4.83751	3.1077	-0.01306
C	-4.22528	3.88529	-0.01348
C	0.38038	-3.85102	0.03835
C	2.43765	-2.75464	0.17473
H	2.96589	-1.81109	0.19398
C	3.07622	-3.99139	0.24462
H	4.15317	-4.05375	0.32958
C	2.27918	-5.1397	0.2024
H	2.70545	-6.13428	0.25105
C	-1.0815	-3.70972	-0.06312
C	-2.89337	-2.23999	-0.16564
H	-3.23379	-1.21331	-0.15919
C	-3.75462	-3.33123	-0.26478
H	-4.8237	-3.18615	-0.34801
C	-3.18975	-4.61051	-0.25431
H	-3.79662	-5.5047	-0.32772
N	1.09011	-2.68253	0.06725

N	0.93472	-5.06936	0.10069
N	-1.55658	-2.4274	-0.06189
N	-1.85663	-4.79889	-0.15398
F	4.53329	4.30922	-0.66504
F	5.26416	3.47002	1.26536
F	5.9494	2.58784	-0.6799
F	-4.6306	4.28717	1.26018
F	-3.79916	5.02858	-0.68692
F	-5.39778	3.47501	-0.66756
Pt	-0.07228	-0.88168	0.01406

Zero-point correction = 0.325994 (Hartree/Particle)
Thermal correction to Energy = 0.353441
Thermal correction to Enthalpy = 0.354386
Thermal correction to Gibbs Free Energy = 0.260248
Sum of electronic and zero-point Energies = -1783.921056
Sum of electronic and thermal Energies = -1783.893608
Sum of electronic and thermal Enthalpies = -1783.892664
Sum of electronic and thermal Free Energies = -1783.986802

(bpym)PtAr$_2$ (dissociative TS)

Symbolic Z-matrix:
Charge = 0 Multiplicity = 1

C	-1.9366	-1.32169	0.22338
C	-3.15528	-0.80983	0.69084
H	-3.18367	0.12612	1.23521
C	-4.33781	-1.5136	0.4594
H	-5.27994	-1.12165	0.82629
C	-4.30823	-2.72716	-0.23376
C	-3.09577	-3.23622	-0.70906
H	-3.07455	-4.17495	-1.25287
C	-1.91148	-2.5317	-0.49063
H	-0.97863	-2.9272	-0.88181
C	-0.76458	1.40295	0.3852
C	-0.44909	2.30864	1.41645
H	0.01964	1.96261	2.33189
C	-0.74744	3.66305	1.2647
H	-0.50527	4.36221	2.05867
C	-1.37686	4.1148	0.09958
C	-1.71092	3.21345	-0.91606
H	-2.20793	3.56617	-1.81281
C	-1.41123	1.85786	-0.77342
H	-1.67871	1.16048	-1.55832
C	-5.58006	-3.47135	-0.52655

C	-1.64378	5.58523	-0.05819
C	5.66661	-1.4792	-0.15048
C	5.51142	-3.69709	0.34234
H	4.88624	-4.58353	0.42831
C	6.8796	-3.74765	0.60788
H	7.37046	-4.6654	0.91256
C	7.58026	-2.55049	0.46162
H	8.64927	-2.49331	0.65618
C	4.98921	-0.2117	-0.57984
C	3.08813	1.04225	-0.6777
H	2.0433	1.14007	-0.38945
C	3.76154	2.0485	-1.36585
H	3.26736	2.96316	-1.67384
C	5.11362	1.81185	-1.62184
H	5.72253	2.53934	-2.15451
N	4.89577	-2.57124	-0.03048
N	6.9862	-1.41639	0.08013
N	3.68461	-0.0913	-0.29756
N	5.73564	0.69641	-1.22604
F	-6.00138	-3.27424	-1.80779
F	-5.43148	-4.81386	-0.38049
F	-6.60104	-3.09308	0.27921
F	-2.47885	5.85719	-1.08853
F	-2.19576	6.12681	1.05874
F	-0.49623	6.28382	-0.28993
Pt	-0.20885	-0.46746	0.57132

Zero-point correction = 0.322808 (Hartree/Particle)
Thermal correction to Energy = 0.349270
Thermal correction to Enthalpy = 0.350214
Thermal correction to Gibbs Free Energy = 0.255693
Sum of electronic and zero-point Energies = -1783.836882
Sum of electronic and thermal Energies = -1783.810419
Sum of electronic and thermal Enthalpies = -1783.809475
Sum of electronic and thermal Free Energies = -1783.903996

(bpym)(η^2-$Me_3SiCCSiMe_3$)$PtAr_2$ (associative TS)

Symbolic Z-matrix:
Charge = 0 Multiplicity = 1

C	-1.84674	0.70556	0.09654
C	-2.07386	1.65367	-0.91963
H	-1.30021	1.85981	-1.64728
C	-3.28648	2.34245	-0.99596
H	-3.4531	3.06542	-1.7854
C	-4.28552	2.10799	-0.0436

C	-4.06572	1.18186	0.98486
H	-4.83396	1.01074	1.73087
C	-2.85629	0.49041	1.05481
H	-2.69622	-0.21989	1.85573
C	0.86522	1.31257	-0.05265
C	0.69493	2.45775	0.7551
H	-0.11033	2.48441	1.47991
C	1.56378	3.54391	0.66169
H	1.44194	4.40366	1.31117
C	2.60507	3.52318	-0.27653
C	2.74622	2.43309	-1.14305
H	3.54528	2.42536	-1.87475
C	1.87763	1.34519	-1.03371
H	2.00979	0.4961	-1.69597
C	-5.60828	2.7713	-0.15493
C	3.6345	4.58859	-0.24887
C	3.29034	-0.95272	0.51279
C	2.03762	-0.39294	2.37958
H	1.16363	-0.64239	2.96911
C	2.90861	0.66074	2.65021
H	2.7561	1.32126	3.49319
C	3.96999	0.85539	1.75774
H	4.64705	1.69552	1.85484
C	3.46265	-1.86296	-0.64032
C	2.48335	-3.15121	-2.28351
H	1.57443	-3.46597	-2.7826
C	3.73882	-3.63171	-2.6641
H	3.85021	-4.34825	-3.46807
C	4.84474	-3.13877	-1.96703
H	5.85565	-3.4468	-2.20813
N	2.21285	-1.18117	1.29375
N	4.18409	0.03599	0.70535
N	2.33662	-2.2602	-1.28025
N	4.71451	-2.25777	-0.95186
F	-6.58431	1.93854	-0.72008
F	-6.11958	3.15044	1.08828
F	-5.57316	3.91519	-0.94829
F	4.28882	4.74992	-1.4669
F	3.12122	5.83357	0.11156
F	4.64614	4.31483	0.69386
Pt	-0.19096	-0.38525	0.19258
C	-1.35727	-2.28437	-0.47552
C	-1.10633	-2.50682	0.72821
Si	-1.9694	-2.2772	-2.25302
Si	-0.91414	-3.26575	2.43022
C	-3.71519	-1.51755	-2.30401

C	-2.04001	-4.11316	-2.78204
C	-0.74663	-1.28442	-3.32659
C	0.81296	-4.05691	2.44931
C	-2.25855	-4.61528	2.58094
C	-1.19966	-1.98891	3.8272
H	-4.42473	-2.14197	-1.75192
H	-3.72288	-0.51671	-1.87015
H	-4.05616	-1.44634	-3.34346
H	-1.05063	-4.58024	-2.72755
H	-2.71698	-4.67109	-2.12702
H	-2.40709	-4.19803	-3.81112
H	0.28635	-1.50473	-3.05315
H	-0.89858	-1.50334	-4.38946
H	-0.90786	-0.21468	-3.16377
H	-0.48501	-1.15939	3.90575
H	-2.19128	-1.53497	3.72649
H	-1.17408	-2.53263	4.77988
H	-2.1778	-5.12474	3.548
H	-3.26191	-4.18449	2.50033
H	-2.13868	-5.35916	1.78681
H	0.81667	-4.91828	1.77229
H	1.53797	-3.33426	2.07729
H	1.09923	-4.39906	3.44929

Zero-point correction = 0.556210 (Hartree/Particle)
Thermal correction to Energy = 0.603073
Thermal correction to Enthalpy = 0.604017
Thermal correction to Gibbs Free Energy = 0.474965
Sum of electronic and zero-point Energies = -2678.475460
Sum of electronic and thermal Energies = -2678.428598
Sum of electronic and thermal Enthalpies = -2678.427653
Sum of electronic and thermal Free Energies = -2678.556706

(η^2-$Me_3SiCCSiMe_3$)$PtAr_2$

Charge = 0 Multiplicity = 1

C	0.63790	0.90980	-0.23214
C	0.25022	1.99502	0.56730
H	-0.48738	1.86207	1.34890
C	0.81412	3.25522	0.36009
H	0.51571	4.08873	0.98670
C	1.74767	3.44650	-0.66184
C	2.11974	2.37203	-1.47615
H	2.84117	2.51853	-2.27337
C	1.56883	1.10917	-1.26254
H	1.87786	0.28124	-1.88753

C	-1.88023	-0.31240	0.16802
C	-2.46322	0.52253	-0.80333
H	-1.84536	0.95564	-1.58253
C	-3.82798	0.81024	-0.78878
H	-4.25905	1.44993	-1.55160
C	-4.64076	0.28304	0.21952
C	-4.08548	-0.53800	1.20561
H	-4.71299	-0.94030	1.99427
C	-2.72052	-0.82571	1.17631
H	-2.30663	-1.45729	1.95874
C	2.39793	4.78447	-0.85877
C	-6.11807	0.54779	0.21927
F	3.61208	4.85703	-0.23968
F	2.62685	5.05748	-2.16945
F	1.65445	5.80376	-0.36306
F	-6.62622	0.64466	1.47573
F	-6.44305	1.69391	-0.42941
F	-6.81602	-0.45128	-0.39489
Pt	0.02489	-0.92872	0.14890
C	2.08797	-1.73299	0.77736
C	1.79190	-2.30233	-0.29446
Si	2.86107	-0.96945	2.29476
Si	1.59111	-3.31844	-1.84163
C	3.71892	0.61055	1.74990
C	4.09257	-2.22420	2.96982
C	1.49241	-0.62165	3.53487
C	-0.02229	-4.26955	-1.66508
C	3.07160	-4.47462	-1.95759
C	1.51679	-2.14499	-3.30867
H	4.47040	0.40740	0.98011
H	3.00512	1.33150	1.34323
H	4.22567	1.07501	2.60382
H	3.59212	-3.15662	3.25178
H	4.86130	-2.46260	2.22710
H	4.59400	-1.82664	3.85986
H	0.96867	-1.54147	3.81582
H	1.90522	-0.17372	4.44612
H	0.75719	0.06987	3.11289
H	0.67309	-1.45493	-3.20839
H	2.43627	-1.55781	-3.40398
H	1.38427	-2.71111	-4.23780
H	2.99331	-5.10881	-2.84823
H	4.00733	-3.90978	-2.02564
H	3.13276	-5.12787	-1.08088
H	-0.01004	-4.91351	-0.77937
H	-0.86977	-3.58093	-1.57640

H	-0.19515	-4.90419	-2.54176

Zero-point correction = 0.423269 (Hartree/Particle)
Thermal correction to Energy = 0.460443
Thermal correction to Enthalpy = 0.461388
Thermal correction to Gibbs Free Energy = 0.346592
Sum of electronic and zero-point Energies = -2151.084172
Sum of electronic and thermal Energies = -2151.046998
Sum of electronic and thermal Enthalpies = -2151.046053
Sum of electronic and thermal Free Energies = -2151.160849

(η^2-$Me_3SiCCSiMe_3$)$PtAr_2$ (reductive elimination TS)

Charge = 0 Multiplicity = 1

C	1.03932	-0.9283	0.00888
C	1.4281	-1.54312	1.2194
H	1.16469	-1.088	2.16718
C	2.141	-2.73669	1.22392
H	2.41354	-3.20004	2.16572
C	2.49944	-3.34464	0.0163
C	2.14548	-2.73976	-1.19599
H	2.42154	-3.20665	-2.13576
C	1.43427	-1.54675	-1.19924
H	1.17516	-1.09412	-2.14939
C	1.03316	0.93423	0.00654
C	1.42544	1.55214	-1.20275
H	1.17026	1.09543	-2.15199
C	2.12939	2.74941	-1.20171
H	2.40382	3.21553	-2.14236
C	2.4783	3.35956	0.00949
C	2.12233	2.75251	1.21821
H	2.39113	3.21976	2.15913
C	1.41693	1.55441	1.21588
H	1.15584	1.09971	2.16449
C	3.31116	-4.60553	0.0065
C	3.28141	4.62591	-0.00348
F	2.92621	-5.45536	-0.98172
F	4.63691	-4.36189	-0.20006
F	3.22396	-5.28819	1.17498
F	3.19966	5.3047	1.16755
F	4.60689	4.39205	-0.22254
F	2.88208	5.47586	-0.98603
Pt	-0.82695	-0.00289	0.00164
C	-2.87523	-0.00552	0.62671
C	-2.87171	-0.00984	-0.6353
Si	-3.28986	-0.00067	2.44086
Si	-3.2768	-0.01836	-2.45158

C	-2.53134	-1.55286	3.18416
C	-5.16574	0.00378	2.60787
C	-2.52475	1.55106	3.17832
C	-2.51394	1.53147	-3.19529
C	-5.15181	-0.02295	-2.6285
C	-2.50851	-1.57264	-3.18029
H	-2.96788	-2.45515	2.74332
H	-1.45346	-1.57886	2.99484
H	-2.6947	-1.58839	4.26729
H	-5.59972	0.88988	2.1325
H	-5.60359	-0.88243	2.13628
H	-5.46175	0.00667	3.66329
H	-2.95355	2.4535	2.73028
H	-2.69265	1.59396	4.2605
H	-1.44594	1.56922	2.99366
H	-1.43101	-1.59172	-2.98814
H	-2.94156	-2.4734	-2.73293
H	-2.66912	-1.61809	-4.26346
H	-5.44218	-0.02805	-3.68547
H	-5.58819	-0.90815	-2.15367
H	-5.59228	0.86415	-2.16103
H	-2.95099	2.43522	-2.75802
H	-1.4367	1.55677	-3.00242
H	-2.67349	1.56479	-4.27907

Zero-point correction = 0.421765 (Hartree/Particle)
Thermal correction to Energy = 0.458529
Thermal correction to Enthalpy = 0.459473
Thermal correction to Gibbs Free Energy = 0.344986
Sum of electronic and zero-point Energies = -2151.061284
Sum of electronic and thermal Energies = -2151.024520
Sum of electronic and thermal Enthalpies = -2151.023575
Sum of electronic and thermal Free Energies = -2151.138063

Chapter 3. Lewis Acid-Base Interactions between Platinum(II) Diaryl Complexes and Bis(perfluorophenyl)Zinc: Reductive Elimination Induced by a Z-Type Ligand

INTRODUCTION

Understanding the interaction of a transition metal with its surrounding ligands is a central focus of organometallic chemistry. The vast majority of ligands are Lewis bases that interact with transition metal centers by the donation of electron density. In fewer cases, Lewis basic transition metals can coordinate to Lewis acids (termed Z-type ligands) to form retro-dative σ-bonding interactions.[1] Often, the Lewis acidic component is incorporated into a multi-dentate ligand to favor coordination.[2] There are relatively few examples of unsupported Z-type interactions, particularly those featuring metal–metal bonds, termed metal-only Lewis pairs.[3]

Although Group 13 elements (B, Al, Ga) feature prominently in reports of Z-type ligands, interactions of this type with Group 12 elements (Zn, Cd, Hg) remain rare.[3,4] To our knowledge, there are no examples of Z-type bonds featuring organozinc complexes. Transient Pd–Zn interactions during the Negishi reaction have been proposed to lower the energy barrier of transmetalation for organozinc complexes relative to analogous organotin reagents.[5] These heterobimetallic intermediates have also been proposed to lead to undesirable *cis*/*trans* isomerization of $L_2PdR^1R^2$ complexes (R^1,R^2 = alkyl or aryl) and secondary transmetalation events to form homocoupling products under Negishi cross-coupling conditions.[6] Understanding the binding motifs and reactivity of organozinc complexes with Group 10 organometallic complexes has the potential to provide insight into the behavior of these proposed intermediates.

Herein, we report binding of the organozinc Lewis acid bis(perfluorophenyl)zinc, $ZnAr^F_2$, to platinum(II) diaryl complexes supported by 1,10-phenanthroline (phen), 2,2′-bipyridine (bpy), and bis(dimethylphosphino)ethane (dmpe) ligands. In the solid state, the nature of the Pt–Zn interaction is found to depend on the chelating ligand, such that the (phen)$PtAr_2$ complex has an unsupported Pt–Zn bond while the dmpe complex features a Pt–Zn contact bridged by the aryl ligands. In solution, facile reductive elimination is promoted by zinc coordination for complexes with phen or bpy ligands, whereas aryl exchange occurs between platinum and zinc for the dmpe-supported bimetallic complex.

RESULTS AND DISCUSSION

The $ZnAr^F_2$ Lewis acid was selected for its expected potent Lewis acidity due to incorporation of fluorinated substituents.[7] Addition of $ZnAr^F_2(\eta^2$-toluene)[8] to a solution of (phen)$PtAr_2$ (**1**, Ar = 4-*tert*-butylphenyl) led to immediate formation of the heterobimetallic compound (phen)$PtAr_2(ZnAr^F_2)$ (**2**, eq 1). In contrast, no interaction was observed between **1** and $ZnBr_2$ or $Zn(OC_6F_5)_2$ (in benzene-d_6 by ^{1}H and ^{19}F NMR spectroscopy). Yellow crystals of **2** were formed by vapor diffusion of pentane into a toluene solution at -35 °C. Treatment of (bpy)$PtAr_2$ (**3**, Ar = 4-*tert*-butylphenyl) with $ZnAr^F_2(\eta^2$-toluene) allowed isolation of an analogous (bpy)$PtAr_2(ZnAr^F_2)$ adduct (**4**).

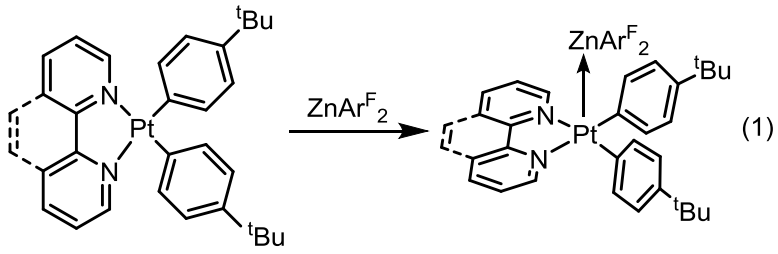

(phen)$PtAr_2$ (**1**)
(bpy)$PtAr_2$ (**3**)

(phen)$PtAr_2(ZnAr^F_2)$ (**2**)
(bpy)$PtAr_2(ZnAr^F_2)$ (**4**)

X-ray crystallographic studies confirmed the presence of an unsupported platinum–zinc interaction in **2** (Figure 1), with the zinc center occupying the apical site of a square pyramidal platinum complex. The platinum–zinc distance of 2.5526(5) Å is longer than the distance in the recently reported [$(Cy_3P)_2$Pt–$ZnBr_2$] complex[9] (2.4040(6) Å) but is on the shorter end of the known range for known platinum–zinc interactions (~2.34–3.00 Å).[10] The zinc-bound perfluorophenyl ligands of **2** are significantly bent away from the platinum center, with a C–Zn–C angle of 134.8°.

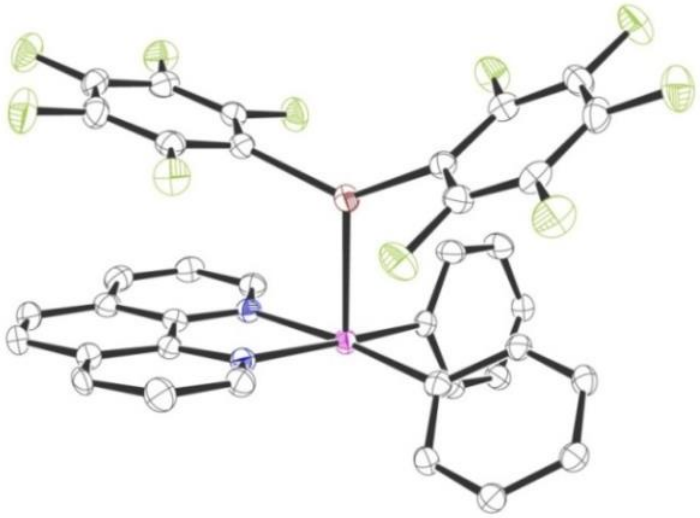

Figure 1. Molecular structure of **2**, with *p*-^{t}Bu groups and hydrogen atoms omitted for clarity and thermal ellipsoids shown at 50 %.

NMR characterization confirmed that the platinum–zinc interaction persists in benzene-d_6 solution at 25 °C. The ^{1}H NMR signal for the *ortho*-aryl protons was shifted upfield, and the $^2J(^{195}Pt–^1H)$ coupling constant decreases upon zinc binding (8.19 ppm, J_{PtH} = 69 Hz for **1**; 7.67 ppm, J_{PtH} = 50 Hz for **2**). Similar trends were observed for copper(I) and silver(I) triflate binding to organoplatinum(II) complexes.[11] There is a minor change in the ^{195}Pt NMR chemical shift upon $ZnAr^F_2$ binding (δ =-3355 ppm for **1** and -3167 ppm for **2**).[12] The bpy derivatives **3** and **4** exhibited similar chemical shift and coupling constant perturbations upon zinc binding (see Experimental Section).

To probe the effect of the platinum-bound chelating ancillary ligand on zinc coordination, the dmpe analogue was selected for comparison. Treatment of a solution of (dmpe)$PtAr_2$ (**5**, Ar = 4-*tert*-butylphenyl) with $ZnAr^F_2(\eta^2$-toluene) led to the zinc adduct (dmpe)$PtAr_2(ZnAr^F_2)$ (**6**, eq 2). Colorless crystals of **6** were isolated by vapor diffusion of pentane into a toluene solution at -35 °C.

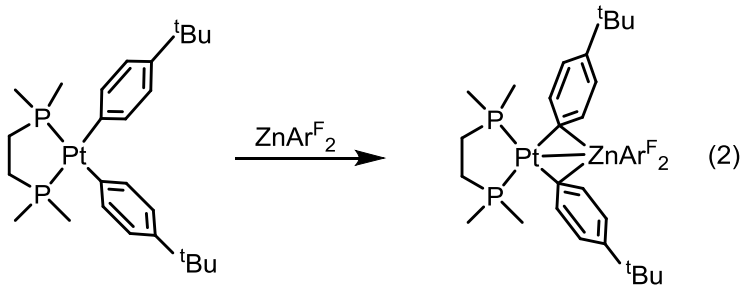

X-ray crystallographic studies revealed a different binding mode of zinc in **6** compared with that in **2** (Figure 2). Rather than occupying the apical position, the zinc atoms adopts a position near the *ipso* carbon atoms of the 4-*tert*-butylphenyl groups, and 0.895 Å above the least-squares platinum square plane.[13] The platinum–zinc distance of 2.7368(4) Å in **6** is significantly longer than the distance in **2** (2.5526(5) Å). The *tert*-butylphenyl groups are unsymmetrically bridging between the platinum and zinc centers, as evidenced by close contacts between the zinc and the *ipso* carbon atoms (2.307(4) and 2.367(4) Å) and the tilting of the aryl rings (Pt–C_{ipso}–C_{para} angles of ~163°).

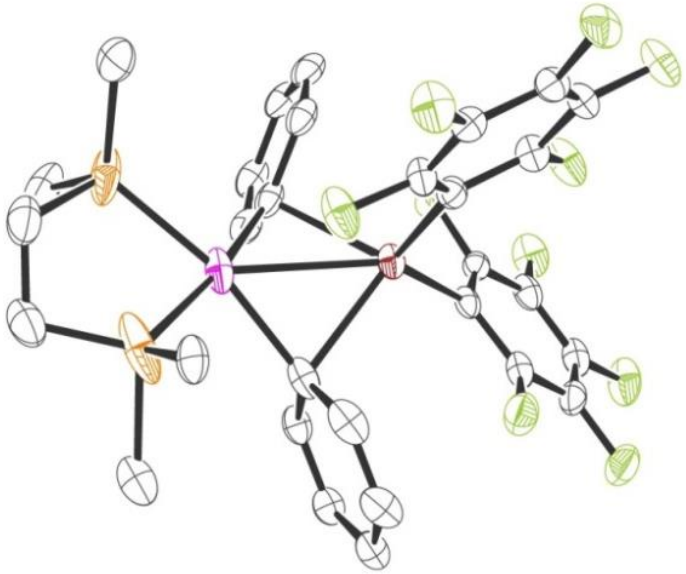

Figure 2. Molecular structure of **6**, with *p*-^{t}Bu groups and hydrogen atoms omitted for clarity and thermal ellipsoids shown at 50 %.

Complex **6** remains intact in benzene-d_6 solution at 25 °C. The *ortho*-aryl ^{1}H NMR signal is shifted downfield upon zinc coordination, from 7.85 ppm in **5** to 8.03 ppm for **6**, and the $^2J(^{195}\text{Pt}–^1\text{H})$ coupling constant decreases from 57 Hz to 42 Hz. The $^{31}\text{P}\{^1\text{H}\}$ NMR chemical shift is relatively insensitive to zinc binding (δ = 21.2 and 29.4 ppm for **5** and **6**, respectively); however, the $J(^{195}\text{Pt}–^{31}\text{P})$ coupling constant increases significantly upon zinc coordination (J_{PtP} = 1630 Hz for **5** and 2142 Hz for **6**). This increase in the $J(^{195}\text{Pt}–^{31}\text{P})$ coupling constant is consistent with a weaker *trans* influence of the aryl groups upon interaction with zinc.[14] There is a small change in ^{195}Pt chemical shift between **5** and **6** (δ = -4506 and -4544 ppm, respectively).

To investigate the effect of zinc binding on reactivity, a solution of (phen)$PtAr_2(ZnAr^F_2)$ (**2**) was heated to 60 °C in benzene-d_6, resulting in quantitative biaryl reductive elimination within 15 minutes, along with formation of Pt(0) and (phen)$ZnAr^F_2$ byproducts (eq 3). In the absence of added $ZnAr^F_2$, reductive elimination did not proceed from (phen)$PtAr_2$ (**1**) over 48 hours at 200 °C, demonstrating that the zinc substituent dramatically accelerates reductive elimination.

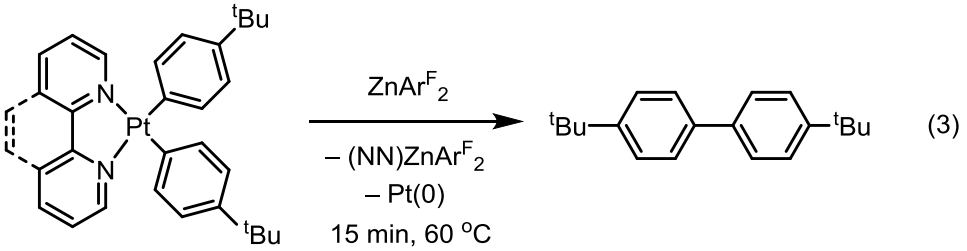

(3)

Quantitative reductive elimination was also observed upon heating (bpy)$PtAr_2(ZnAr^F_2)$ (**4**) for 15 minutes at 60 °C in benzene-d_6. The thermolysis of (bpy)$PtAr_2$ (**3**) in the absence of additives at 150 °C has previously been reported to form *tert*-butylbenzene and a platinum–bipyridine polymer.[15] These products are generated by a roll-over cyclometalation reaction, which proceeds by dissociation and rotation of one pyridyl group, followed by C–H activation at the remote C3 pyridyl position.[16] In the current work, addition of $ZnAr^F_2$ switches the reaction selectivity to produce a biaryl rather than arene product.

Coordination of additives to Group 10 metals has been proposed to reduce electron density at the metal center and thereby facilitate reductive elimination.[17] A range of activators have been employed to promote reductive elimination, including electron-withdrawing olefins, Brønsted acids, alkyl halides, and strong oxidants.[18] The current work represents a rare example of reductive elimination promoted by a dative, heterobimetallic interaction.

In contrast to the phen- and bpy-containing complexes, for (dmpe)$PtAr_2(ZnAr^F_2)$ (**6**), there is aryl exchange between platinum and zinc to produce exclusively (dmpe)$Pt(C_6F_5)_2$ and $Zn(4\text{-}^t\text{Bu-Ph})_2$ at 60 °C (eq 4). There is no evidence of an interaction between (dmpe)$Pt(C_6F_5)_2$ and either $ZnAr^F_2$ or $Zn(4\text{-}^t\text{Bu-Ph})_2$, suggesting that the platinum center exhibits diminished nucleophilic character due to the perfluorinated aryl substituents.

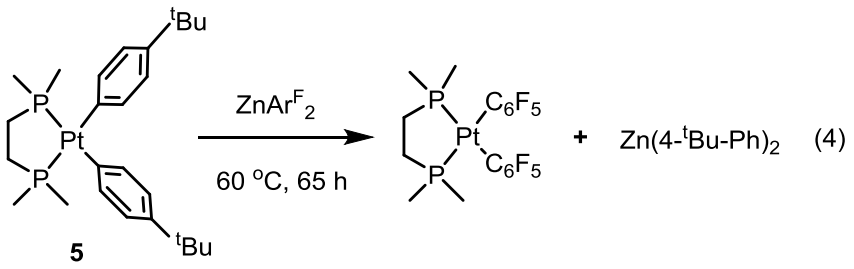

We propose that coordination of $ZnAr^F_2$ favors reductive elimination from **2** and **4** by both withdrawing electron density from platinum and increasing steric congestion at the metal center.[19] In the case of the bpy complex **4**, the binding of zinc also prevents roll-over cyclometalation by blocking the intramolecular C–H activation pathway that requires a vacant coordination site.[18d,e] For the dmpe complex **6**, the stronger *trans* effect of the phosphorus-based ligand may weaken the platinum–aryl bonds, particularly once $ZnAr^F_2$ binds, which favors aryl exchange over reductive elimination.

CONCLUSIONS

Dative, heterobimetallic interactions are observed between platinum(II) diaryl complexes and $ZnAr^F_2$ in both solution and the solid state. The (phen)$PtAr_2(ZnAr^F_2)$ complex features an unsupported Pt–Zn bond, and NMR spectroscopy confirms that this interaction is retained in solution. A more complex binding situation is observed for the dmpe analogue, which features additional interactions between the platinum-bound aryl ligands and zinc. These binding motifs demonstrate that the Lewis acid-base interactions between platinum(II) and $ZnAr^F_2$ are highly sensitive to the nature of the platinum-bound bidentate ligand.

The reactivity of the Pt–Zn complexes is also controlled by the platinum-bound ancillary ligand. For the dmpe complex, aryl transmetalation between Pt and Zn is exclusively observed. This aryl exchange is reminiscent of the secondary transmetalation pathways that have been proposed for Negishi catalysts. For the phen and bpy derivatives, reductive elimination is promoted by a Pt–Zn interaction. This result raises the possibility that Pd–Zn interactions may be present during the reductive elimination step, as well as transmetalation events, of Negishi cross-coupling reactions. Future work is needed to determine whether reductive elimination induced by an organozinc Z-type ligand interaction is a viable mechanism under catalytic conditions.

EXPERIMENTAL SECTION

General Considerations. Unless otherwise noted, all experiments were conducted using standard Schlenk techniques or in a nitrogen atmosphere glovebox. Solvents were stored in PTFE-valved flasks after drying using a Vacuum Atmospheres solvent purification system. Deuterated solvents were purchased from Cambridge Isotope Laboratory and were degassed and dried using appropriate drying agents prior to use. $Pt(SEt_2)_2$(4-*tert*-butylphenyl)$_2$ was prepared by a method analogous to that of van Koten and coworkers,[20] and $Zn(C_6F_5)_2(\eta^2$-toluene) was

prepared according to a literature procedure.[8] The ligands 1,10-phenanthroline, 2,2′-bipyridyl, and bis(dimethylphosphino)ethane were purchased from Aldrich and used as received.

Solution NMR spectroscopy was performed using Bruker NMR spectrometers at 20 °C unless otherwise noted. ^{1}H NMR spectra were calibrated internally to the residual proteo solvent relative to tetramethylsilane, ^{19}F NMR chemical shifts are referenced to 1,3,5-tris(trifluoromethyl)benzene, ^{31}P NMR chemical shifts are reported relative to H_3PO_4, and ^{195}Pt NMR chemical shifts are referenced to K_2PtCl_4 in D_2O. Elemental analyses were performed by the University of California, Berkeley College of Chemistry Microanalytical Facility. For elemental analysis results of samples containing solvent molecules, the percentage of solvent was confirmed by ^{1}H NMR spectroscopy.

Single crystal X-ray diffraction was performed at the UC Berkeley CHEXRAY crystallographic facility. Measurements were performed on a Bruker APEX-II CCD area detector with Mo Kα radiation (λ = 0.71073 Å) monochromated using QUAZAR multilayer mirrors. Crystals were maintained at 100(2) K during collection. Data collection, refinement, and reduction were performed with Bruker APEX2 software (v. 2013.4 or 2014.1). Structures were refined with SHELXL-2013 direct methods[21] or SHELXT-2014 with refinement of F^2 against all reflections by full-matrix least squares. Non-hydrogen atoms were refined anisotropically, and hydrogen atoms were included at geometrically-calculated positions and refined using a riding model.

Synthesis of (phen)Pt(4-^{t}Bu-Ph)$_2$ (1). A solution of $Pt(SEt_2)_2$(4-*tert*-butylphenyl)$_2$ (116 mg, 0.180 mmol) in 8 mL of benzene was added to a stirred suspension of 1,10-phenanthroline (32.0 mg, 0.180 mmol) in 2 mL of benzene under air. After 16 hours, volatiles were removed under reduced pressure. Following trituration with pentane (3 x 5 mL), (phen)Pt(4-^{t}Bu-Ph)$_2$ (**1**) was isolated as a yellow powder (92.0 mg, 80 % yield). ^{1}H NMR (C_6D_6) δ 9.00 (d, J = 5.0 Hz, 2H, phen H2 and H9), 8.19 (d with Pt satellites, J_{PtH} = 69 Hz, J_{HH} = 7.8 Hz, 4H, *o*-Ar), 7.46 (d, J = 7.7 Hz, 4H, *m*-Ar), 7.21 (d, J = 8.2 Hz, 2H, phen H4 and H7), 6.82 (s, 2H, phen H5 and H6), 6.37 (dd, J = 8.2, 5.0 Hz, 2H, phen H3 and H8); 1.42 (s, 18H, ^{t}Bu);^{1}H NMR (CD_2Cl_2) δ 8.80 (d, J = 5.0 Hz, 2H, phen H2 and H9), 8.58 (d, J = 8.2 Hz, 2H, phen H4 and H7), 7.97 (s, 2H, phen H5 and H6), 7.74 (dd, J = 8.2, 5.0 Hz, 2H, phen H3 and H8), 7.46 (d with Pt satellites, J_{PtH} = 67 Hz, J_{HH} = 7.8 Hz, 4H, *o*-Ar), 7.11 (d, J = 7.8 Hz, 4H, *m*-Ar), 1.33 (s, 18H, ^{t}Bu); ^{13}C{^{1}H} NMR (CD_2Cl_2) δ 150.38 (phen C2 and C9), 148.06 (phen), 144.65 (*ipso*-Ar), 141.50 (*p*-Ar), 138.15 (*o*-Ar), 137.16 (phen C4 and C7), 130.84 (phen), 127.76 (phen H5 and H6), 126.23 (phen H3 and H8), 124.50 (*m*-Ar), 34.35 (–*C*(CH_3)$_3$), 31.96 (–C(*C*H_3)$_3$); ^{195}Pt{^{1}H} NMR (CD_2Cl_2) δ -3355. Anal. Calcd for $C_{32}H_{34}N_2Pt$•0.67C_6H_6 (%) C 62.32, H 5.52, N 4.04; Found C 62.57, H 5.15, N 3.85.

Synthesis of (phen)Pt(4-^{t}Bu-Ph)$_2$[Zn(C_6F_5)$_2$] (2). A solution of **1** (9.6 mg, 0.015 mmol) and Zn(C_6F_5)$_2$(η^2-toluene) (7.5 mg, 0.015 mmol) was prepared in 0.5 mL of toluene. The solution was filtered, and vapor diffusion of pentane into the toluene solution at –35 °C afforded yellow crystals of (phen)Pt(4-^{t}Bu-Ph)$_2$[Zn(C_6F_5)$_2$] (**2**, 9.5 mg, 56 % yield). ^{1}H NMR (C_6D_6) δ 8.93 (d, J = 5.0 Hz, 2H, phen H2 and H9), 7.67 (d with Pt satellites, J_{PtH} = 50 Hz, J_{HH} = 7.8 Hz, 4H, *o*-Ar), 7.30 (d, J = 8.1 Hz, 4H, *m*-Ar), 7.19 (d, J = 8.2 Hz, 2H, phen H4 and H7), 6.89 (s, 2H, phen H5 and H6), 6.51 (dd, J = 8.1, 5.0 Hz, 2H, phen H3 and H8), 1.33 (s, 18H, ^{t}Bu); ^{13}C{^{1}H} NMR (C_6D_6) δ 151.60 (phen 2 and 9), 147.70 (phen), 147.05 (*ipso*-Ar), 138.66 (*o*-Ar), 138.23 (phen), 137.93 (phen C4 and C7), 136.09 (*p*-Ar), 127.19 (phen C5 and C6), 126.03 (*m*-Ar), 125.57 (phen C3 and C8), 34.65 (–*C*(CH_3)$_3$), 32.03 (–C(*C*H_3)$_3$); C_6F_5 resonances not observed;

^{19}F NMR (C_6D_6) δ -116.97, -156.23, -160.81; ^{195}Pt{^{1}H} NMR (C_6D_6) δ -3167. Anal. Calcd for $C_{44}H_{34}N_2PtZn•0.5C_7H_8$ (%) C 52.47, H 3.52, N 2.58; Found C 52.27, H 3.56, N 2.75.

Synthesis of (bpy)Pt(4-^{t}Bu-Ph)$_2$ (3). A solution of $Pt(SEt_2)_2$(4-*tert*-butylbenzene)$_2$ (116 mg, 0.180 mmol) in 8 mL of benzene was added to a stirred suspension of 2,2′-bipyridyl (28.0 mg, 0.180 mmol) in 2 mL of benzene under air. After 16 hours, volatiles were removed under reduced pressure. Following trituration with pentane (3 x 5 mL), yellow crystals of (bpy)Pt(4-^{t}Bu-Ph)$_2$ (**3**) were isolated by recrystallization from a toluene/hexanes solution at –30 °C (87.1 mg, 73 % yield).^{1}H NMR (CD_2Cl_2) δ 8.49 (dt, *J* = 5.3, 1.2 Hz, 2H, bpy H6), 8.15 – 8.04 (m, 4H, bpy H3 and H4), 7.41 (td, *J* = 5.8, 2.7 Hz, 2H, bpy H5), 7.36 (d with Pt satellites, J_{PtH} = 60 Hz, J_{HH} = 6.0 Hz, 4H, *o*-Ar), 7.06 (d, *J* = 6.0 Hz, 4H, *m*-Ar), 1.30 (s, 18H, ^{t}Bu); ^{13}C{^{1}H} NMR (CD_2Cl_2) δ 156.61 (bpy C2, 150.35 (bpy C6), 144.55 (*ipso*-Ar), 142.09 (*p*-Ar), 137.86 (*o*-Ar and bpy C4), 127.55 (bpy C5), 124.50 (*m*-Ar), 122.80 (bpy C3), 34.31 (–*C*(CH_3)$_3$), 31.92 (–C(*C*H_3)$_3$); ^{195}Pt{^{1}H} NMR (CD_2Cl_2) δ -3328. Anal. Calcd for $C_{30}H_{34}N_2Pt·0.33C_7H_8$ (%) C59.89, H 5.70, N 4.32; Found C 59.56, H 5.70, N 4.32.

Synthesis of (bpy)Pt(4-^{t}Bu-Ph)$_2$[Zn(C_6F_5)$_2$] (4). A solution of **2** (11 mg, 0.017 mmol) and Zn(C_6F_5)$_2$(η^2-toluene) (9.2 mg, 0.019 mmol) was prepared in 0.5 mL of toluene. The solution was filtered, and vapor diffusion of pentane into the toluene solution at –35 °C afforded yellow crystals of (bpy)Pt(4-^{t}Bu-Ph)$_2$[Zn(C_6F_5)$_2$] (**4**, 11 mg, 64 % yield). ^{1}H NMR (C_6D_6) δ 8.60 (d, *J* = 5.5 Hz, 2H, bpy H6), 7.59 (d with Pt satellites, J_{PtH} = 42 Hz, J_{HH} = 7.8 Hz, 4H, *o*-Ar), 7.25 (d, *J* = 7.8 Hz, 4H, *m*-Ar), 6.74 (t, *J* = 7.8 Hz, 2H, bpy H4), 6.60 (d, *J* = 8.1 Hz, 2H, bpy H3), 6.18 (t, *J* = 6.6 Hz, 2H, bpy H5), 1.26 (s, 18H, ^{t}Bu); ^{13}C{^{1}H} NMR (CD_2Cl_2) δ 155.94 (bpy C2), 151.22 (bpy C6), 147.79 (*ipso*-Ar), 138.23 (*o*-Ar), 138.11 (bpy C4), 136.01 (*p*-Ar), 126.85 (bpy C5), 126.02 (*m*-Ar), 122.15 (bpy C3), 34.59 (–*C*(CH_3)$_3$), 31.93 (–C(*C*H_3)$_3$); ^{195}Pt{^{1}H} NMR (C_6D_6) δ -3150. Anal. Calcd for $C_{42}H_{34}F_{10}N_2PtZn$ (%) C 49.59, H 3.37, N 2.75; Found C 49.44, H 3.23, N, 3.10.

Synthesis of (dmpe)Pt(4-^{t}Bu-Ph)$_2$ (5). Bis(dimethylphosphino)ethane (30.0 μL, 0.180 mmol) was added to a stirred solution of $Pt(SEt_2)_2$(4-*tert*-butylbenzene)$_2$ (116 mg, 0.180 mmol) in 8 mL of toluene. After 20 minutes, volatiles were removed under reduced pressure, and the resulting white powder was triturated with hexanes (3 x 4 mL) to afford (dmpe)Pt(4-^{t}Bu-Ph)$_2$ (**5**, 93.6 mg, 85 % yield). ^{1}H NMR (C_6D_6) δ 7.85 (dd with Pt satellites, J_{PtH} = 57 Hz, J_{HH} = 5.0 Hz, J_{PH} = 7.0 Hz, 4H, *o*-Ar), 7.33 (d, J_{HH} = 5.0 Hz, 4H, *m*-Ar), 1.28 (s, 18H, ^{t}Bu), 0.95 – 0.74 (m, 16H, dmpe); ^{13}C{^{1}H} NMR (C_6D_6) δ 159.45 (*ipso*-Ar), 144.12 (*p*-Ar), 137.42 (J_{PtH} = 37 Hz, *o*-Ar), 125.01 (J_{PtH} = 63 Hz, *m*-Ar), 34.40 (–*C*(CH_3)$_3$), 32.24 (–C(*C*H_3)$_3$), 29.38 (br, dmpe), 11.96 (d, J_{PH} = 27 Hz, dmpe); ^{31}P NMR (C_6D_6) δ 21.23 (s with Pt satellites, J_{PtP} = 1630.5 Hz); ^{195}Pt{^{1}H} NMR (C_6D_6) δ -4506 (t, J_{PtP} = 1631.0 Hz). Anal. Calcd for $C_{26}H_{42}P_2Pt$ (%) C 51.06, H 6.92; Found C 50.99, H 6.74.

Synthesis of (dmpe)Pt(4-^{t}Bu-Ph)$_2$[Zn(C_6F_5)$_2$] (6). A solution of **5** (10. mg, 0.016 mmol) and Zn(C_6F_5)$_2$(η^2-toluene) (8.1 mg, 0.016 mmol) was prepared in 0.5 mL of toluene. The solution was filtered, and vapor diffusion of pentane into the toluene solution at –35 °C afforded colorless crystals of (dmpe)Pt(4-^{t}Bu-Ph)$_2$[Zn(C_6F_5)$_2$] (**6**, 11 mg, 68 % yield). ^{1}H NMR (C_6D_6) δ 8.03 (dd with Pt satellites, J_{PtH} = 42.0 Hz, J_{PH} = 7.9 Hz, J_{HH} = 6.0 Hz, 4 H, *o*-Ar), 7.36 (d, J_{HH} = 6.0 Hz, 4H, *m*-Ar), 1.23 (s, 18H, ^{t}BuAr), 0.64 (m, 4H, dmpe), 0.55 (m, 12H, dmpe); ^{13}C{^{1}H} NMR (C_6D_6) δ 151.56 (*p*-Ar), 141.69 (J_{PtH} = 24 Hz, *o*-Ar), 127.51 (J_{PtH} = 45 Hz, *m*-Ar), 34.66 (–*C*(CH_3)$_3$), 31.64 (–C(*C*H_3)$_3$), 27.89 (br, dmpe), 10.90 (d, J_{PH} = 32 Hz, dmpe), *ipso*-carbon and Zn-Ar^F groups not observed; ^{31}P NMR (C_6D_6) δ 29.37 (s with Pt satellites, J_{PtP} = 2142.3 Hz); ^{19}F

NMR (C_6D_6) δ -111.77, -147.84, -155.07; ^{195}Pt{^{1}H} NMR (C_6D_6) δ -4544 (t, J_{PtP} = 2138.8 Hz). Anal. Calcd for $C_{38}H_{42}F_{10}P_2PtZn$ (%) C 45.14, H 4.19; Found C 44.76, H 4.50.

Attempted thermolysis of (phen)Pt(4-^{t}Bu-Ph)$_2$ (1). A solution of **1** (3.2 mg, 0.0050 mmol) was prepared in 0.500 mL of mesitylene-d_{12} in a J. Young NMR tube. The NMR tube was heated to 200 ^{o}C in a temperature-controlled oil bath. No reaction was observed by ^{1}H NMR spectroscopy after 48 hours.

Biaryl reductive elimination from (phen)Pt(4-^{t}Bu-Ph)$_2$[Zn(C_6F_5)$_2$] (2). A solution of **1** (3.2 mg, 0.0050 mmol), Zn(C_6F_5)$_2$(η^2-toluene) (25 mg, 0.050 mmol), and ferrocene as an internal standard was prepared in 0.5 mL of benzene-d_6. The NMR tube was stored at 0 °C prior to use. The tube was placed in an NMR spectrometer with the temperature pre-equilibrated to 60 °C. Complete conversion to 4,4′-di-*tert*-butylbiphenyl[22] and (phen)Zn(C_6F_5)$_2$[23] was observed by ^{1}H and ^{19}F NMR spectroscopy within 15 minutes. ^{1}H NMR of 4,4′-di-*tert*-butylbiphenyl: δ 7.58 (d, J = 8.2 Hz, 4H), 7.37 (d, J = 8.1 Hz, 4H), 1.28 (s, 18H); ^{1}H NMR of (phen)Zn(C_6F_5)$_2$: δ 9.05 (d, J = 4.4 Hz, 2H), 7.22 (dd, J = 8.2, 1.4 Hz, 2H), 6.86 (s, 2H), 6.75 (dd, J = 8.2, 4.8 Hz, 2H); ^{19}F NMR of (phen)Zn(C_6F_5)$_2$ δ -116.04 (br), -156.84 (br), -161.01 (br).

Biaryl reductive elimination from (phen)Pt(4-^{t}Bu-Ph)$_2$[Zn(C_6F_5)$_2$] (2) in the presence of P^{t}Bu$_3$. A solution of **1** (3.2 mg, 0.0050 mmol), Zn(C_6F_5)$_2$(η^2-toluene) (25 mg, 0.050 mmol), and tri-*tert*-butylphosphine (10. mg, 0.050 mmol) was prepared in 0.5 mL of benzene-d_6 in a J. Young NMR tube. heating the NMR tube for 24 hours in a temperature-controlled oil bath, complete conversion to 4,4′-di-*tert*-butylbiphenyl, (phen)Zn(C_6F_5)$_2$, and Pt(P^{t}Bu$_3$)$_2$[24] was observed by ^{1}H, ^{19}F, and ^{31}P NMR spectroscopy.

Biaryl reductive elimination from (bpy)Pt(4-^{t}Bu-Ph)$_2$[Zn(C_6F_5)$_2$] (4). A solution of **3** (3.1 mg, 0.0050 mmol) and Zn(C_6F_5)$_2$(η^2-toluene) (25 mg, 0.050 mmol) was prepared in 0.5 mL of benzene-d_6 in a J. Young NMR tube. The NMR tube was heated to 60 °C in a temperature-controlled oil bath. Complete conversion to 4,4′-di-*tert*-butylbiphenyl and (bpy)Zn(C_6F_5)$_2$[25] was observed by ^{1}H and ^{19}F NMR spectroscopy within 15 minutes. ^{1}H NMR of (bpy)Zn(C_6F_5)$_2$: δ 8.87 (d, J = 5.0 Hz, 2H), 6.87 (m, 4H), 6.65 (m, 2H).

Attempted thermolysis of (dmpe)Pt(4-^{t}Bu-Ph)$_2$ (5). A solution of **5** (3.1 mg, 0.0050 mmol) was prepared in 0.5 mL of toluene-d_8 in a J. Young NMR tube. The NMR tube was heated to 60 °C in a temperature-controlled oil bath. No reaction was observed by ^{1}H or ^{31}P NMR spectroscopy after 24 hours.

Thermolysis of (dmpe)Pt(4-^{t}Bu-Ph)$_2$[Zn(C_6F_5)$_2$] (6). A solution of **5** (3.1 mg, 0.0050 mmol) and Zn(C_6F_5)$_2$(η^2-toluene) (25.0 mg, 0.0500 mmol) was prepared in 0.5 mL of toluene-d_8 in a J. Young NMR tube. The NMR tube was heated to 60 °C in a temperature-controlled oil bath. After 65 hours, complete conversion to (dmpe)Pt(C_6F_5)$_2$[26] and bis(4-*tert*-buylphenyl)zinc[27] was observed by ^{1}H, ^{19}F, and ^{31}P NMR spectroscopy. ^{1}H NMR of bis(4-*tert*-butylphenyl)zinc: δ 7.56 (d, J = 7.7 Hz, 4H), 7.53 (d, J = 7.7 Hz, 4H), 1.46 (s, 18H); ^{19}F NMR of (dmpe)Pt(C_6F_5)$_2$: δ -118.9 (m with Pt satellites, J_{PtF} = 330 Hz, 4F), -162.1 (m, 2F), -163.2 (m, 4F); ^{31}P NMR of (dmpe)Pt(C_6F_5)$_2$: δ 26.5 (bm, J_{PtP} = 2245 Hz).

REFERENCES

(1) (a) Green, M. L. H. *J. Organomet. Chem.* **1995**, *500*, 127; (b) Hill, A. F. *Organometallics* **2006**, *25*, 4741; (c) Parkin, G. *Organometallics* **2006**, *25*, 4744.
(2) Amgoune, A.; Bourissou, D. *Chem. Commun.* **2011**, *47*, 859.

(3) Bauer, J.; Braunschweig, H.; Dewhurst, R. D. *Chem. Rev.* **2012**, *112*, 4329.
(4) (a) Kim, M.; Taylor, T. J.; Gabbaï, F. P. *J. Am. Chem. Soc.* **2008**, *130*, 6332. (b) López-de-Luzuriaga, J. M.; Monge, M.; Olmos, M. E.; Pascual, D.; Lasanta, T. *Chem. Commun.* **2011**, *47*, 6795. (c) Lasanta, T.; López-de-Luzuriaga, J. M.; Monge, M.; Olmos, M. E.; Pascual, D. *Chem. Eur. J.* **2013**, *19*, 4754.
(5) (a) Fuentes, B.; García-Melchor, M.; Lledós, A.; Maseras, F.; Casares, J. A.; Ujaque, G.; Espinet, P. *Chem. Eur. J.* **2010**, *16*, 8596; (b) Álvarez, R.; de Lera, A. R.; Aurrecoechea, J. M.; Aritz, D. *Organometallics* **2007**, *26*, 2799.
(6) (a) van Asselt, R.; Elsevier, C. J. *Organometallics* **1994**, *13*, 1972; (b) Casares, J. A.; Espinet, P.; Fuentes, B.; Salas, G. *J. Am. Chem. Soc.* **2007**, *129*, 3508; (c) Liu, Q.; Lan, Y.; Liu, J.; Li, G.; Wu, Y.-D.; Lei, A. *J. Am. Chem. Soc.* **2009**, *131*, 10201; (d) delPozo, J.; Gioria, E.; Casares, J. A.; Álvarez, R.; Espinet, P. *Organometallics* **2015**, *34*, 3120.
(7) Noltes, J. G.; van den Hurk, J. W. G. *J. Organomet. Chem.* **1964**, *1*, 377.
(8) Walker, D. A.; Woodman, T. J.; Hughes, D. L.; Bochmann, M. *Organometallics* **2001**, *20*, 3772.
(9) Ma, M; Sidiropoulos, A.; Ralte, L.; Stasch, A.; Jones, C. *Chem. Commun.* **2013**, *49*, 48.
(10) As determined from a survey of the Cambridge Crystallographic Database, November, 2015.
(11) Moret, M.-E.; Chen, P. *J. Am. Chem. Soc.* **2009**, *131*, 5675.
(12) Still, B. M.; Kumar, P. G. A.; Aldrich-Wright, J. R.; Price, W. S. *Chem. Soc. Rev.* **2007**, *36*, 665.
(13) Plane defined to include the phosphorus and platinum atoms. If the plane is defined to also include the ipso aryl carbons, the zinc is 1.236 Å above the plane.
(14) (a) MacKay, K. M.; MacKay, R. A.; Henderson, W. *Introduction to Modern Inorganic Chemistry*, 6th Ed; Melson Thornes Ltd.: London, 2002; p 174. (b) Clark, H. C.; Milne, C. R. *Can. J. Chem.* **1979**, *57*, 958.
(15) Skapski, A. C.; Sutcliffe, V. F.; Young, G. B. *J. Chem. Soc., Chem. Commun.* **1985**, 609.
(16) Butschke, B.; Schwarz, H. *Chem. Sci.* **2012**, *3*, 308.
(17) Johnson, J. B.; Rovis, T. *Angew. Chem. Int. Ed.* **2008**, *47*, 840.
(18) (a) Yamamoto, T.; Yamamoto, A.; Ikeda, S. *J. Am. Chem. Soc.* **1971**, *93*, 3350; (b) Komiya, S.; Akai, Y.; Tanaka, K.; Yamamoto, T.; Yamamoto, A. *Organometallics* **1985**, *4*, 1130; (c) Gollaszewski, A.; Schwartz, J. *Organometallics* **1985**, *4*, 417; (d) Sustmann, R.; Lau, J. *Chem. Ber.* **1986**, *119*, 2531; (e) Sustmann, R.; Lau, J.; Zipp, M. *Tetrahedron Lett.* **1986**, *27*, 5207; (f) Kurosawa, H.; Kijimaru, H.; Miyoshi, M.-A.; Ohnishi, H.; Ikeda, I. *J. Mol. Catal.* **1992**, *74*, 481; (g) Markies, B. A.; Canty, A. J.; Boersma, J.; van Koten, G. *Organometallics* **1994**, *13*, 2053; (h) Yamamoto, T.; Abla, M.; Murakami, Y. *Bull. Chem. Soc. Jpn.* **2002**, *75*, 1997; (i) Yamamoto, T.; Yamaguchi, I.; Abla, M. *J. Organomet. Chem.* **2003**, *671*, 179; (j) Yahav, A.; Goldberg, I.; Vigalok, A. *J. Am. Chem. Soc.* **2003**, *125*, 13634; (k) Popp, B. V.; Stahl, S. S. *J. Am. Chem. Soc.* **2006**, *128*, 2804; (l) Lanci, M. P.; Remy, M. S.; Kaminsky, W.; Mayer, J. M.; Sanford, M. S. *J. Am. Chem. Soc.* **2009**, *131*, 15618.
(19) We cannot exclude the possibility that $ZnAr^{F}_{2}$ abstracts the phen or bpy ligand prior to reductive elimination.

(20) Lacabra, M. A. C.; Canty, A. J.; Lutz, M.; Patel, J.; Spek, A. L.; Sun, H.; van Koten, G. *Inorg. Chim. Acta* **2002**, *327*, 15.
(21) Sheldrick, G. M. *Acta. Cryst. A* **2008**, ***64***, 112.
(22) Cook, A. K.; Sanford, M. S. *J. Am. Chem. Soc.* **2015**, *137*, 3109.
(23) Noltes, J. G.; van den Hurk, J. W. G. *J. Organomet. Chem.* **1965**, *3*, 222.
(24) Goel, R. G.; Ogini, W. O.; Srivastava, R. C. *J. Organomet. Chem.* **1981**, *214*, 405.
(25) Martin, E.; Clegg, W.; Harrington, R. W.; Hughes, D. L.; Hursthouse, M. B.; Male, L.; Lancaster, S. J. *Polyhedron* **2010**, *29*, 405.
(26) Hughes, R. P.; Ward, A. J.; Golden, J. A.; Incarvito, C. D.; Rheingold, A. L.; Zakharov, L. N. *Dalton Trans.* **2004**, 2720.
(27) Ilies, L.; Okabe, J.; Yoshikai, N.; Nakamura, E. *Org. Lett.* **2010**, *12*, 2838.

Chapter 3. Appendix

Table A1. Crystal data and structure refinement for **2**.

Identification code	almx88	
Empirical formula	C51 H42 F10 N2 Pt Zn	
Formula weight	1133.32	
Temperature	100(2) K	
Wavelength	0.71073 Å	
Crystal system	Monoclinic	
Space group	P 21/c	
Unit cell dimensions	a = 12.9950(13) Å	α= 90°.
	b = 16.7483(16) Å	β= 106.136(2)°.
	c = 21.185(2) Å	γ = 90°.
Volume	4429.1(7) $Å^3$	
Z	4	
Density (calculated)	1.700 Mg/m^3	
Absorption coefficient	3.777 mm^{-1}	
F(000)	2240	
Crystal size	0.120 x 0.100 x 0.040 mm^3	
Theta range for data collection	1.575 to 25.373°.	
Index ranges	-15<=h<=15, -20<=k<=20, -25<=l<=25	
Reflections collected	90981	
Independent reflections	8095 [R(int) = 0.0344]	
Completeness to theta = 25.000°	100.0 %	
Absorption correction	Semi-empirical from equivalents	
Max. and min. transmission	0.3529 and 0.2655	
Refinement method	Full-matrix least-squares on F^2	
Data / restraints / parameters	8095 / 0 / 593	
Goodness-of-fit on F^2	1.156	
Final R indices [I>2sigma(I)]	R1 = 0.0312, wR2 = 0.0722	
R indices (all data)	R1 = 0.0355, wR2 = 0.0747	
Extinction coefficient	n/a	
Largest diff. peak and hole	2.648 and -0.649 $e.Å^{-3}$	

Table A2. Crystal data and structure refinement for **6**.

Identification code	ALMX57	
Empirical formula	C38 H42 F10 P2 Pt Zn	
Formula weight	1011.11	
Temperature	100(2) K	
Wavelength	0.71073 Å	
Crystal system	Monoclinic	
Space group	P 21/n	
Unit cell dimensions	a = 10.9506(3) Å	α= 90°.
	b = 19.9969(6) Å	β= 96.0540(10)°.
	c = 17.6775(6) Å	γ = 90°.
Volume	3849.4(2) $Å^3$	
Z	4	
Density (calculated)	1.745 Mg/m^3	
Absorption coefficient	4.412 mm^{-1}	
F(000)	1992	
Crystal size	0.120 x 0.100 x 0.070 mm^3	
Theta range for data collection	1.542 to 25.358°.	
Index ranges	-13<=h<=13, 0<=k<=23, 0<=l<=21	
Reflections collected	7042	
Independent reflections	7042	
Completeness to theta = 25.000°	100.0 %	
Absorption correction	Semi-empirical from equivalents	
Max. and min. transmission	0.303439 and 0.250108	
Refinement method	Full-matrix least-squares on F^2	
Data / restraints / parameters	7042 / 0 / 558	
Goodness-of-fit on F^2	1.206	
Final R indices [I>2sigma(I)]	R1 = 0.0252, wR2 = 0.0560	
R indices (all data)	R1 = 0.0315, wR2 = 0.0622	
Extinction coefficient	n/a	
Largest diff. peak and hole	0.823 and -1.459 $e.Å^{-3}$	

Chapter 4. Lewis Acidity of Bis(perfluorocatecholato)silane: Aldehyde Hydrosilation Catalyzed by a Neutral Silicon Compound

INTRODUCTION

Lewis acidic main group compounds have emerged as broadly applicable reagents. In particular, $B(C_6F_5)_3$ and other electron-deficient boranes can serve as activators for transition metal compounds,[1] and as alternatives to metal-based catalysts.[2]

In contrast to Group 13 species, silicon Lewis acids remain relatively rare.[3] Silicon tetrachloride is the common silicon-based Lewis acid of choice in catalytic applications;[4] however, the reactive Si–Cl bonds are readily cleaved by nucleophilic reagents, limiting its utility. Several recent reports have shown that cationic silylium ions promote catalytic imine reduction and Diels-Alder reactions.[5] Silylium compounds, in combination with phosphines, engage in frustrated Lewis pair reactions that activate carbon dioxide and dihydrogen.[6] Additionally, Leighton and coworkers have demonstrated that chiral silicon complexes can serve as reagents for asymmetric crotylation reactions and as catalysts for Diels-Alder additions.[7] Based on these promising results, we were interested in exploring the behavior of neutral silicon compounds as potent Lewis acids. Herein, we report the synthesis and reactivity of a neutral bis(perfluorocatecholato)silane Lewis acid, which represents the first example of a neutral silicon species that catalyzes aldehyde hydrosilation.

RESULTS AND DISCUSSION

The bis(catecholato)silane motif was selected due to its ease of preparation and stability, and fluorinated catechol ligands were employed to enhance the Lewis acidic properties. The novel complex bis(perfluorocatecholato)silane, $Si(cat^F)_2$ (**1**), was easily prepared by treatment of silicon tetrachloride with 2 equiv of tetrafluorocatechol in acetonitrile. In the absence of Lewis bases, **1** has very limited solubility in standard organic solvents including benzene, dichloromethane, and acetonitrile.

Reactions with simple anionic and neutral Lewis bases were investigated to probe the binding properties of $Si(cat^F)_2$. First, addition of tris(dimethylamino)sulfonium difluorotrimethylsilicate (TASF) to $Si(cat^F)_2$ in tetrahydrofuran led to the immediate formation of a bis(perfluorocatecholato)fluorosilicate complex (**2**, eq 1). Single crystal X-ray diffraction confirmed the structure of **2**, which exhibits an approximate square pyramidal geometry at silicon (Figure 1). There is π-stacking between the perfluorocatechol rings of two silicate units in the solid state (d = 3.08–3.61 Å).[8] The silicon–fluorine bond distance in **2** (1.602(2) Å) is nearly identical to that reported previously for $[Si(cat)_2F][NEt_4]$.[9] This fluoride binding demonstrates that $Si(cat^F)_2$ can readily accommodate an added Lewis base to form a pentacoordinate species, a general step that is necessary for catalytic applications.

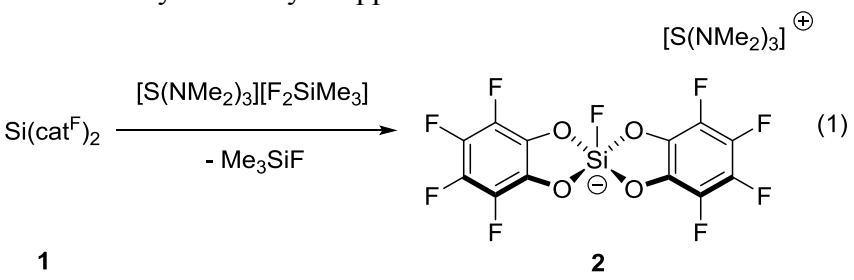

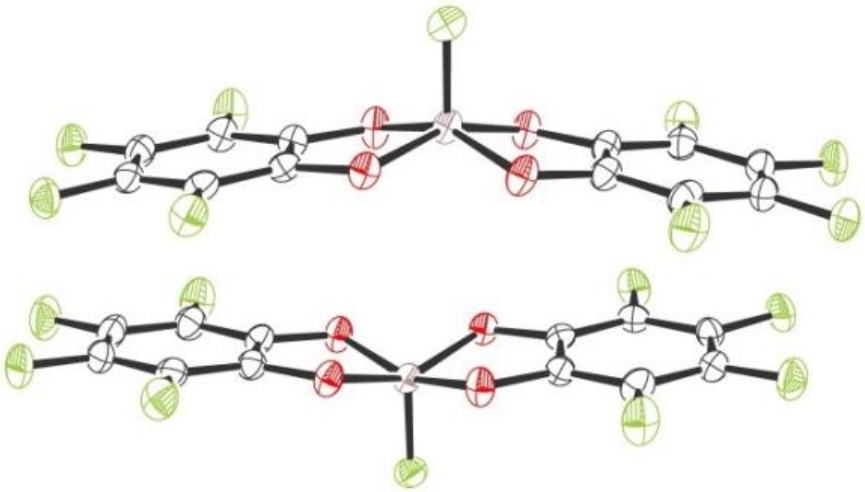

Figure 1. ORTEP diagram of **2**, with thermal elipsoids at 50% probability. Tris(dimethylamino)sulfonium cations are omitted for clarity.

The Gutmann-Beckett method, which evaluates the change in the ^{31}P chemical shift of triethylphosphine oxide upon complexation, was applied as a gauge of Lewis acidity.[10] A change of + 35.9 ppm in the ^{31}P NMR chemical shift of $OPEt_3$ was observed upon treatment with 1 equiv of $Si(cat^F)_2$ in dichloromethane-d_2. Only a slightly smaller change in chemical shift was observed using $Si(cat)_2$ ($\Delta\delta = +32.5$ ppm). These differences are substantially larger than the change observed upon binding to $B(C_6F_5)_3$ ($\Delta\delta = +26.6$ ppm), and suggest that $Si(cat^F)_2$ is a stronger Lewis acid toward $OPEt_3$ than $Si(cat)_2$ or $B(C_6F_5)_3$, although both silicon complexes induce large changes in ^{31}P NMR chemical shifts upon complexation.

In contrast to the strong Lewis acidity implied by the Guttmann-Beckett analysis with $OPEt_3$, $Si(cat^F)_2$ does not readily bind aldehydes or ketones. The combination of 1 equiv of *trans*-crotonaldehyde and $Si(cat^F)_2$ resulted in negligible (<2 %) conversion to a $Si(cat^F)_2$–crotonaldehyde adduct (assessed by ^{1}H NMR spectroscopy in dichloromethane-d_2). This suggests that $Si(cat^F)_2$ displays a substantially diminished affinity for "soft" Lewis bases relative to typical boron Lewis acids, which readily coordinate to carbonyl groups.[2a,11]

Replacing aldehyde moieties with the strongly coordinating amide functional group promoted coordination, and quantitative adduct formation was observed between N,N'-diisopropylbenzamide and $Si(cat^F)_2$ (**3**, eq 2). Upon binding to either $Si(cat^F)_2$ or $B(C_6F_5)_3$, the two N-bound isopropyl groups of the benzamide appear as separate, sharp signals, whereas there is coalescence of these signals in the room temperature ^{1}H NMR spectrum of the free benzamide.[12] This behavior can be rationalized by invoking strong nitrogen π-donation upon formation of the Lewis acid-base adduct, which slows the exchange of the *E* and *Z* isopropyl groups via rotation about the C(amide)–N bond. In contrast to **1**, the parent bis(catecholato)silane complex $Si(cat)_2$ does not react with N,N'-bisdiisopropylbenzamide (by ^{1}H NMR spectroscopy in dichloromethane-d_2 solvent), indicating that the perfluoro derivative displays an enhanced binding affinity for this substrate.

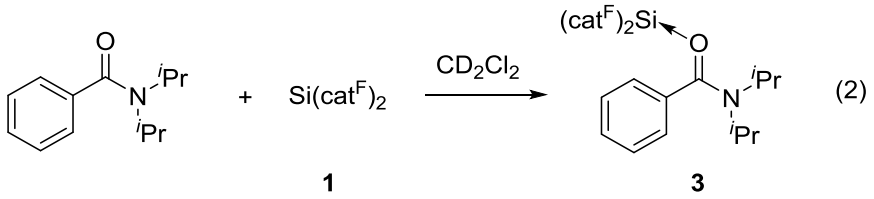

Single crystals of **3** were grown from a mixture of *o*-difluorobenzene and toluene at – 30 ^{o}C (Figure 2). In comparison to the analogous $B(C_6F_5)_3$ adduct, the C(amide)–O bond of **3** is shorter (1.32(1) vs. 1.304(3) Å) and the C(amide)–N bond is longer (1.28(1) vs. 1.297(3) Å).[12] The C=O stretching frequency of **3** (ν_{CO} = 1606 cm^{-1}) is intermediate between values for free benzamide and the $B(C_6F_5)_3$ adduct (1625 and 1570 cm^{-1}, respectively). Thus, both bond length and IR spectroscopic comparisons suggest that $B(C_6F_5)_3$ is more activating than **1** toward benzamides.

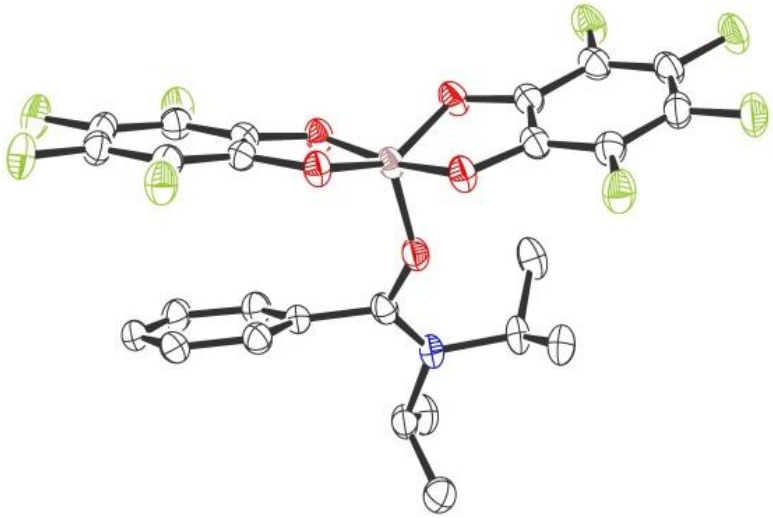

Figure 2. ORTEP diagram of compound **3** with all thermal elipsoids shown at 50% probability.

Hydrosilation of aldehydes was used to assess the catalytic properties of $Si(cat^F)_2$. Main–group–catalyzed hydrosilation is well known for both neutral and cationic boron Lewis acids.[2a,13] In contrast, only cationic silylium ions have previously been reported as hydrosilation catalysts.[2b,14] These silylium-ion catalyzed carbonyl reductions often result in over-reduction to the deoxygenated hydrocarbon products, rather than the presumed initial silyl ether complex.

Initial studies showed that $Si(cat^F)_2$ is an efficient catalyst for the hydrosilation of 4-nitrobenzaldehyde with triethylsilane at room temperature, to exclusively form the corresponding silyl ether product (Table 1, entry 1). In contrast, we found the previously reported $Si(cat)_2$ and $Si(C_6F_5)_4$ complexes to be essentially inactive as catalysts (Table 1, entries 2, 3). To our knowledge, $Si(cat^F)_2$ represents the first neutral silicon Lewis acid to serve as a catalyst for aldehyde hydrosilation.

Table 1. Hydrosilation trials with neutral silicon catalysts.

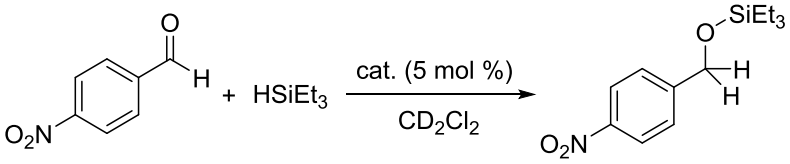

Entry	Catalyst	Time (h)	Temp. (^{o}C)	Yield (%)
1	$Si(cat^{F})_2$	0.5	25	> 95
2	$Si(cat)_2$	48	25	2
3	$Si(C_6F_5)_4$	48	45	0

Reaction conditions: 4-nitrobenzaldehyde (0.30 M), triethylsilane (0.30 M), and catalyst (0.015 M) in dichloromethane-d_2 (0.5 mL).

Catalytic amounts of $Si(cat^{F})_2$ also promoted the silylcyanation of 4-nitro-benzaldehyde with trimethylsilylcyanide at 45 ^{o}C (eq 3). Previous studies of main group silylcyanation catalysis typically involve (i) combinations of Lewis acid and Lewis base catalysts, such as the Shibasaki bifunctional aluminium and phosphine oxide system,[15] or (ii) simple Lewis base activators, including fluoride, phosphines, and amines.[16] In the current study, $Si(cat^{F})_2$ behaves as a single component Lewis acid silylcyanation catalyst.

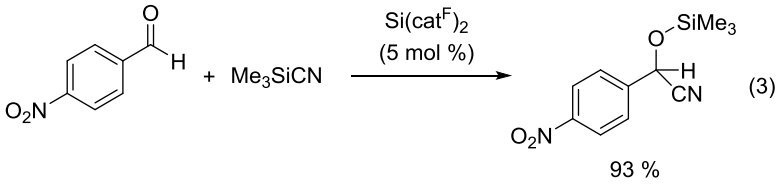

Hydrosilation catalysis was further evaluated through study of the silane substrate scope (Table 2). Tertiary alkyl and aryl silanes exhibited high activity in hydrosilations of 4-nitrobenzaldehyde (entries 1–4). Bulky silanes such as triisopropylsilane and bis(trimethylsilyl)phenylsilane were also tolerated (entries 5, 6). In contrast, $B(C_6F_5)_3$ does not react with these sterically demanding substrates, which has been attributed to front strain that prevents silane coordination.[2b] Silanes incorporating trimethylsiloxy- and dimethyl-amido-groups were also efficiently transformed (entries 7, 8). Secondary silanes underwent hydrosilation in low conversion (entry 9) and the primary silanes surveyed (H_3SiPh and $H_3Si^{t}Bu$) were completely inactive.

Table 2. Silane scope for hydrosilation catalysis[a]

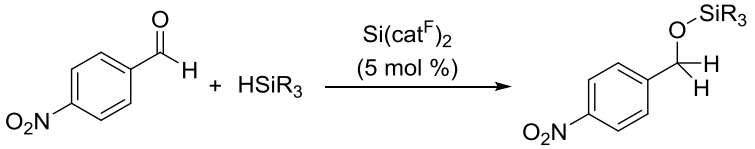

Entry	Silane	Time (h)	Yield (%)
1	$HSiPh_3$	1	94
2	$HSiPh_2Me$	0.5	>95
3	$HSiPhMe_2$	0.5	>95
4	HSi^tBuMe_2	0.5	91
5	HSi^iPr_3	0.5	>95
6	$HSi(SiMe_3)_2Ph$	1	93
7	$HSi(OSiMe_3)_2Me$	0.5	>95
8	$HSi(NMe_2)_2Me$	0.5	92
9	$H_2SiPhMe$	2	42

[a]Reaction conditions: 4-nitrobenzaldehyde (0.30 M), silane (0.30 M), and **1** (0.015 M) in CD_2Cl_2 at 25 °C. Yields were determined by ^1H NMR integration relative to an internal standard. [b]45 °C.

A variety of benzaldehydes were investigated for conversion to the corresponding silyl ethers (Scheme 1). Electron-deficient aldehydes were required for productive catalysis. The nitrile functional group was tolerated (entry c), whereas many Lewis acid catalysts, notably $B(C_6F_5)_3$, are inactive in the presence of these strongly coordinating groups.[2b] No inhibitory effect was observed for *ortho* substituents (entries h, i). Aldehydes were selectively and exclusively hydrosilated in the presence of ketones and esters (entries j, k). Lastly, an electron-deficient cinnemaldehyde derivative underwent exclusive 1,2-addition (entry l).

Scheme 1. Hydrosilation aldehyde scope[a]

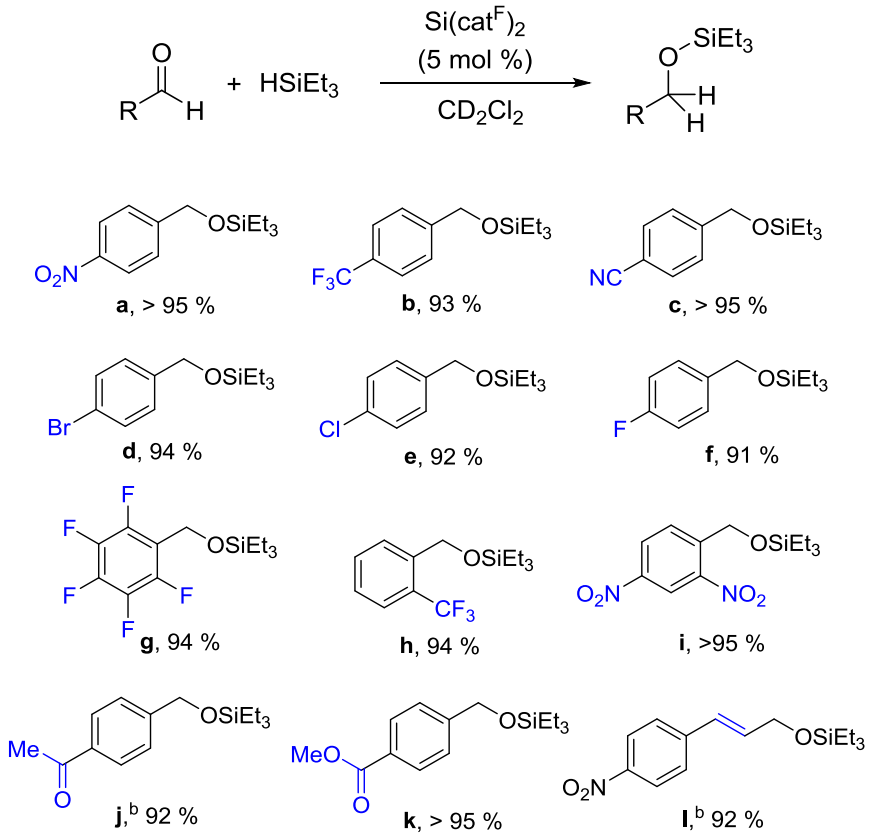

[a]Reaction conditions: aldehyde (0.30 M), triethylsilane (0.30 M), and **1** (0.015 M) in CD_2Cl_2 at 25 °C. Yields were determined by ^{1}H NMR integration relative to an internal standard. [b]0.45 M $HSiEt_3$.

In order to distinguish between possible mechanistic pathways, experiments were performed to determine whether Si(cat^F)$_2$ binds to and activates the aldehyde or silane substrate during hydrosilation catalysis.[17] No changes were observed in the ^{1}H NMR spectrum of $HSiEt_3$ upon addition of Si(cat^F)$_2$ (in dichloromethane-d_2). Previous work by the Piers and Bergman groups has cited loss of J_{HH} coupling between the Si–H and CH_2 protons of silicon-bound alkyl groups as evidence for the intervention of a transient Lewis acid adduct.[2b,18] Additionally, no scrambling occurred between a 1:1 mixture of $HSiPhMe_2$ and $DSiPh_2Me$ upon treatment with 10 mol % Si(cat^F)$_2$ in dichloromethane-d_2. Attempts to observe hydrosilation of alkenes or silation of phenols with catalytic Si(cat^F)$_2$ were unsuccessful. In contrast, $B(C_6F_5)_3$, which is known to operate via a silane activation mechanism, is efficient for these catalytic transformations.[2d,19] Taken together, these observations suggest that Si(cat^F)$_2$, unlike $B(C_6F_5)_3$, does not bind to the silane substrate during catalysis.

An optically active silane substrate was employed to provide further mechanistic insight. Analogous enantiospecificity studies have been reported as evidence for the silane coordination mechanism operative for $B(C_6F_5)_3$ and transition metal catalysts.[20] Reactions were performed

with 5 mol % $Si(cat^F)_2$ for the hydrosilation of 4-nitro-benzaldehyde with enantiopure R-(+)-methyl(1-napthyl)phenylsilane[21] to furnish the silyl ether product in 95 % yield (eq 4). The reaction proceeded with predominant stereochemical retention; however, the enantiomeric excess was highly dependent on solvent polarity, with increased racemization in more polar media (70 % *ee* in benzene, 40 % *ee* in *o*-dichlorobenzene, and 12 % *ee* in dichloromethane).

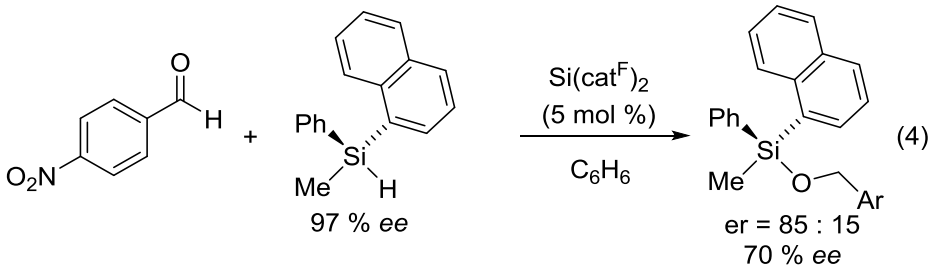

(4)

To investigate the decrease in enantiospecificity, studies were performed in the presence of tetrabutylammonium tetrakis(pentafluorophenyl)borate, $NBu_4BAr^F_4$. Salt effects on organic S_N1 reactions have provided insight into ionic dissociation steps, typically in polar solvents;[22] however, there are fewer examples of salt effects in nonpolar solvents.[23] For the hydrosilation shown in eq 4, the addition of $NBu_4BAr^F_4$ had a deleterious effect on the enantiospecificity (26 % *ee* in the presence of 150.0 mM $NBu_4BAr^F_4$, compared to 70 % *ee* in the absence of salt).

A proposed mechanism that accounts for the predominant stereochemical retention, as well as the observed solvent and salt effects, is shown in Scheme 2. The aldehyde first coordinates to $Si(cat^F)_2$ (**A**), which is followed by hydride transfer from the silane substrate to the activated aldehyde. We suggest that this leads to a silylium alkoxysilicate intimate ion pair intermediate (**B**) that can undergo rapid silicon–oxygen bond formation, with displacement of the catalyst, within the ion pair prior to silylium rotation, resulting in stereochemical retention. Loss of stereospecificity is caused by the formation of a solvent separated ion pair or ion aggregate (**C**), which is favored in more polar solvents or upon increasing salt concentration. An alternative mechanism featuring a four-membered cyclic transition state has been proposed for related silane additions to activated carbonyls.[24] This concerted, asynchronous addition should afford complete stereochemical retention, and is inconsistent with the observed racemization under more polar conditions. For comparison, a catalytically competent silane–$Si(cat^F)_2$ adduct should lead to inversion in the major product,[20a] allowing us to exclude this possible mechanism.

Scheme 2. Proposed hydrosilation mechanism

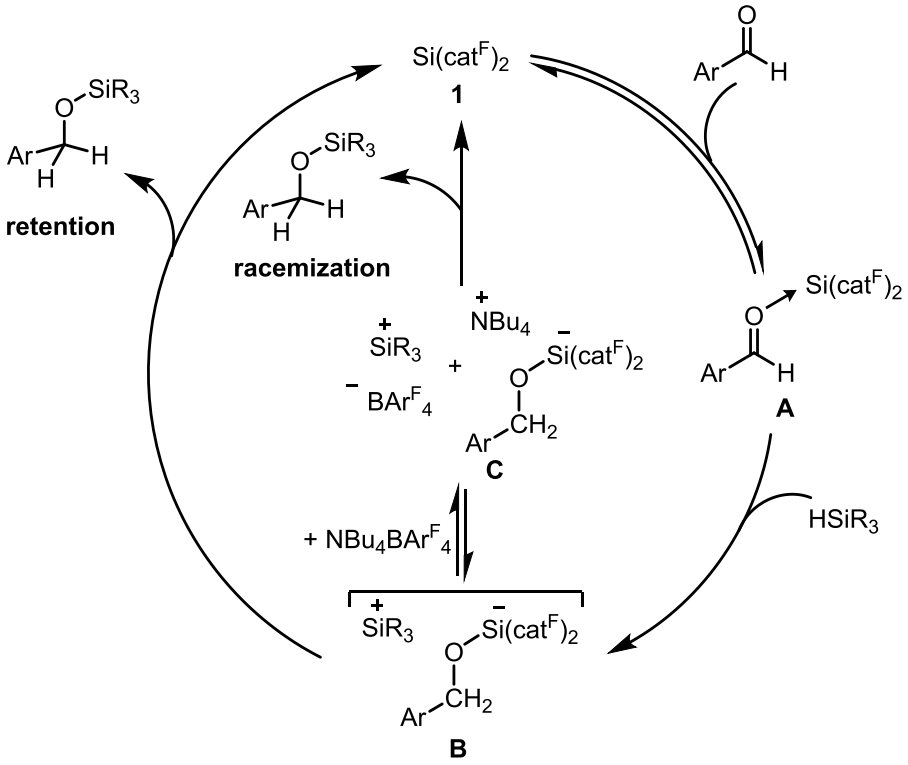

CONCLUSION

In conclusion, bis(perfluorocatecholato)silane (**1**) was prepared, and reactions to assess its Lewis acidity were investigated. Coordination of fluoride, triethylphosphine oxide, and N,N'-diisopropylbenzamide demonstrate the ability of Si(cat^F)$_2$ to bind several common classes of Lewis bases. Additionally, hydrosilation and silylcyanation of electron-deficient aldehydes were catalyzed by Si(cat^F)$_2$ under mild conditions. A stereogenic silicon substrate was employed in combination with solvent and salt effect studies to provide evidence for a carbonyl activation mechanism involving an ionic intermediate. We hope that future work will expand upon the use of neutral, yet potent, silicon Lewis acids in catalytic transformations.[25]

EXPERIMENTAL SECTION

General. All experiments were conducted with dry, oxygen-free solvents using standard Schlenk techniques or in a N_2 atmosphere glovebox. Solvents were stored in PTFE-valved flasks after drying using Vacuum Atmospheres solvent purification systems or by distillation from appropriate drying agents. Deuterated solvents were purchased from Cambridge Isotope Laboratory and dried before use. Tetrafluorocatechol was purchased from Matrix Scientific and was dried by storage as a diethyl ether solution over 3 Å molecular sieves for 48 hours. Tris(dimethylamino)sulfonium difluorotrimethylsilicate and triethylphosphine oxide were purchased from Sigma-Aldrich and used as received. Bis(catecholato)silane,

tetrakis(pentafluorophenyl)silicon, and diphenylmethylsilyl deuteride ($MePh_2SiD$) were prepared according to previously reported methods.[26,27,28] *R*-(+)-methyl(1-napthyl)phenylsilane was prepared as previously reported,[21,29] and its enantiomeric excess (97 % *ee*) was determined by polarimetry ($[\alpha]_D$ = + 32.75 found vs + 33.7 reported (*c* 4.00 cyclohexane)).

Analytical methods. Solution NMR spectroscopy was performed using Bruker NMR spectrometers at 20 °C. ^{1}H and ^{13}C NMR spectra were calibrated internally to resonances for either the solvent or the residual proteo solvent relative to tetramethylsilane. ^{19}F NMR chemical shifts were referenced to 1,3,5-tris(trifluoromethyl)benzene. ^{29}Si NMR chemical shifts were measured relative to an external reference of tetramethylsilane in $CDCl_3$. Elemental analyses were performed by the University of California, Berkeley College of Chemistry Microanalytical Facility. Enantiomeric excesses were measured on a Shimadzu VP Series Chiral HPLC using a Chiralpak IB column with hexanes/isopropanol (99:1) eluent. High resolution EI-MS data were acquired in the QB3/College of Chemistry Mass Spectrometry Facility at the University of California, Berkeley. Low resolution mass spectral data were obtained on a 6890N gas chromatograph system coupled to a 5973N mass selective detector (Agilent Technologies).

X-ray structural determinations were performed on Bruker MicroSTAR-H APEX II or Bruker APEX II Quazar diffractometers. Both are Kappa Geometry with DX and are 3-circle diffractometers that couple a CCD detector with a sealed-tube source of monochromated Cu-Kα (MicroSTAR) or Mo Kα radiation (Quazar). Structures were solved using the SHELXTL (version 5.1) program library (G. Sheldrick, Bruker Analytical Systems, Madison, WI). All software and sources of scattering factors are contained in the SHELXTL (version 5.1) program library.

Synthesis of bis(perfluorocatecholato)silane (1). A solution of tetrachlorosilane (0.20 mL, 1.75 mmol) was prepared in 12 mL of acetonitrile. This solution was cooled to 0 °C and was added dropwise to a cold (0 °C) solution of tetrafluorocatechol (0.62 g, 3.41 mmol) in 8 mL of acetonitrile. The reaction vessel warmed to 25 °C overnight. After 20 hours, the mixture was filtered to allow collection of a white powder, which was washed with acetonitrile and solvent was removed under vacuum (0.41 g, 53 %). Isolated product contains 2 equivalents of acetonitrile per silicon center, as assessed by ^{1}H NMR spectroscopy and elemental analysis. ^{19}F NMR (CD_2Cl_2) δ -164.77 (dd, J = 16.5, 10.5 Hz), -169.96 (dd, J = 16.4, 10.7 Hz). ^{13}C and ^{29}Si NMR data could not be obtained due to limited solubility. Anal. Calcd for $C_{16}H_6F_8N_2O_4Si$: C, 40.86; H, 1.29; N, 5.96; found C, 40.83; H, 1.08; N, 5.96.

Synthesis of tris(dimethylamino)sulfonium bis(perfluorocatecholato)fluorosilicate (2). A solution of tris(dimethylamino)sulfonium difluorotrimethylsilicate (11.0 mg, 0.040 mmol) in THF (5 mL) was added dropwise to a stirred suspension of **1** (18.8 mg, 0.040 mmol) in THF (2 mL). After 10 minutes, solvent was evaporated under reduced pressure. The colorless solid was washed with 2 mL of diethyl ether and trace solvent was removed *in vacuo*. Colorless crystals were grown by vapor diffusion of diethyl ether into an *o*-difluorobenzene solution of **2** at –30 °C (15.7 mg, 68 %). ^{1}H NMR (THF-d_8) 2.95 (s); ^{13}C NMR (THF-d_8) 133.20 (d, J_{CF} = 4.5 Hz), 132.76 (br), 132.54 (br d, J_{CF} = 240 Hz), 35.61; ^{19}F NMR (THF-d_8) δ -134.59 (1F), -170.74 (dd, J_{FF} = 16.5, 12.3 Hz, 4F), -178.41 (dd, J_{FF} = 16.4, 12.4 Hz, 4F); ^{29}Si NMR (THF-d_8) –103.28 (d, J_{SiF} = 197 Hz). Anal. Calcd for $C_{18}H_{18}F_9N_3O_4SSi$: C, 37.83; H, 3.17; N, 7.35; S, 5.61 found C, 37.92; H, 2.80; N, 7.15, S, 5.91.

Gutmann-Beckett method for assessing Lewis acidity of (1). A solution of **1** (5.0 mg, 0.011 mmol) and triethylphosphine oxide (1.5 mg, 0.011 mmol) was prepared in dichloromethane-d_2 (0.50 mL). ^{1}H and ^{31}P NMR spectra were identical using either 1 or 3 equiv

of **1**. ^{1}H NMR (CD_2Cl_2) δ 2.06 (dq, *J* = 11.7, 7.7 Hz, 6H), 1.11 (dt, *J* = 19.2, 7.7 Hz, 9H); ^{19}F NMR (CD_2Cl_2) δ -166.09 (dd, *J* = 16.3, 11.2 Hz, 4F), -172.02 (dd, *J* = 16.3, 11.2 Hz, 4F); ^{31}P NMR (CD_2Cl_2) δ 86.56.

Synthesis of Bis(perfluorocatecholato)silane–N,N'-diisopropylbenzamide (3). Compound **1** (36.5 mg, 0.0776 mmol) and N,N'-diisopropylbenzamide (16.0 mg, 0.0776 mmol) were dissolved in 6 mL of a 1:1 mixture of toluene and *o*-difluorobenzene. After 10 minutes, the solution was filtered and stored at –30 ^{o}C overnight to afford colorless crystals (20.1 mg, 86 %). ^{1}H NMR (CD_2Cl_2) δ 7.43 (t, *J* = 7.4 Hz, 1H), 7.35 (m, 4H), 4.07 (sept, *J* = 6.7 Hz, 1H), 3.88 (sept, *J* = 6.8 Hz, 1H), 1.43 (d, *J* = 6.9 Hz, 6H), 1.26 (d, *J* = 6.7 Hz, 6H); ^{13}C NMR (CD_2Cl_2) δ 171.63, 135.90 (br d, J_{CF} = 245 Hz), 135.18 (br d, J_{CF} = 254 Hz), 132.89, 132.83, 129.49, 129.03, 126.97, 57.08, 51.98, 20.49, 20.13; ^{19}F NMR (CD_2Cl_2) δ -166.35 (m, 4F), -172.68 (m, 4F); ^{29}Si NMR (CD_2Cl_2) δ –101.48. IR: $\nu_{C=O}$ = 1606 cm^{-1}. Anal. Calcd for $C_{25}H_{19}F_8NO_5Si$: C, 50.59; H, 3.23; N, 2.36; found C, 50.97; H, 3.16; N, 2.25.

General hydrosilylation procedure. In a typical experiment, a J. Young NMR tube was charged with 0.50 mL of a dichloromethane-d_2 solution of **1** (3.5 mg, 0.0075 mmol), aldehyde (0.15 mmol), silane (0.15 mmol), and a known amount of 1,3,5-tris(trifluoromethyl)benzene or hexamethylbenzene as an internal standard. The reaction progress was followed by ^{1}H NMR spectroscopy until substrate conversion ceased, and the yield was determined by ^{1}H NMR integration relative to the internal standard. Subsequently, the reaction mixture was directly charged onto a short silica plug and chromatographed. The solvent was removed under reduced pressure to yield the pure silyl ethers as typically colorless oils.

For the hydrosilylation of 4-nitro-benzaldehyde with methylphenylsilane (Table 2, entry 9), upon reaction completion, the crude reaction mixture was exposed to air and quenched with methanol (5 mL). Aqueous hydrochloric acid (5 mL of a 1 N solution) was added, and the biphasic mixture was stirred for 2 hours at room temperature. A series of extractions was performed with dichloromethane (10 mL × 4). The combined organic layers were washed with brine, stirred over anhydrous $MgSO_4$, filtered, and the organic solvent was removed *in vacuo*. The residue was purified by column chromatography to allow isolation of 4-nitrobenzyl alcohol (identified by ^{1}H and ^{13}C NMR spectroscopy, 42 % yield).

Attempt to observed silane H/D exchange. A solution of dimethylphenylsilane (12.1 mL, 0.079 mmol), diphenylmethylsilyl deuteride (15.7 mL, 0.079 mmol), and **1** (3.0 mg, 0.0079 mmol) was prepared in 0.5 mL of dichloromethane-d_2. No H/D exchange between silanes was observed over 24 h at 25 ^{o}C.

Chiral silane experiments. A solution of 4-nitrobenzaldehyde (11.9 mg, 0.0785 mmol), *R*-(+)-methyl(1-napthyl)phenylsilane (20.0 mg, 0.0785 mmol), and **1** (3.0 mg, 0.0079 mmol) was prepared in 0.5 mL of benzene-d_6. The reaction was complete within 30 minutes at 25 ^{o}C, as assessed by ^{1}H NMR spectroscopy. The solution was quenched by addition of a drop of triethylamine, and was analyzed by chiral HPLC. Samples analyzed as aliquots collected throughout the reaction (after 10, 20, or 30 minutes) showed identical enantiomeric excesses. Similarly, catalyst loading (5, 10, or 20 mol %) also had no effect on the measured *ee* of the hydrosilylation product.

Table 3. Dependence of the observed enantiospecificity on solvent.

Solvent	**enantiomeric ratio (retention : inversion)**	**% *ee***
benzene	85 : 15	70
benzene/*o*-dichlorobenzene (1:1)	79 : 21	58
o-dichlorobenzene	70 : 30	40
dichloromethane	56 : 44	12

Table 4. Dependence of the observed enantiospecificity on salt concentration.

$[NBu_4B(C_6F_5)_4]$ (mM)	**enantiomeric ratio (retention : inversion)**	**% *ee***
0	85 : 15	70
50.0	72 : 28	44
100.0	67 : 33	34
150.0	63 : 37	26

Characterization of hydrosilylation products

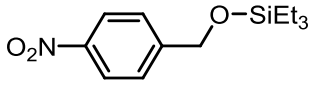

(4-Nitro-benzyloxy)-triethyl-silane. ^{1}H NMR (CD_2Cl_2) δ 8.18 (d, *J* = 10 Hz, 2H), 7.52 (d, *J* = 10 Hz, 2H), 4.84 (s, 2H), 0.99 (t, *J* = 10 Hz, 9H), 0.69 (q, *J* = 9 Hz, 6H); ^{13}C NMR (CD_2Cl_2) δ 149.65, 147.29, 126.74, 123.73, 64.01, 6.86, 4.69. MS (EI, +ve): *m/z* 267 $[M]^+$, 238 $[M–Et]^+$.

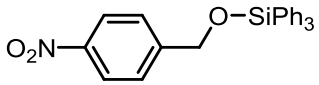

(4-Nitro-benzyloxy)-triphenyl-silane. ^{1}H NMR (CD_2Cl_2) δ 8.19 (d, *J* = 8.3 Hz, 2H), 7.70 (d, *J* = 7.1 Hz, 6H), 7.56 (d, *J* = 8.4 Hz, 2H), 7.54 – 7.47 (m, 3H), 7.48 – 7.42 (m, 6H), 5.03 (s, 2H); ^{13}C NMR (CD_2Cl_2) δ 148.87, 147.78, 135.99, 134.13, 131.08, 128.77, 127.35, 124.14, 65.37. HRMS (*m*/*z*): $[M]^+$ calcd for $C_{25}H_{21}NO_3Si$, 411.1291; found, 411.1290.

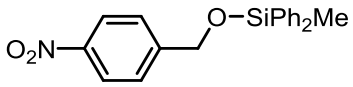

(4-Nitro-benzyloxy)-diphenylmethyl-silane. ^{1}H NMR (CD_2Cl_2) δ 8.19 (d, *J* = 8.6 Hz, 2H), 7.67 – 7.64 (m, 4H), 7.54 (d, *J* = 8.3 Hz, 2H), 7.50 – 7.39 (m, 6H), 4.92 (s, 2H), 0.74 (s, 3H); ^{13}C NMR (CD_2Cl_2) δ 148.94, 147.64, 135.89, 134.83, 130.68, 128.56, 127.21, 123.99, 64.79, -2.93. MS (EI, +ve): 334 $[M–Me]^+$.

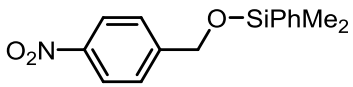

(4-Nitro-benzyloxy)-phenyldimethyl-silane. ^{1}H NMR (CD_2Cl_2) δ 8.17 (d, *J* = 8.6 Hz, 2H), 7.67 – 7.60 (m, 2H), 7.50 (d, *J* = 8.3 Hz, 2H), 7.46 – 7.34 (m, 3H), 4.81 (s, 2H), 0.46 (s, 6H); ^{13}C NMR (CD_2Cl_2) δ 149.15, 147.60, 137.54, 134.02, 130.42, 128.51, 127.07, 123.95, 64.22, -1.89. MS (EI, +ve): 272 $[M–Me]^+$.

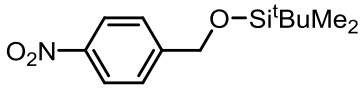

(4-Nitro-benzyloxy)-tert-butyldimethyl-silane. ^{1}H NMR (CD_2Cl_2) δ 8.18 (d, *J* = 8.4 Hz, 2H), 7.51 (d, *J* = 8.4 Hz, 3H), 4.84 (s, 2H), 0.96 (s, 9H), 0.13 (s, 6H); ^{13}C NMR (CD_2Cl_2) δ 149.88, 126.90, 123.94, 100.56, 64.55, 26.17, 18.79, -5.13. MS (EI, +ve): *m/z* 210 $[M–^{t}Bu]^+$.

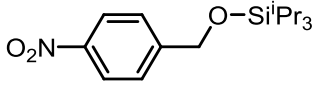

(4-Nitro-benzyloxy)-triisopropyl-silane. ^{1}H NMR (CD_2Cl_2) δ 8.19 (d, *J* = 8.5 Hz, 2H), 7.55 (d, *J* = 8.4 Hz, 2H), 4.94 (s, 2H), 1.15 – 1.25 (m, 3H), 1.10 (d, *J* = 7.4 Hz, 18H); ^{13}C NMR (CD_2Cl_2) δ 150.05, 147.51, 126.70, 123.95, 64.81, 18.34, 12.54. MS (EI, +ve): 266 $[M–^{i}Pr]^+$. HRMS (*m*/*z*): $[M]^+$ calcd for $C_{16}H_{27}NO_3Si$, 309.1760; found, 309.1759.

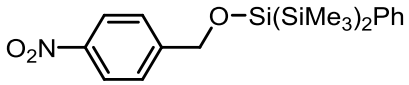

(4-Nitro-benzyloxy)-bis(trimethylsilyl)phenyl-silane. ^{1}H NMR (CD_2Cl_2) δ 8.22 (d, *J* = 8.7 Hz, 2H), 7.56 (d, *J* = 8.4 Hz, 2H), 7.53 – 7.50 (m, 2H), 7.45 – 7.31 (m, 3H), 4.89 (s, 2H), 0.21 (s, 18H); ^{13}C NMR (CD_2Cl_2) δ 149.65, 147.61, 138.29, 133.89, 129.29, 128.60, 126.84, 124.02, 67.17, -0.70. HRMS (*m*/*z*): $[M–Me]^+$ calcd for $C_{18}H_{26}NO_3Si$, 388.1221; found, 388.1215.

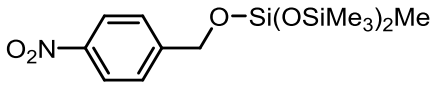

(4-Nitro-benzyloxy)-bis(trimethylsiloxy)methyl-silane. ^{1}H NMR (CD_2Cl_2) δ 8.20 (d, *J* = 8.4 Hz, 2H), 7.54 (d, *J* = 8.3 Hz, 2H), 4.89 (s, 2H), 0.13 (s, 21H); ^{13}C NMR (CD_2Cl_2) δ 149.31, 147.49, 127.14, 123.97, 63.32, 1.88, -3.54. MS (EI, +ve): *m/z* 373 $[M]^+$, 358 $[M–Me]^+$. HRMS (*m*/*z*): $[M]^+$ calcd for $C_{14}H_{27}NO_5Si_3$, 373.1197; found, 373.1190.

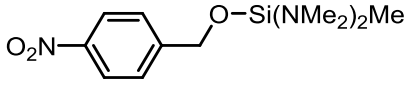

(4-Nitro-benzyloxy)-bis(dimethylamino)methyl-silane. ^{1}H NMR (CD_2Cl_2) δ 8.19 (d, *J* = 8.2 Hz, 2H), 7.38 (d, *J* = 8.3 Hz, 2H), 3.52 (s, 2H), 2.46 (s, 3H), 2.11 (s, 12H); ^{13}C NMR (CD_2Cl_2) δ 147.84, 143.22, 129.79, 123.22, 89.40, 41.12, 37.99, 37.88. The silyl ether product was unstable upon exposure to air, and mass spectral data could not be obtained. Instead, the silyl ether product was deprotected to afford the benzyl alcohol derivative. The reaction mixture was first quenched with methanol (5 mL), followed by aqueous hydrochloric acid (5 mL of a 1 N solution). The biphasic mixture was vigorously stirred for 3 hours at 25 ^{o}C. Extractions were performed using dichloromethane (10 mL × 4). The combined organic layers were washed with brine, stirred over anhydrous $MgSO_4$, filtered, and the organic solvent was removed *in vacuo*. The residue was purified by column chromatography. The isolated product was identified as 4-nitrobenzyl alcohol by ^{1}H and ^{13}C NMR spectroscopy.

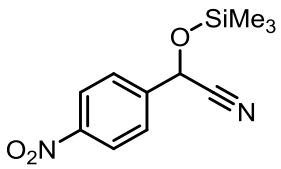

2-(4-nitrophenyl)-2-(trimethylsiloxy)acetonitrile. ^{1}H NMR (CD_2Cl_2) δ 8.38 (d, *J* = 8.6 Hz, 2H), 7.80 (d, *J* = 8.3 Hz, 2H), 5.75 (s, 1H), 0.38 (s, 9H); ^{13}C NMR (CD_2Cl_2) δ 149.08, 143.72, 127.75, 124.67, 118.88, 63.30, -0.12. HRMS (*m*/*z*): $[M]^+$ calcd for $C_{11}H_{14}N_2O_3Si$, 250.0774; found, 250.0777.

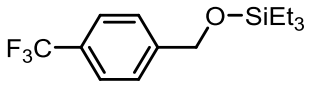

(4-Trifluoromethyl-benzyloxy)-triethyl-silane. ^{1}H NMR (CD_2Cl_2) δ 7.61 (d, *J* = 7 Hz, 2H), 7.50 (d, *J* = 7 Hz, 2H), 4.82 (s, 2H), 1.01 (t, *J* = 8 Hz, 9H), 0.69 (q, *J* = 8 Hz, 6H); ^{13}C NMR (CD_2Cl_2) δ 146.27, 129.30, 129.02, 126.55, 125.40 (q, $J_{F—C}$ = 3.8 Hz), 64.13, 6.70, 4.26; ^{19}F NMR (CD_2Cl_2) – 59.97. MS (EI, +ve): *m/z* 290 $[M]^+$, 261 $[M–Et]^+$.

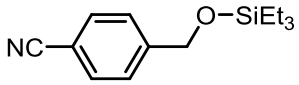

(4-cyano-benzyloxy)-triethyl-silane. ^{1}H NMR (CD_2Cl_2) δ 7.63 (d, *J* = 8.4 Hz, 2H), 7.46 (d, *J* = 7.9 Hz, 2H), 04.79 (s, 2H), 0.98 (t, *J* = 8.0 Hz, 5H), 0.67 (q, *J* = 8.0 Hz, 3H); ^{13}C NMR (CD_2Cl_2) δ 147.68, 132.60, 126.94, 119.45, 111.13, 64.38, 7.07, 4.90. MS (EI, +ve): *m/z* 218 $[M–Et]^+$.

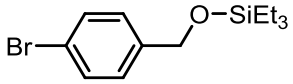

(4-bromo-benzyloxy)-triethyl-silane. ^{1}H NMR (CD_2Cl_2) δ 7.46 (d, *J* = 8.1 Hz, 2H), 7.24 (d, *J* = 8.1 Hz, 2H), 4.68 (s, 2H), 0.98 (t, *J* = 8.0 Hz, 9H), 0.66 (q, *J* = 8.0 Hz, 6H); ^{13}C NMR (CD_2Cl_2) δ 141.78, 132.23, 128.97, 121.48, 64.95, 7.60, 5.45. MS (EI, +ve): *m/z* 300 $[M]^+$, 273 $[M–Et]^+$.

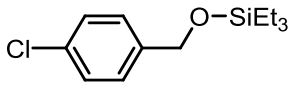

(4-chloro-benzyloxy)-triethyl-silane. ^{1}H NMR (CD_2Cl_2) δ 7.40 – 7.28 (m, 4H), 4.73 (s, 2H), 1.01 (t, *J* = 8.0 Hz, 9H), 0.69 (q, *J* = 8.0 Hz, 6H); ^{13}C NMR (CD_2Cl_2) δ 140.78, 132.91, 128.78, 128.15, 64.44, 7.11, 4.96. MS (EI, +ve): *m/z* 227 $[M–Et]^+$.

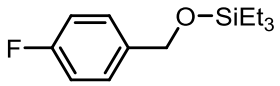

(4-fluoro-benzyloxy)-triethyl-silane. ^{1}H NMR (C_6D_6) δ 7.09 (dd, *J* = 8.4, 5.4 Hz, 2H), 6.84 (t, *J* = 8.7 Hz, 2H), 4.47 (s, 2H), 0.97 (t, *J* = 8.0 Hz, 9H), 0.58 (q, *J* = 8.0 Hz, 6H); ^{13}C NMR (C_6D_6) δ 162.64 (d, *J* = 244.1 Hz), 137.72 (d, *J* = 3.1 Hz), 128.33 (d, *J* = 7.6 Hz), 115.45 (d, *J* = 21.3 Hz), 64.41, 7.25, 5.09; ^{19}F NMR (C_6D_6) δ –115.08. MS (EI, +ve): *m/z* 211 $[M–Et]^+$.

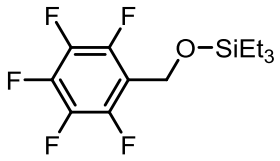

(2,3,4,5,6-pentafluoro-benzyloxy)-triethyl-silane. ^{1}H NMR (CD_2Cl_2) δ 4.76 (t, J = 1.8 Hz, 2H), 0.96 (t, J = 8.0 Hz, 9H), 0.65 (q, J = 8.0 Hz, 6H); ^{13}C NMR (CD_2Cl_2) δ 145.99 (br d, J_{CF} = 253 Hz), 141.55 (br d, J_{CF} = 253 Hz), 138.08 (br d, J_{CF} = 253 Hz), 114.67, 53.01, 6.88, 4.69; ^{19}F NMR (CD_2Cl_2) δ –141.96 (dd, J_{FF} = 22.3, 8.5 Hz), –153.42 (t, J_{FF} = 22.6 Hz), –160.67 (td, J_{FF} = 21.5, 8.4 Hz). MS (EI, +ve): *m/z* 283 $[M–Et]^+$. HRMS (*m*/*z*): $[M–Et]^+$ calcd for $C_{11}H_{12}OF_5Si$, 283.0578; found, 283.0580.

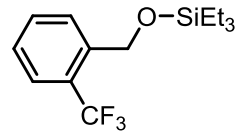

(2-trifluoromethyl-benzyloxy)-triethyl-silane. ^{1}H NMR (CD_2Cl_2) δ 7.84 (d, J = 7.8 Hz, 1H), 7.62 (d, J = 10 Hz, 1H), 7.59 (t, J = 10 Hz, 1H), 7.37 (t, J = 7.6 Hz, 1H), 4.93 (s, 2H), 1.00 (t, J = 7.9 Hz, 9H), 0.70 (q, J = 7.9 Hz, 6H); ^{13}C NMR (CD_2Cl_2) δ 140.78, 132.57, 128.09, 127.29, 126.54, 125.87, 124.11, 61.15, 7.06, 4.92; ^{19}F NMR (CD_2Cl_2) – 58.29. HRMS (*m*/*z*): $[M–Et]^+$ calcd for $C_{12}H_{16}OF_3Si$, 261.0923; found, 261.0923.

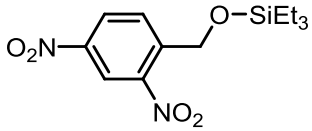

(2,4-dinitro -benzyloxy)-triethyl-silane. ^{1}H NMR (CD_2Cl_2) δ 8.93 (d, J = 2.3 Hz, 2H), 8.51 (dd, J = 8.7, 2.3 Hz, 2H), 8.23 (d, J = 8.7 Hz, 2H), 5.19 (s, 2H), 1.00 (t, J = 8.0 Hz, 9H), 0.73 (q, J = 8.0 Hz, 6H); ^{13}C NMR (CD_2Cl_2) δ 147.12, 146.55, 145.76, 129.99, 128.13, 120.36, 62.10, 6.84, 4.61. MS (EI, +ve): *m/z* 312 $[M]^+$, 283 $[M–Et]^+$. HRMS (*m*/*z*): $[M–Et]^+$ calcd for $C_{11}H_{15}N_2O_5Si$, 283.0750; found, 283.0750.

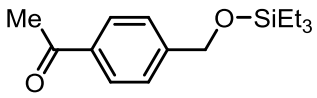

(4-acetyl-benzyloxy)-triethyl-silane. ^{1}H NMR (CD_2Cl_2) δ 7.94 (d, J = 7.9 Hz, 2H), 7.46 (d, J = 7.8 Hz, 2H), 4.81 (s, 2H), 2.58 (s, 3H), 1.00 (t, J = 7.9 Hz, 9H), 0.69 (q, J = 7.9 Hz, 6H); ^{13}C NMR (CD_2Cl_2) δ 192.02, 147.61, 136.60, 128.82, 126.52, 64.69, 27.01, 7.12, 4.97. MS (EI, +ve): *m/z* 235 $[M–Et]^+$. HRMS (*m*/*z*): calcd for $C_{15}H_{24}O_2Si$, 264.1546; found, 264.1549.

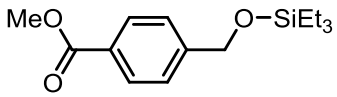

Methyl 4-(triethylsilyloxymethyl)benzoate. ^{1}H NMR (CD_2Cl_2) δ 7.99 (d, *J* = 8.3 Hz, 2H), 7.42 (d, *J* = 7.9 Hz, 2H), 4.79 (s, 2H), 3.88 (s, 3H), 0.99 (t, *J* = 7.9 Hz, 9H), 0.67 (q, *J* = 8.0 Hz, 6H); ^{13}C NMR (CD_2Cl_2) δ 167.36, 147.46, 129.95, 129.45, 126.40, 64.69, 52.41, 7.10, 4.95. MS (EI, +ve): *m/z* 251 $[M–Et]^+$.

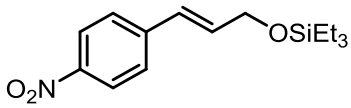

[3-(4-nitrophenyl)-2-propenyl]oxy-triethyl-silane. ^{1}H NMR (CD_2Cl_2) δ 8.17 (d, *J* = 8.8 Hz, 2H), 7.54 (d, *J* = 8.8 Hz, 2H),6.74 (d, *J* = 15 Hz, 1H), 6.54 (dt, *J* = 15.8, 4.5 Hz, 1H), 4.40 (dd, *J* = 4.5, 2.0 Hz, 2H), 4.30 – 4.27 (m, 1H), 1.01 (t, *J* = 9 Hz, 9H), 0.68 (q, *J* = 8.0 Hz, 6H); ^{13}C NMR (CD_2Cl_2) δ 147.35, 144.47, 135.24, 127.44, 127.39, 124.50, 63.50, 7.18, 5.03. MS (EI, +ve): *m/z* 293 $[M]^+$, 264 $[M–Et]^+$. HRMS (*m/z*): $[M]^+$ calcd for $C_{15}H_{23}NO_3Si$, 293.1447; found, 293.1451.

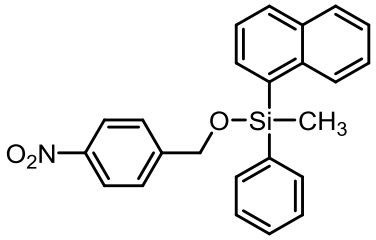

(4-Nitro-benzyloxy)-phenylmethyl(1-napthyl)-silane. ^{1}H NMR (C_6D_6) δ 8.27 (d, *J* = 8.2 Hz, 1H), 7.84 (d, *J* = 6.8 Hz, 1H), 7.77 (d, *J* = 8.4 Hz, 2H), 7.71 (d, *J* = 8.2 Hz, 1H), 7.66 – 7.55 (m, 3H), 7.30 (t, *J* = 7.5 Hz, 1H), 7.23 – 7.07 (m, 5H), 6.86 (d, *J* = 8.3 Hz, 2H), 4.42 (d, *J* = 3.9 Hz, 2H), 0.66 (s, 3H); ^{13}C NMR (C_6D_6) δ 148.20, 147.73, 137.91, 136.68, 136.07, 134.95, 134.37, 133.78, 131.94, 130.82, 129.75, 129.03, 128.82, 126.98, 126.92, 126.46, 125.74, 123.84, 64.74, -1.42. HRMS (*m/z*): $[M]^+$ calcd for $C_{24}H_{21}NO_3Si$, 399.1291; found, 399.1298.

REFERENCES

(1) (a) Piers, W. E.; Chivers, T. *Chem. Soc. Rev.* **1997**, *26*, 345; (b) Chen, E. Y.-X.; Marks, T. J. *Chem. Rev.* **2000**, *100*, 1391; (c) Stern, C. L.; Marks, T. J. *J. Am. Chem. Soc.* **1994**, *116*, 10015; (d) Bochmann, M.; Lancaster, S. J.; Hursthouse, M. B.; Malik, K. M. A. *Organometallics* **1994**, *13*, 2235; (e) Bochmann, M.; Dawson, D. M. *Angew. Chem. Int. Ed. Engl.* **1996**, *35*, 2226.
(2) (a) Parks, D. J.; Piers, W. E. *J. Am. Chem. Soc.* **1996**, *118*, 9440; (b) Parks, D. J.; Blackwell, J. M..; Piers, W. E. *J. Org. Chem.* **2000**, *65*, 3090; (c) Chandrasekhar, S.; Reddy, C. R.; Babu, B.

N. *J. Org. Chem.* **2002**, *67*, 9080; (d) Rubin, M.; Schwier, T.; Gevorgyan, V. *J. Org. Chem.* **2002**, *67*, 1936; (e) Ishihara, K.; Hanaki, N.; Yamamoto, H. *Synlett* **1993**, 577.
(3) Revunova, K.; Nikonov, G. I. *Dalton Trans.* **2015**, *44*, 840.
(4) (a) Denmark, S. E.; Beutner, G. L.; Wynn, T.; Eastgate, M. D. *J. Am. Chem. Soc.* **2005**, *127*, 3774; (b) Denmark, S. E.; Chung, W. *J. Org. Chem.* **2008**, *73*, 4582; (c) Azizi, N.; Baghi, R.; Ghafuri, H.; Boloutchian, M.; Hashemi, M. *Synlett* **2010**, 379.
(5) (a) Müther, K.; Mohr, J.; Oestreich, M. *Organometallics* **2013**, *32*, 6643; (b) Nödling, A. R.; Müther, K.; Rohde, V. H. G.; Hilt, G.; Oestreich, M. *Organometallics* **2014**, *33*, 302.
(6) (a) Reißmann, M.; Schäfer, A.; Jung, S.; Müller, T. *Organometallics* **2013**, *32*, 6736; (b) Herrington, T. J.; Ward, B. J.; Doyle, L. R.; McDermott, J.; White, A. J. P. ; Hunt, P. A.; Ashley, A. E. *Chem. Commun.* **2014**, *50*, 12753.
(7) (a) Suen, L. M.; Steigerwald, M. L.; Leighton, J. L. *Chem. Sci.* **2013**, *4*, 2413; (b) Kubota, K.; Hamblett, C. L.; Wang, X.; Leighton, J. L. *Tetrahedron* **2006**, *62*, 11397.
(8) This range represents the shortest and longest distances measured between the least-squares mean plane defined by the catecholate ligands of the molecule containing Si1 to individual atoms of the Si2-containing silicate complex.
(9) Harland, J. J.; Day, R. O.; Vollano, J. F.; Sau, A. C.; Holmes, R. R. *J. Am. Chem. Soc.***1981**, *103*, 5269.
(10) (a) Mayer, U.; Gutmann, V.; Gerger, W. *Monatsh. Chem.***1975**, *106*, 1235; (b) Beckett, M. A.; Strickland, G. C.; Holland, J. R.; Varma, K. S. *Polymer* **1996**, *37*, 4629.
(11) Childs, R. F.; Mulholland, D. L.; Nixon, A. *Can. J. Chem.* **1982**, *60*, 801.
(12) Parks, D. J.; Piers, W. E.; Parvez, M.; Atencio, R.; Zaworotko, M. J. *Organometallics* **1998**, *17*, 1369.
(13) Denmark, S. E.; Ueki, Y. *Organometallics* **2013**, *32*, 6631.
(14) (a) Kira, M.; Hino, T.; Sakurai, H. *Chem. Lett.* **1992**, 555; (b) Müther, K.; Oestreich, M. *Chem. Commun.* **2011**, *47*, 334.
(15) Hamashima, Y.; Sawada, D.; Kanai, M.; Shibasaki, M. *J. Am. Chem. Soc.* **1999**, *121*, 2641.
(16) (a) Kim, S. S.; Rajagopal, G.; Song, D. H. *J. Organomet. Chem.* **2004**, *689*, 1734; (b) Denmark, S. E.; Chung, W. *J. Org. Chem.* **2006**, *71*, 4002.
(17) NMR kinetics experiments were attempted for the hydrosilation of 2-trifluoromethylbenzaldehyde with a 10-fold excess of triethylsilane at 30 ^{o}C. Unfortunately, the kinetics data were complex and could not be fit to a standard rate law, in part due to complications from catalyst decomposition.
(18) Koller, J.; Bergman, R. G. *Organometallics* **2012**, *31*, 2530.
(19) Blackwell, J. M.; Foster, K. L.; Beck, V. H.; Piers, W. E. *J. Org. Chem.* **1999**, *64*, 4887.
(20) (a) Rendler, S.; Oestreich, M. *Angew. Chem. Int. Ed.* **2008**, *47*, 5997; (b) Metsänen, T. T.; Hrobárik, P.; Klare, H. F. T.; Kaupp, M.; Oestreich, M. *J. Am. Chem. Soc.* **2014**, *136*, 6912; (c) Shinke, S.; Tsuchimoto, T.; Kawakami, Y. *Silicon Chem.* **2007**, *3*, 243.
(21) (a) Sommer, L. H.; Frye, C. L.; Parker, G. A.; Michael, K. W. *J. Am. Chem. Soc.* **1964**, *86*, 3271; (b) Ojima, Y.; Yamaguchi, K.; Mizuno, N. *Adv. Synth. Catal.* **2009**, *351*, 1405.
(22) (a) Winstein, S.; Klinedinst, P. E.; Robinson, G. C. *J. Am. Chem. Soc.* **1961**, *83*, 885; (b) Allen, A. D.; Tidwell, T. T.; Tee, O. S. *J. Am. Chem. Soc.* **1993**, *115*, 10091; (c) Loupy, A.; Tchoubar, B. *Salt Effects in Organic and Organometallic Chemistry*; VCH: Weinheim, Germany, 1992.

(23) (a) Winstein, S.; Friedrich, E. C.; Smith, S. *J. Am. Chem. Soc.* **1964**, *86*, 305; (b) Perrin, C. L.; Pressing, J. *J. Am. Chem. Soc.* **1971**, *93*, 5705; (c) Tellers, D. M.; Yung, C. M.; Arndtsen, B. A.; Adamson, D. R.; Bergman, R. G. *J. Am. Chem. Soc.* **2002**, *124*, 1400.
(24) (a) Doyle, M. P.; West, C. T. *J. Org. Chem.* **1975**, *40*, 3835; (b) Doyle, M. P.; West, C. T.; Donnelly, S. J.; McOsker, C. C. *J. Organomet. Chem.* **1976**, *117*, 129; (c) Sakata, K.; Fujimoto, H. *J. Org. Chem.* **2013**, *78*, 12505.
(25) The work in this chapter was adapted with permission from Liberman-Martin, A. L.; Bergman, R. G.; Tilley, T. D. *J. Am. Chem. Soc.*, **2015**, *137*, 5328.
(26) Allcock, H. R.; Nugent, T. A.; Smeltz, L. A. *Synth. Inorg. Met.-Org. Chem.* **1972**, *2*, 97.
(27) Tamborski, C.; Soloski, E. J.; Dec, S. M. *J. Organomet. Chem.* **1965**, *4*, 446.
(28) Savela, R.; Zawartka, W.; Leino, R. *Organometallics* **2012**, *31*, 3199.
(29) Ojima, Y.; Yamaguchi, K.; Mizuno, N. *Adv. Synth. Catal.* **2009**, *351*, 1405.

Chapter 4. Appendix

Chiral HPLC traces

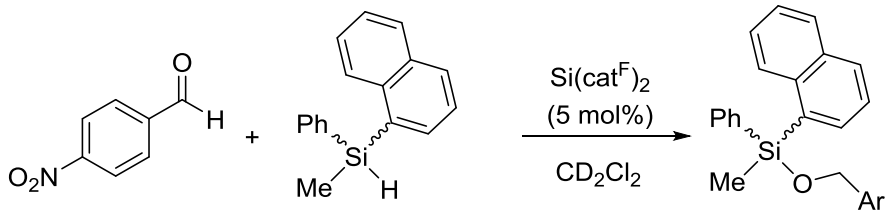

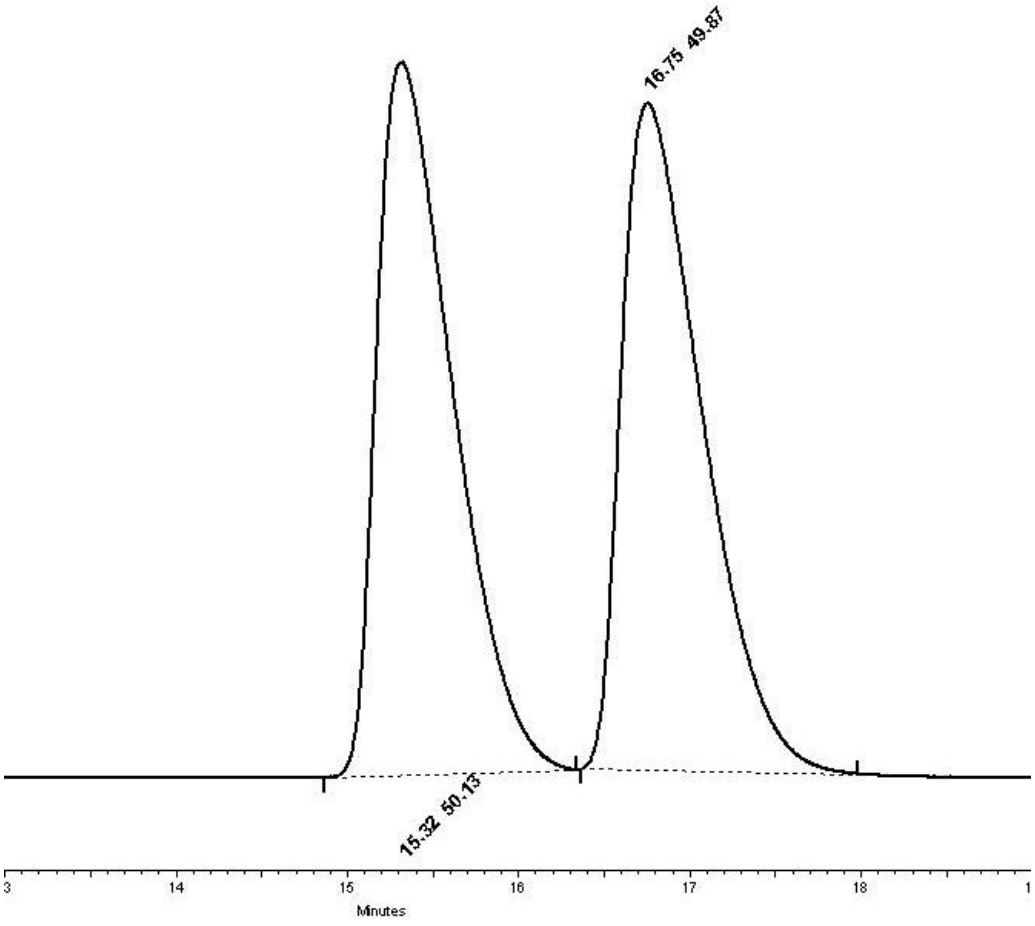

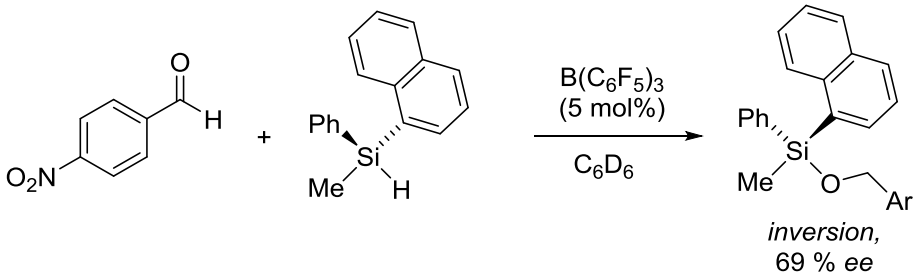

inversion,
69 % *ee*

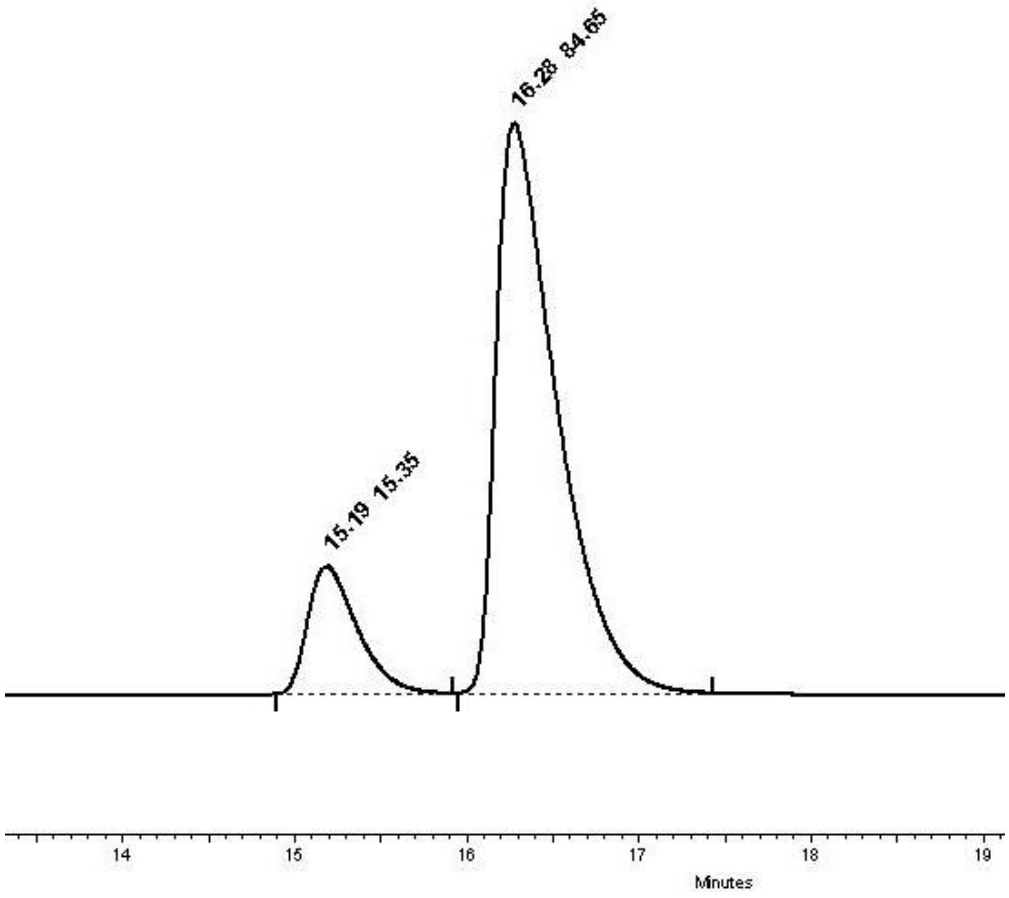

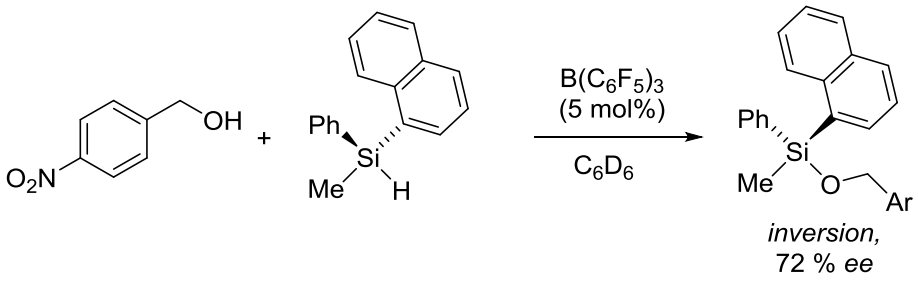
OH
O_2N
+
Ph
Si
Me
H
$B(C_6F_5)_3$
(5 mol%)
C_6D_6
Ph
Si
Me
O
Ar
inversion,
72 % *ee*

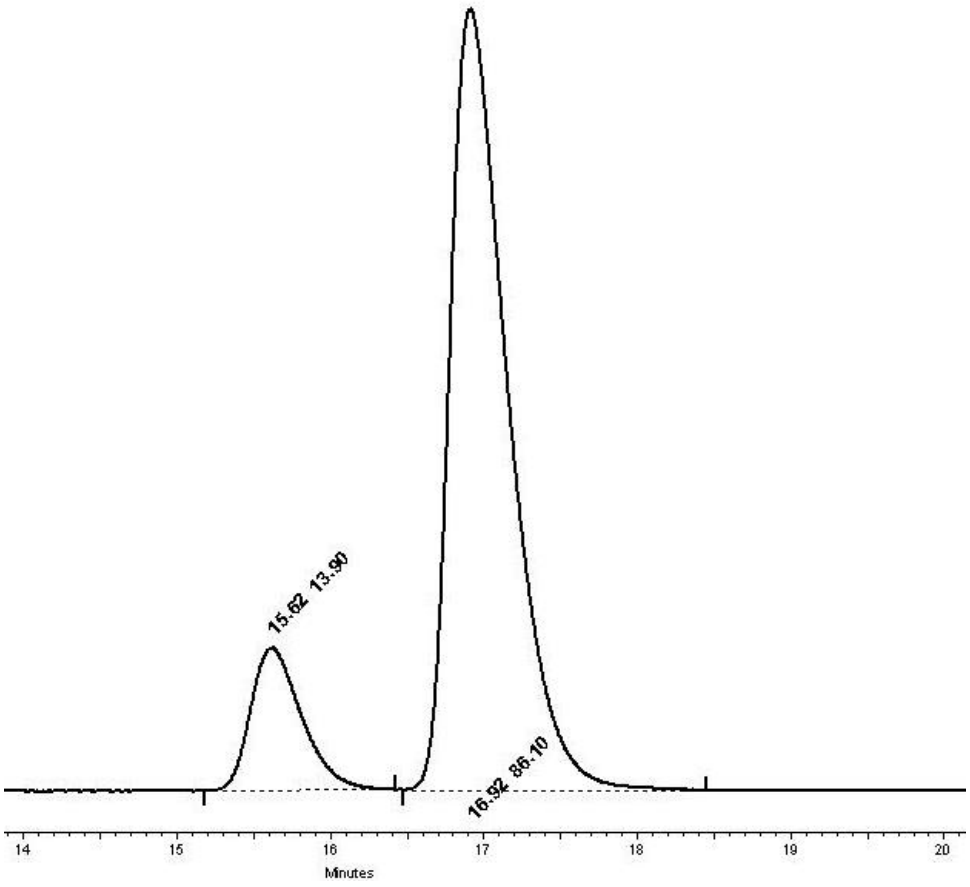
15.62 13.90
16.92 86.10
14
15
16
17
18
19
20
Minutes

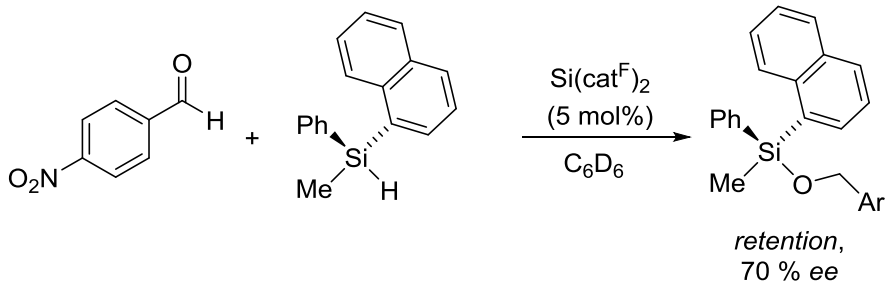

retention,
70 % *ee*

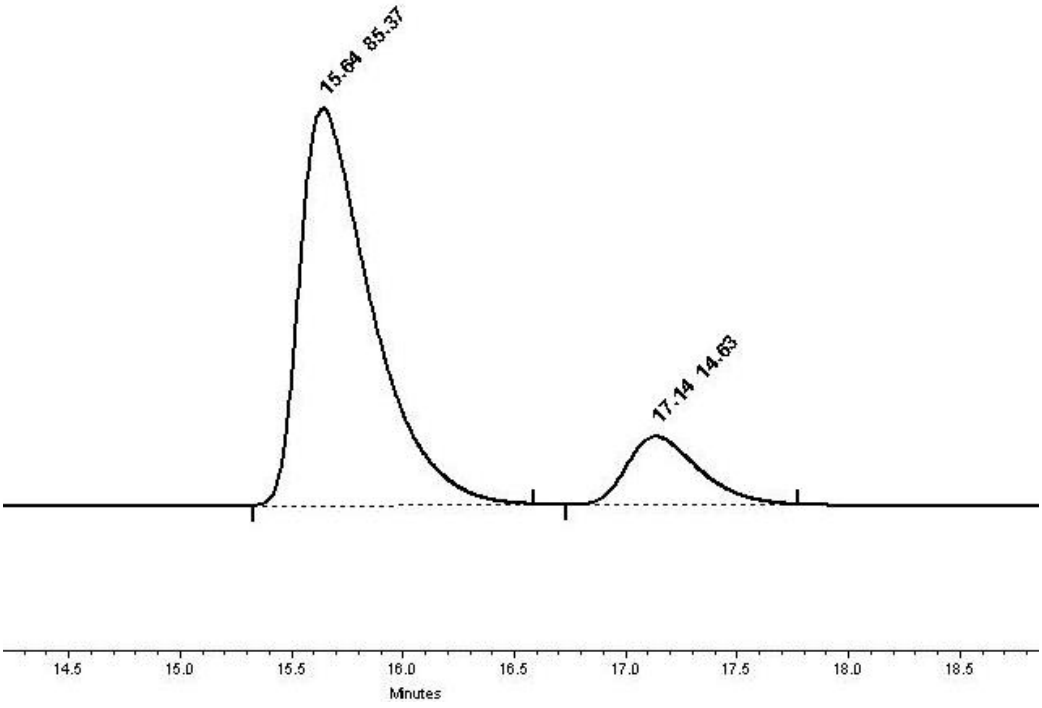

Table A1. Crystal data and structure refinement for **2**.

Empirical formula	$C_{18}H_{18}F_9N_3O_4SSi$	
Formula weight	571.50	
Temperature	100(2) K	
Wavelength	0.71073 Å	
Crystal system	Triclinic	
Space group	P -1	
Unit cell dimensions	a = 10.302(2) Å	α= 94.143(9)°.
	b = 11.005(2) Å	β= 92.813(11)°.
	c = 19.949(4) Å	γ = 95.037(9)°.
Volume	2243.7(8) $Å^3$	
Z	4	
Density (calculated)	1.692 Mg/m^3	
Absorption coefficient	0.305 mm^{-1}	
F(000)	1160	
Crystal size	0.15 x 0.10 x 0.09 mm^3	
Theta range for data collection	1.863 to 31.591°	
Index ranges	-14<=h<=15, -12<=k<=14, -28<=l<=27	
Reflections collected	51799	
Independent reflections	11537 [R(int) = 0.0682]	
Completeness to theta = 25.00°	99.8 %	
Absorption correction	Semi-empirical from equivalents	
Max. and min. transmission	0.7301 and 0.6254	
Refinement method	Full-matrix least-squares on F^2	
Data / restraints / parameters	11537 / 0 / 661	
Goodness-of-fit on F^2	1.090	
Final R indices [I>2sigma(I)]	R1 = 0.0555, wR2 = 0.1483	
R indices (all data)	R1 = 0.0710, wR2 = 0.1620	
Largest diff. peak and hole	0.616 and -1.193 $e.Å^{-3}$	

Table A2. Crystal data and structure refinement for **3**.

Empirical formula	$C_{31}H_{23}F_{10}NO_5Si$	
Formula weight	707.59	
Temperature	100(2) K	
Wavelength	1.54178 Å	
Crystal system	Monoclinic	
Space group	c 2/c	
Unit cell dimensions	a = 33.591(2) Å	α= 90°.
	b = 13.3628(8) Å	β= 106.444(2)°.
	c = 14.0068(8) Å	γ = 90°.
Volume	6030.1(6) $Å^3$	
Z	8	
Density (calculated)	1.559 Mg/m^3	
Absorption coefficient	1.651 mm^{-1}	
F(000)	2880	
Crystal size	0.040 x 0.030 x 0.010 mm^3	
Theta range for data collection	2.743 to 68.433°	
Index ranges	-40<=h<=40, -16<=k<=16, -16<=l<=12	
Reflections collected	36472	
Independent reflections	5457 [R(int) = 0.0272]	
Completeness to theta = 67.00°	98.8 %	
Absorption correction	Semi-empirical from equivalents	
Max. and min. transmission	0.7531 and 0.7011	
Refinement method	Full-matrix least-squares on F^2	
Data / restraints / parameters	5457 / 0 / 433	
Goodness-of-fit on F^2	1.032	
Final R indices [I>2sigma(I)]	R1 = 0.0466, wR2 = 0.1317	
R indices (all data)	R1 = 0.0491, wR2 = 0.1342	
Largest diff. peak and hole	0.791 and -0.575 $e.Å^{-3}$	